

AD 656480

AD

**USAAVLABS TECHNICAL REPORT 66-33**  
**BOUNDARY LAYER CONTROL SYSTEM INSTALLATION**  
**FOR THE YCV-2B AIRPLANE**

**By**

**C. A. Cordner**

**May 1967**

**U. S. ARMY AVIATION MATERIEL LABORATORIES**  
**FORT EUSTIS, VIRGINIA**

**CONTRACT DA 44-177-AMC-35(T)**  
**RYAN AERONAUTICAL COMPANY**  
**SAN DIEGO, CALIFORNIA**

*Distribution of this  
document is unlimited*



**RECEIVED**

**AUG 21 1967**

**CFSTI**

1-202

### Disclaimers

When Government drawings, specifications, or other data are used for any purpose other than in connection with a definitely related Government procurement operation, the United States Government thereby incurs no responsibility nor any obligation whatsoever; and the fact that the Government may have formulated, furnished, or in any way supplied the said drawings, specifications, or other data is not to be regarded by implication or otherwise as in any manner licensing the holder or any other person or corporation, or conveying any rights or permission, to manufacture, use, or sell any patented invention that may in any way be related thereto.

Trade names cited in this report do not constitute an official endorsement or approval of the use of such commercial hardware or software.

### Disposition Instructions

Destroy this report when no longer needed. Do not return it to originator.

ACCESSION TO	
CESTI	WHITE SUPPLY
DDG	DATE ACQUISITION
UNANNOUNCED	
JUSTIFICATION	
BY <i>Kn</i>	
DISTRIBUTION AVAILABLE TO ALL	
DIST.	APPROVAL OF SPECIAL
1	



DEPARTMENT OF THE ARMY  
U. S. ARMY AVIATION MATERIEL LABORATORIES  
FORT EUSTIS, VIRGINIA 23604

This report has been reviewed by the U. S. Army Aviation Materiel Laboratories. The conclusions and recommendations made in this report are considered to be technically sound. The results of the investigations, although negative in nature, will supply useful information for future work of this type.

Task 1P121401A14178  
Contract DA 44-177-AMC-35(T)  
USAAVLABS Technical Report 66-33  
May 1967

312  
600

**BOUNDARY LAYER CONTROL SYSTEM INSTALLATION  
FOR THE YCV-2B AIRPLANE**

**Final Report**

**RYAN REPORT NO. 65B017A**

**This research was supported by the Advanced Research Projects Agency of the Department of Defense and was monitored by the U.S. Army Aviation Materiel Laboratories (USAAVLABS) under Contract DA 44-177-AMC-35(T).**

**by  
C. A. Cordner**

**Prepared by  
RYAN AERONAUTICAL COMPANY  
SAN DIEGO, CALIFORNIA**

**for**

**U.S. ARMY AVIATION MATERIEL LABORATORIES  
FORT EUSTIS, VIRGINIA**

**Distribution of this  
document is unlimited**



### ABSTRACT

This is the final report of a program conducted by the Ryan Aeronautical Company, San Diego, California, under Contract DA 44-177-AMC-35(T) with the U.S. Army Aviation Materiel Laboratories (USAAVLABS), Fort Eustis, Virginia. The interim report for the program was Ryan Report No. 64B053 dated 6 April 1964.

The results of a theoretical analysis, predesign study, and bench tests to determine the feasibility of further development of a high lift, jet-pumped boundary layer control (BLC) system for an aircraft, such as the YCV-2B Caribou, are presented in this report. No classified data were developed during the program.

Technical data of the YCV-2B Caribou were obtained from USAAVLABS and from the U.S. Army Aviation Materiel Command, St. Louis, Missouri.

## CONTENTS

	Page
ABSTRACT	iii
LIST OF ILLUSTRATIONS	vi
LIST OF TABLES	ix
LIST OF SYMBOLS	x
SUMMARY	1
CONCLUSIONS	2
RECOMMENDATIONS	4
DESCRIPTION OF THE SYSTEM CONCEPT	5
EXPERIMENTAL PROCEDURE	12
TESTS	26
INSTRUMENTATION	51
REFERENCES	56
DISTRIBUTION	57
APPENDIX I - THEORETICAL DEVELOPMENT OF A BOUNDARY LAYER CONTROL JET PUMP	59
APPENDIX II - DIGITAL COMPUTER PROGRAMS	88
APPENDIX III - SYSTEM OF EQUATIONS FOR THE SOLUTION OF TWO-DIMENSIONAL MIXING FLOW OF CONCENTRIC STREAMS OF FLUIDS	143
APPENDIX IV - SMOKE TUNNEL TESTS	146

## ILLUSTRATIONS

<u>Figure</u>		<u>Page</u>
1	Airfoil Shown With Suction Slot	7
2	Airfoil Shown With Blowing Slot	7
3	Conceptual Schematic of the Multiple Cell Boundary Layer Control	8
4	Schematic Drawing of Jet Pump	9
5	Schematic Drawing of the BLC System as Installed in the YCV-2B Caribou	10
6	Typical Installation of the BLC System	11
7	Jet Pump and Ducts	11
8	Motor Assembly - Type 1 (Material: Hastelloy X)	15
9	Jet Pump Primary Motor	15
10	Primary Motor (Material: Hastelloy X)	18
11	Duct System	19
12	Plaster Mold for Suction Duct	23
13	Plaster Mold for Blowing Duct	23
14	Plaster Mold for Elbow	24
15	Plaster Forming Mold for Duct	24
16	Diffuser with 7° Angle	25
17	Assembly of Test Duct	25
18	View of Bellmouth	25
19	Configurations Tested	28
20	Schematic Drawing of Bench Test Arrangement	29
21	Schematic Drawing of Pressure Probe Location	30
22	Final Arrangement for Cold Flow Tests	31
23	Operator's Control Panel	31
24	View of Primary Motor During Test	31
25	Primary Motor Performance - Run 18	37
26	Kinetic Energy Values - Cold Flow	38
27	Kinetic Energy Values - Hot Flow	38
28	Entrainment Ratio Versus Primary Weight Flow - Cold Flow	39
29	Entrainment Ratio Versus Primary Weight Flow - Hot Flow	39
30	Fuel/Air Ratio Versus Combustor Temperature - Primary Motor	40
31	Location of Microphone With Respect to Primary Motor	49
32	Noise Level Versus Frequency Spectrum	50

<u>Figure</u>		<u>Page</u>
33	Photograph Record of Pressure Data	52
34	Primary Motor Failure	53
35	IBM 704 Input Format	102
36	Blowing Wing Coefficient - Look-Up Values	123
37	Blowing Wing Coefficient - Look-Up Values	124
38	Input Matrix Format	125
39	Control Card	126
40	Control Card	127
41	Comment 2 Control Cards	128
42	Look-Up Card for Plain Flaps	129
43	Look-Up Card for Single Slotted Flaps	130
44	Tork Coefficients	139
45	Model Airfoils Tested	147
46	Fifteen-Percent-Thick Suction Flap Airfoil - Smoke Tunnel Test Runs 3, 6, 9, and 12	151
47	Fifteen-Percent-Thick Suction Flap Airfoil - Smoke Tunnel Test Runs 15, 18, 21, and 24	152
48	Seventeen-Percent-Thick Suction Flap Airfoil - Smoke Tunnel Test Runs 27, 30, 33, and 36	153
49	Seventeen-Percent-Thick Suction Flap Airfoil - Smoke Tunnel Test Runs 39, 42, 45, and 48	154
50	Blowing Flap Airfoil - Smoke Tunnel Test Runs 59, 62, 65, and 68	155
51	Blowing Flap Airfoil - Smoke Tunnel Test Runs 71, 74, 77, and 80	156
52	Blowing Aileron - Smoke Tunnel Test Runs 90 Through 98	157
53	Blowing Aileron - Smoke Tunnel Test Runs 99 Through 106	158
54	Suction Elevator Airfoil - Smoke Tunnel Test Runs 49 Through 53	159
55	Suction Elevator Airfoil - Smoke Tunnel Test Runs 56 Through 56	160
56	Effect of $C_{QS}$ on $\Delta C_{l_r}$ , Fifteen-Percent Suction Flap Airfoil	161
57	Effect of $C_{QS}$ on $\Delta C_{l_r}$ , Blowing Aileron	162
58	Effect of $C_{QS}$ on Blowing Elevator, $\delta_e = \pm 15^\circ$	163

<u>Figure</u>		<u>Page</u>
59	Fifteen-Percent-Thick Airfoil With Suction Flap Deflected 60° at Zero Angle of Attack	164
60	Fifteen-Percent-Thick Airfoil With Suction Flap Deflected 90° at 25 fps Tunnel Velocity	165
61	Fifteen-Percent-Thick Airfoil With Suction Flap Deflected 90° at 14 Angle of Attack	166
62	Seventeen-Percent-Thick Airfoil With Suction Flap Deflected 60° at 25 fps Tunnel Velocity	167
63	Seventeen-Percent-Thick Airfoil With Suction Flap Deflected 90° at Zero Angle of Attack	168
64	Seventeen-Percent-Thick Airfoil With Suction Flap Deflected 90° and 80° at 10° Angle of Attack and 50 fps Tunnel Velocity	169
65	Seventeen-Percent-Thick Airfoil With Suction Flap Deflected 80° at 10° Angle of Attack	170
66	Seventeen-Percent-Thick Airfoil With Suction Flap Deflected 80° at 25 fps Tunnel Velocity	171
67	Seventeen-Percent-Thick Airfoil With Suction Flap Deflected 80° at 10 fps Tunnel Velocity and 14° Angle of Attack	172
68	Seventeen-Percent-Thick Airfoil With Blowing Flap Deflected 60° and 80° at Zero Angle of Attack and 25 fps Tunnel Velocity	173
69	Seventeen-Percent-Thick Airfoil With Blowing Flap Deflected 90° at 25 fps Tunnel Velocity	174
70	Airfoil With Blowing Aileron Deflected 10° and 20° at Zero Angle of Attack and 25 fps Tunnel Velocity	175
71	Airfoil With Blowing Aileron Deflected 40° and 60° at Zero Angle of Attack and 25 fps Tunnel Velocity	176
72	Airfoil With Suction Elevator Deflected +15° at Zero Angle of Attack and 25 fps Tunnel Velocity	177
73	Airfoil With Suction Elevator Deflected -15° at Zero Angle of Attack and 25 fps Tunnel Velocity	178
74	Airfoil With Suction Elevator Deflected -15° at 25 fps Tunnel Velocity	179
75	Airfoil With Blowing Elevator Deflected ±15° at 25 fps Tunnel Velocity	180
76	Seventeen-Percent-Thick Suction Flap Airfoil, $\delta_F = 60^\circ$	181
77	Blowing Flap Airfoil, $\delta_F = 60^\circ$	182

## TABLES

<u>Table</u>		<u>Page</u>
I	Summary of Primary Motor Performance	36
II	Summary of Selected Data - Test No. 8 - Cold Flow	41
III	Summary of Selected Data - Test No. 9 - Cold Flow	42
IV	Summary of Selected Data - Test No. 10 - Cold Flow	43
V	Summary of Selected Data - Test No. 11 - Cold Flow	44
VI	Summary of Selected Data - Test No. 18 - Hot Flow	44
VII	Summary of Selected Data - Test No. 34 - Hot Flow	45
VIII	Summary of Selected Data - Test No. 35 - Hot Flow	46
IX	Summary of Selected Data - Test No. 36 - Hot Flow	47
X	Instrumentation List	54

# SYMBOLS

$A$	Cross-sectional area, ft <sup>2</sup>
$a$	Cross-sectional area of nozzle sections, in. <sup>2</sup>
$A_{XD}$	Area at the exit of the diffuser or mixing tube, ft <sup>2</sup>
$A_{SJ}$	Cross-sectional area of the secondary jet at the plane of the primary motor outlet, in. <sup>2</sup>
$AR$	Aspect ratio
$b=l$	Span, ft
$C_{f/c}$	Ratio of flap chord to airfoil chord
$C_l$	Coefficient of lift
$C_{l_{P.F.}}$	Theoretical potential flow lift coefficient
$C_{l_R}$	Reaction lift coefficient
$C_{l_{TOT}}$	Total coefficient of lift
$C_{l_\Gamma}$	Circulation lift coefficient
$\Delta C_{l_B}$	Blowing induced circulation lift coefficient
$\Delta C_{l_{R_B}}$	Blowing momentum reaction lift coefficient
$\Delta C_{l_{R_{SS}}}$	Direct thrust lift coefficient

$\Delta C_{l_S}$	Suction induced circulation lift coefficient
$\Delta C_{l_{\Gamma_{SS}}}$	Slipstream induced circulation
$C_M$	Running torsion coefficient
$C'_M$	Torsion coefficient
$C_{M_o}$	Aerodynamic pitching moment coefficient of local airfoil due to camber
$C_{Q_B} = \frac{Q_B}{V_o S_B} \text{ (at } \rho_o \text{)}$	= Blowing air volume flow coefficient
$C_{Q_S} = \frac{Q_S}{V_o S_S} \text{ (at } \rho_o \text{)}$	= Suction air volume flow coefficient
$C_\mu = 2(s/c)_B \cdot q_J/q_o$	= Blowing air momentum coefficient
$c$	Chord, ft
$\bar{c}$	Wing mean aerodynamic chord
$c_p$	Specific heat at constant pressure, $\frac{\text{Btu}}{\text{lb } o_R}$
$c_{p_t} = \frac{P_{T_M} - P_{T_{SJ}}}{1/2 \rho_M V_M^2}$	Loss coefficient, pressure
$c_v$	Specific heat at constant volume, $\frac{\text{Btu}}{\text{lb } o_R}$
$CK_t$	Loss coefficient due to contraction
$d$	Diameter, in.
$D$	Diameter, ft
$D_{ACT}$	Actual throat diameter of primary motor nozzle, in.



$D_{SS}$	Slipstream diameter at quarter chord, ft.
$DPPT = \Delta P + \frac{P_1 A}{T_{A A}}$	Density correction factor
$E$	Kinetic energy - ft-lb
$e$	Error
$E_m$	Error between $m_1$ and $m_2$ based on $m_1/m_2$
$E_{T_{cc}} = \frac{T_{cc A}}{T_{cc}^o}$	Combustion chamber temperature error
$E_{T_{PJ}} = \frac{T'_{PJ}}{T_{PJ}}$	Exit temperature error of the primary motor jet
$F$	Fuel to air weight flow ratio
$F_1, F_{T/F_1}, F_{O/F_1}$	As defined in Ryan Report 62B046 and incorporated in Tables of Look-Up (See Figures 35, and 39 and Pages 141, 142)
$f$	Friction loss coefficient
$g$	Acceleration of gravity, 32.174 ft/sec. <sup>2</sup>
$h$	Enthalpy, Btu /lb
$h$	Fuel sight gage height, inches
$i_w$	Incidence of wing root chord referenced to fuselage longitudinal axis
$J$	Joule's equivalent = 778 ft-lb/Btu
$K_{SS}$	Ratio of local slipstream dynamic pressure to free stream dynamics pressure
$K$	Loss coefficient - blowing duct
$k = \frac{c_p}{c_v}$	Specific heat ratio

$k_S$	$= \frac{\Delta C_S}{C_{Q_S} k_t}$	
$k_t$	Thickness correction	
$l=b$	Span, ft	
$M$	Mach number	
$m$	$= \frac{W_{SJ}}{W_{PJ}} =$	Entrainment ratio
$m_1$	Entrainment ratio based on inlet duct and nozzle data	
$m_2$	Entrainment ratio based on mixing duct-diffuser and nozzle data	
$N_o$	Impelling power, ft-lb/sec	
$N_{SS}$	Exponent used in $K_{SS}$ equation	
NUM	Numerator of expression for A as used in $K_{SS}$ equation	
$p$	Pressure, lb/in. <sup>2</sup>	
$P$	Pressure, lb/ft. <sup>2</sup>	
$P_{cc_A}$	$= P_{cc} + P_{ATM}$	Combustion chamber pressure, psia
$P_{S_{x_D}}$	Static pressure at end of mixing tube or diffuser, psia	
$P_1$	Air pressure upstream of the metering orifice, psig	
$P_{1A}$	Air pressure upstream of measuring orifice, psia	
$P_2$	Air pressure downstream of the metering orifice, psig	
psia	Pounds per square inch, absolute	

psig	Pounds per square inch, gauge
$\Delta P_{t_{TS}}$	Turn loss, psia
Q	Volume flow, ft <sup>3</sup> /sec
q	Dynamic pressure, lb/ft <sup>2</sup>
$q_{B_x}$	Dynamic pressure at exit of diffuser (at entrance to the blowing duct) lb/ft <sup>2</sup>
R	Gas constant = 53.3 ft-lb/lb°R
$R'_e$	$\frac{\rho V}{\gamma} = \text{Reynolds Number}$
r'	Hydraulic radius, ft
S	Wing area, ft <sup>2</sup>
s	Slot width, ft
(s/c)	Slot width to chord ratio
T	Temperature, °R static, streamwise
T	Propeller thrust, lb
$T_{A_A}$	Air temperature upstream of measuring orifice, °R
$T_C$	Thrust coefficient
$T_{cc_A}$	$= \Delta T_{cc} + T_{A_A}$ Total temperature, absolute, in the combustion chamber, °R
$T'_{cc}$	$= \frac{.1735 P_{cc_A}^2 D_{ACT}^4}{W_{PJ}^2}$ Combustion chamber temperature by continuity equation, °R
$T_{CLXD}$	Centerline temperature at exit to diffuser or mixing tube, °R

$T_{JP}$	Thrust of jet pump, lb
$T'_{PJ}$	Temperature of the primary jet at nozzle exit, based on the continuity equation, °R
$T'$	Temperature based on continuity equation, °R
$T_R$	Thrust of primary motor, lb
$T^0$	Temperature, °R (stagnation, or static)
$T_{W XD}$	Wall temperature at exit to diffuser or mixing tube, °R
$t$	Time, sec
$t/c$	Airfoil thickness to chord ratio
$V$	Velocity, ft/sec
$V_{SJ}$	Velocity of secondary (induced flow) air at inlet to jet pump, ft/sec
$V_{PJ}$	Velocity of the gas at the exit from the primary motor, ft/sec
$W$	Weight flow, lb/sec
$W_{PJ}$	Weight flow of burned fuel/air mixture from primary motor, lb/sec
$W_{SJ}$	Weight of secondary (induced flow) air at inlet to jet pump, lb/sec
$W_M$	$= W_{PJ} + W_{SJ} =$ Mixed flow at end of mixing tube, lb/sec
$X_3$	Distance between propeller disc and wing quarter chord location, ft
$X_{SS}$	Distance between wing station under consideration and thrust center-line, ft

$\alpha$	Angle of attack, deg
$\alpha_V$	$= \frac{V_{SJ}}{V_{PJ}}$ at Station I = velocity ratio
$\alpha_g$	Angle between relative wind and fuselage datum line, degrees
$\alpha_{in}$	Angle of incidence, deg
$\beta$	$= V_M/V_{PJ}$ at Station M = velocity ratio
$\beta$	Final velocity ratio (See University of Wichita Report 294)
$\Gamma$	Circulation, ft <sup>3</sup> /sec
$\gamma$	$=$ Kinematic viscosity of air, $1.57 \times 10^{-4}$ ft <sup>2</sup> /sec
$\Delta$	Incremental change in a value
$\Delta h_{TXD}$	Dynamic head at the exit to the diffuser or mixing tube, in.
$\delta_e$	Elevator deflection, deg
$\delta_F$	Flap deflection, deg
$\delta_{FB}$	Deflection of blowing flap, deg
$\delta_{FS}$	Deflection of suction flap, deg
$\delta_j$	Angle between upper surface of airfoil trailing edge and airfoil chord line, deg
$\delta_{te}$	Deflection of the jet sheet referenced to the relative wind, deg
$\epsilon$	Wing twist angle, deg
$\zeta$	$= \eta_E/\eta_i$ = efficiency ratio
$\eta$	Efficiency
$\eta_E$	Experimental efficien

$\eta_i$	Ideal efficiency (theoretical)
$\eta_T$	Spanwise location of propeller centerline
$\eta_Y$	Wing spanwise location as a decimal fraction of wing semispan
$\lambda_o$	$= \Delta P_{t/q} =$ total pressure loss coefficient per $l/r'$
$\rho$	Density, lb sec <sup>2</sup> /ft <sup>4</sup>
$\rho_{B_x}$	Density at exit of diffuser (at entrance to the blowing duct) lb sec <sup>2</sup> /ft <sup>4</sup>
$\rho_M$	Density at end of mixing tube, lb sec <sup>2</sup> /ft <sup>4</sup>
$\rho_{SI}$	Static inlet (to bellmouth) density lb sec <sup>2</sup> /ft <sup>4</sup>
$\phi_T$	Turn loss coefficient
$\varphi$	$= \frac{A_{PJ}}{A_{SJ}} =$ Area ratio of primary motor exit to cross section of secondary stream at the plane of Station I
$\varphi$	Diffuser angle, deg
$\omega$	Measured weight of fuel, lb

### SUBSCRIPTS

A	Absolute
A	Air - upstream of metering orifice
ACT	Actual
ATM	Atmospheric
AV	Average
a	Air
a	Available
B	Blowing
BX	Blowing exit
CA	Compressed air
cc	Combustion chamber
D	Duct
Di	Diffuser, suction duct
E	Entrance
E	Experimental
EX, ex	Excess
F	Wall friction
f	Fuel
g	Geometric
H	Hydraulic
I	Station I (primary jet station)

i	Ideal; inlet
in	Incidence
J	Jet sheet (blowing air)
M	Mixing tube; station at end of blowing tube, mean
o	Ambient; stagnation; initial; freestream
P	Propeller
$P_o$	Primary jet pressure before expansion in primary nozzle
PJ	Primary jet
$R_B$	Blowing momentum reaction
$R_{SS}$	Direct thrust reaction
S	Static
S	Suction
SI	Static inlet
SJ	Secondary jet
Sl	Slot
SXD	Static head at exit to diffuser or mixing tube
$T_o$	Primary jet temperature before expansion
t	Throat
t	Total
x	Exit



**BLANK PAGE**

## SUMMARY

This report presents the findings of a research and development contract for the investigation of the feasibility of installing a high lift boundary layer control (BLC) system in a YCV-2B airplane. The program was conducted under the authority of Contract DA 44-177-AMC-35 (T) dated 11 June 1963. The contract specified that the contractor conduct work in the areas of preliminary design, technical analysis, and development testing to the extent necessary to determine the feasibility and practicability of improvement of takeoff and landing performance of YCV-2B aircraft.

The contractor's effort was directed primarily to the development of a compressed air/gasoline fuel primary motor for driving the jet pump system. The secondary effort was directed to the design and evaluation of the system and to the performance characteristics. The contractor also conducted a series of smoke tunnel tests to determine qualitatively the effects of BLC on lift characteristics of the YCV-2B airfoils. Difficulty was experienced in the development of the primary motor owing to its inability to contain high temperatures. However, the experimental prototype model was satisfactory for obtaining limited jet pump data. The performance of the jet pump was not able to improve the takeoff or the landing characteristics of the aircraft. Design and technical analysis studies showed that the BLC system could not be installed and operated in the YCV-2B airplane with any reasonable expectancy of success.

Included as a part of this report are equations, computer programs and methods for predicting design parameters, and performance characteristics of jet pumps and boundary layer controls systems.

## CONCLUSIONS

The proposed high lift, jet-pumped boundary layer control (BLC) system is not feasible for an aircraft such as the YCV-2B Caribou. This is the major conclusion resulting from the study. While incontrovertible proof of such a negative conclusion is always very difficult, it is this Contractor's judgment that the conclusion is sound, based on the following considerations:

1. Jet pumps such as those proposed proved to be incapable of producing the required secondary air mass flows throughout the spectrum of flight conditions and within the installation constraints.
2. Reliability of currently available gasoline burning jet pump components is too low. This applies particularly to the igniters and to the nozzle throat sections, which did not long withstand the temperature and erosion conditions inherent in the configuration.
3. System complexity as installed in the aircraft would be excessive. This applies particularly to the problems of maintaining proper fuel/air ratio at all of the required primary motors. Successful operation would require means to balance fuel and airflow to each of the primary motors under conditions where the variables include pressures of incoming air and fuel, temperatures of incoming air and fuel, variation in total primary flow rate, duct ambient temperature and flow field around the primary motors, as well as burning chamber pressure and temperature. The total system for the YCV-2B Caribou would require a minimum of one primary motor, and perhaps several, for each of the fifteen ducts in the system. All would require individual control for stable operation as well as coordinated control for throttling.
4. Undesirable complexity would result from the need for automatic means of controlling the aircraft during BLC takeoff and landing. The very low dynamic pressure ( $q \approx 4$  psf) would result in very low aerodynamic damping, and low speed-regime stability augmentation probably would be necessary. Wind tunnel testing on a large scale model would be required to evaluate aircraft control and probable handling characteristics and to establish criteria for an augmentation system.

5. Insufficient space is available for installing the necessary ducting aft of the wing spar in the Caribou. Spaces in the tail surfaces are even more restricted.
6. Noise levels generated by the supersonic jet stream from the primary motor would be a serious problem from the standpoint of crew comfort as well as from that of structural fatigue.
7. Since the performance of the jet pumps is strongly affected by the external flow conditions at the suction and blowing slots, large-scale wind tunnel tests would be necessary to examine the mutual interrelationships.
8. Consideration of the 1600°F temperature of the primary motors would require careful design and would result in weight penalties to protect against fire damage or heat damage.
9. Time required to recharge the compressed air tanks is restricted by the power available from engine accessory pads. Based on the 1.5 pounds per second maximum flow rate mentioned in the contract for 1-1/2 minutes of operation and on the torque available at the accessory pad, the recharge time would be 45 minutes.

### RECOMMENDATIONS

No further work directed toward development of the proposed jet pump augmented lift BLC system for the YCV-2B Caribou aircraft is recommended.

## DESCRIPTION OF THE SYSTEM CONCEPT

Increased lift coefficients have been obtained on wing/flap arrangements for aircraft when boundary layer control has been used to prevent separation. Two familiar methods of obtaining boundary layer control are (1) by blowing air over the top of the flap and (2) by sucking air at the flap hinge line. The proposed BLC system contemplated use of these two methods in combination. Figures 1 and 2 show the general cross-sectional arrangement of the airfoils, ducts, and slots and flaps for the suction and blowing airfoils.

Figure 3 shows schematically how the air sucked in at one location would also be blown out over another section of the flap. The air is moved through the connecting ducts by means of jet pumps (Figure 4). This system is more fully described by Reference 1. Stored compressed air (replenished by compressors driven by power from main engines) and aircraft fuel supplies the energy to drive the jet pumps. The compressed air tank charge-up occurs during ground run-up or in cruise flight. These are periods when maximum engine power is not being demanded for flight.

The total system concept is shown in Figure 5. A typical arrangement of blowing and sucking sections of the wing, including the overlapping feature of the individual duct system, is shown in Figure 6. Figure 7 shows a breakdown of the major components comprising one of the individual duct systems. Note that the total Caribou BLC system included fifteen assemblies consisting of the jet pump and blowing and sucking ducts, six in each semi-span of the wing, two in the horizontal tail, and one in the vertical fin.

## PRELIMINARY STUDIES

As a part of the work leading up to the submittal of the proposal, the Contractor had carried out preliminary studies and analyses of the system. This work had indicated that the BLC installation would, if successful, reduce take-off and landing distances for the Caribou by about half (Reference 3). Studies had considered the effect of the BLC on lift and drag on cruise performance, and on low-speed flying qualities; they also had included cursory investigations of probable sizing for system components. Some work had been done in the preliminary bench test of the primary jet motors. The Contractor also had

conducted a study on high lift boundary layer control for the Navy, under Contract Nonr 3194(00), which included small scale wind tunnel testing at California Polytechnic College in Pomona, California.

Work had reached a point where further progress required investigation of the concept applied to an actual aircraft, with testing to substantiate the theoretical analysis. The feasibility proposal was then submitted.

#### INTERDEPENDENCY OF SYSTEM COMPONENTS

Interdependencies of various portions of the system presented one of the most difficult problems. For example, the choice of an optimum spanwise distribution of the several blowing and sucking slots depended on balancing the effects of unequal lift contributions from sucking and blowing against the necessity for total blowing airflow, to equal total sucking flow plus the flow introduced by the primary motors. The sizes of the several primary motors, in turn, were dictated by the size and configuration of the duct in which each was to be installed. A more thorough treatment of the theoretical development of boundary layer jet pumps is given in Appendix I, page 59.

As another example, the flap chord to wing chord relationship is affected by the desirability of an elliptical spanwise lift distribution, which again influenced slot widths and jet pump sizes.

A truly optimized system would require simultaneous solutions for all of the variations of aircraft gross weight, engine horsepower, propeller characteristics, thrust, slipstream effects, ground effects, aircraft velocity, angle of attack, airfoil characteristics, flap dimensions, flap deflection angles, distribution of flaps between blowing and sucking types, blowing and sucking slot lengths and widths, primary jet pump power required, and compressed air and fuel flow quantities to the primary motors.

However, the most basic requirement, and one for which the least valid test data were available, was improvement in the performance of the jet pumps. The jet pumps depend, for their proper functioning, on a good primary motor and on efficient mixing. This central requirement was recognized by both Customer and Contractor and therefore dictated the decision to initiate work in the area at the onset of the program.

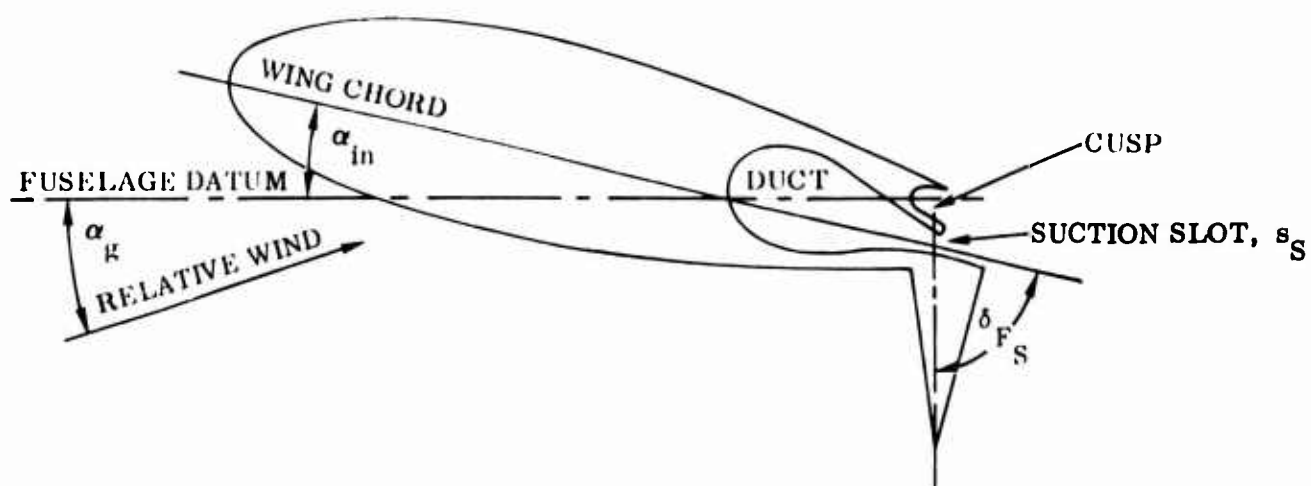


Figure 1. Airfoil Shown With Suction Slot

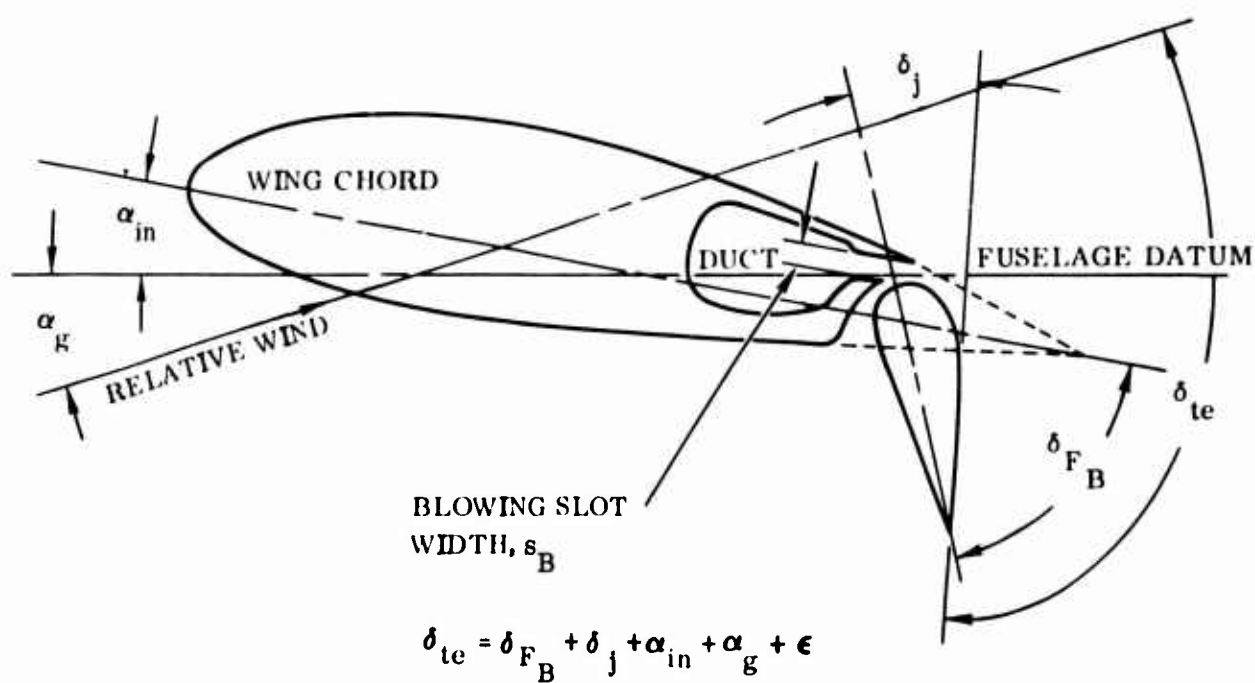


Figure 2. Airfoil Shown With Blowing Slot



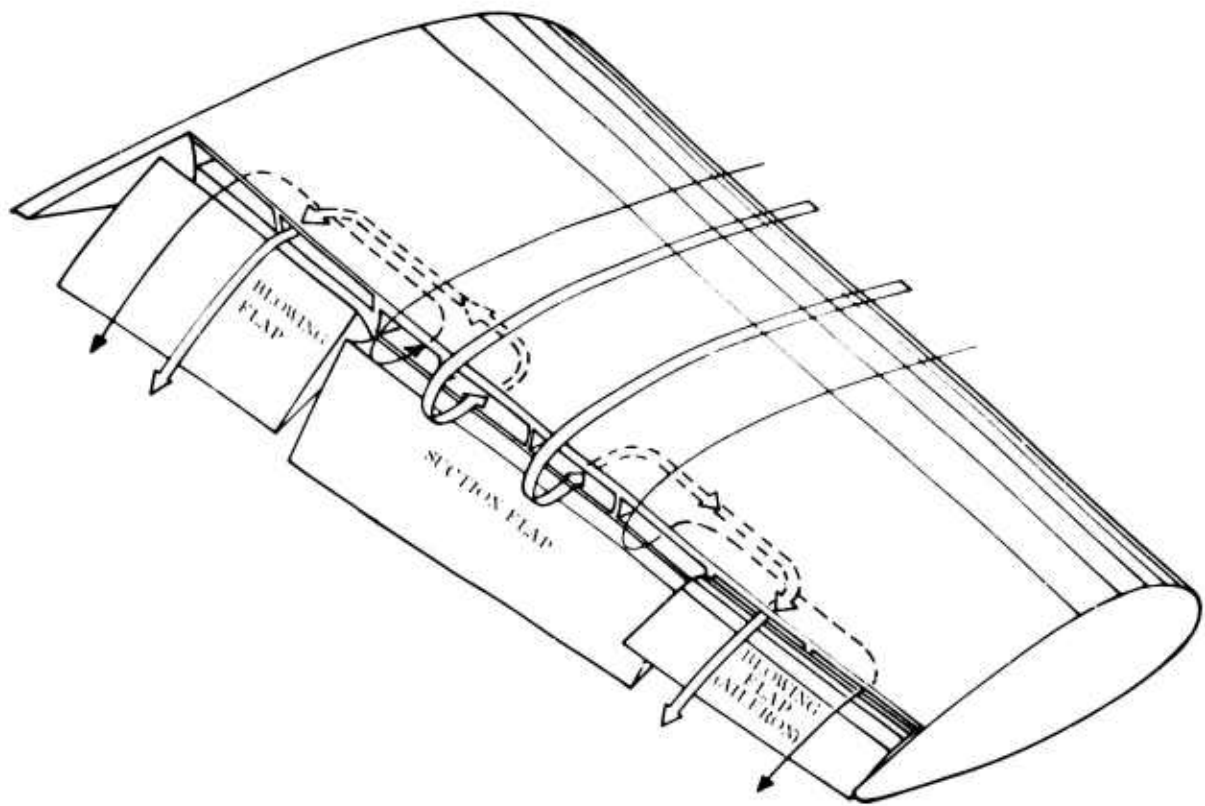
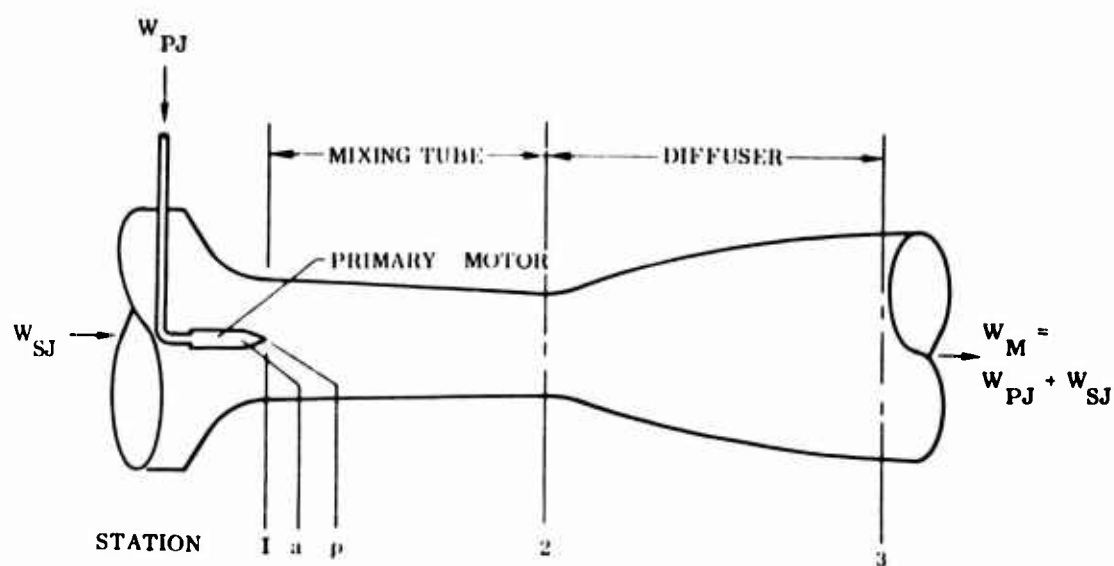


Figure 3. Conceptual Schematic of the Multiple Cell Boundary Layer Control



$$\alpha_v = \frac{v_{SJ}}{v_{PJ}}$$

$$\phi = \frac{A_{PJ}}{A_{SJ}}$$

$$W_{PJ} + W_{SJ} = W_M$$

$$m = \frac{W_{SJ}}{W_{PJ}} = \frac{\rho_{SJ} A_{SJ} v_{SJ}}{\rho_{PJ} A_{PJ} v_{PJ}} = \frac{\rho_{SJ} \alpha_v}{\rho_{PJ} \phi}$$

$$n = \frac{W_M \left( \frac{P_{tM}}{\rho_M} - \frac{P_{tSJ}}{\rho_{SJ}} \right)}{W_{PJ} g J \Delta h_{a-p}}$$

$\Delta h_{a-p}$  = ENTHALPY DROP THROUGH THE PRIMARY NOZZLE

$P_t$  = TOTAL PRESSURE

Figure 4. Schematic Drawing of Jet Pump

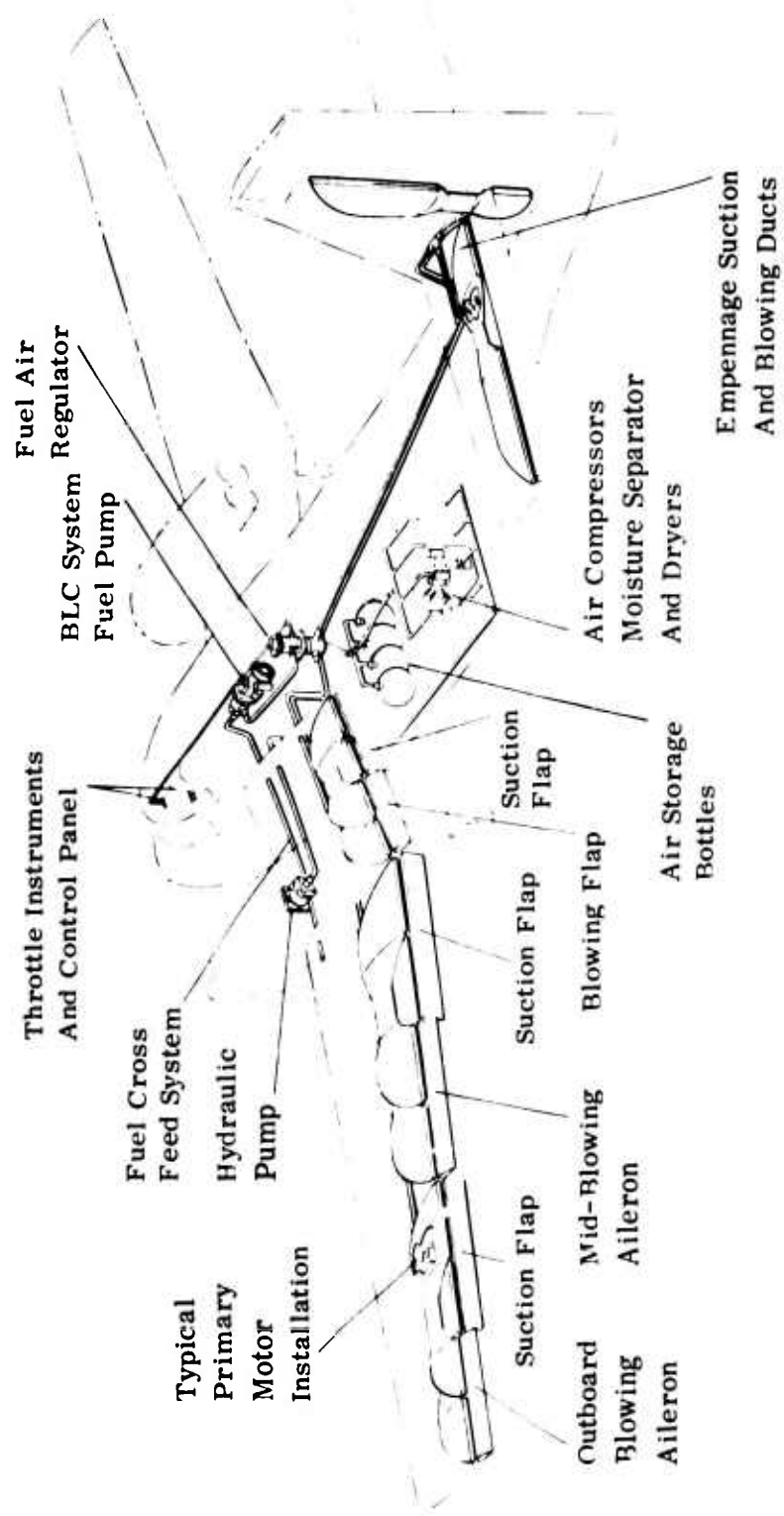


Figure 5. Schematic Drawing of the BLC System as Installed in the YCV-2B Caribou

BLC APPLICATION TO THE CARIBOU

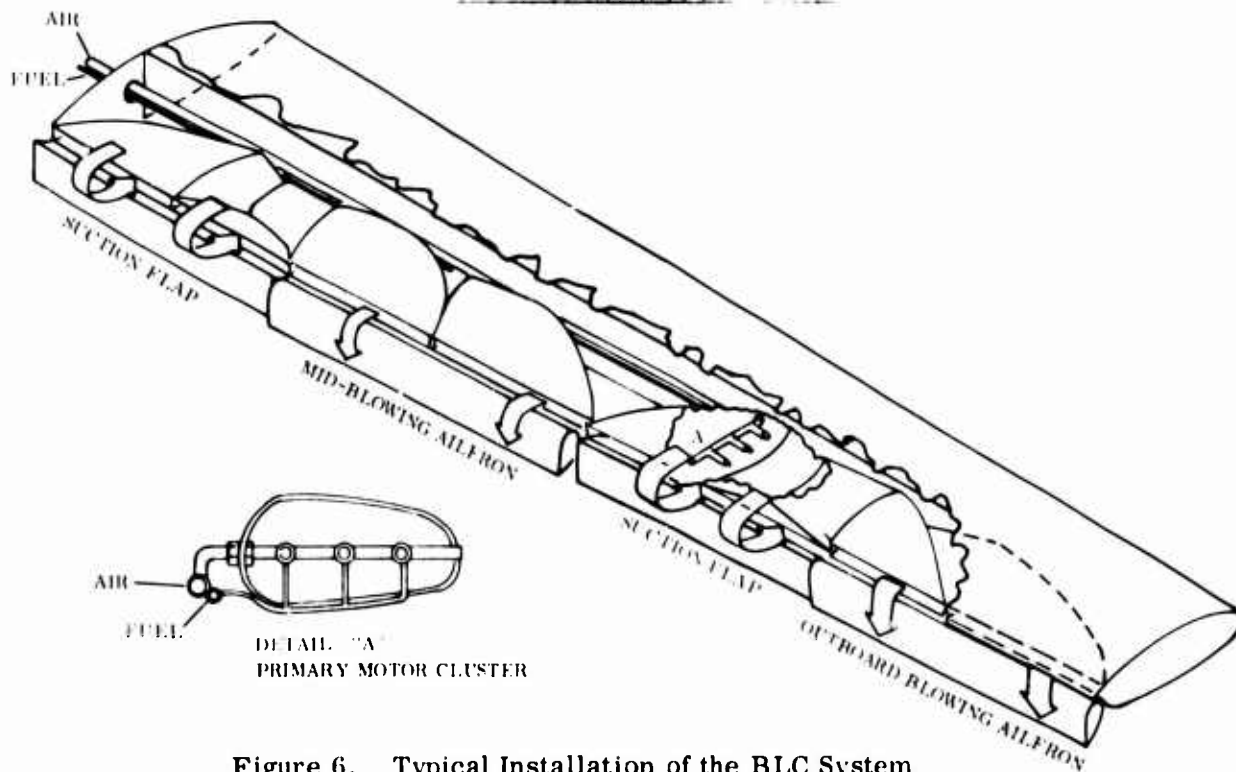


Figure 6. Typical Installation of the BLC System

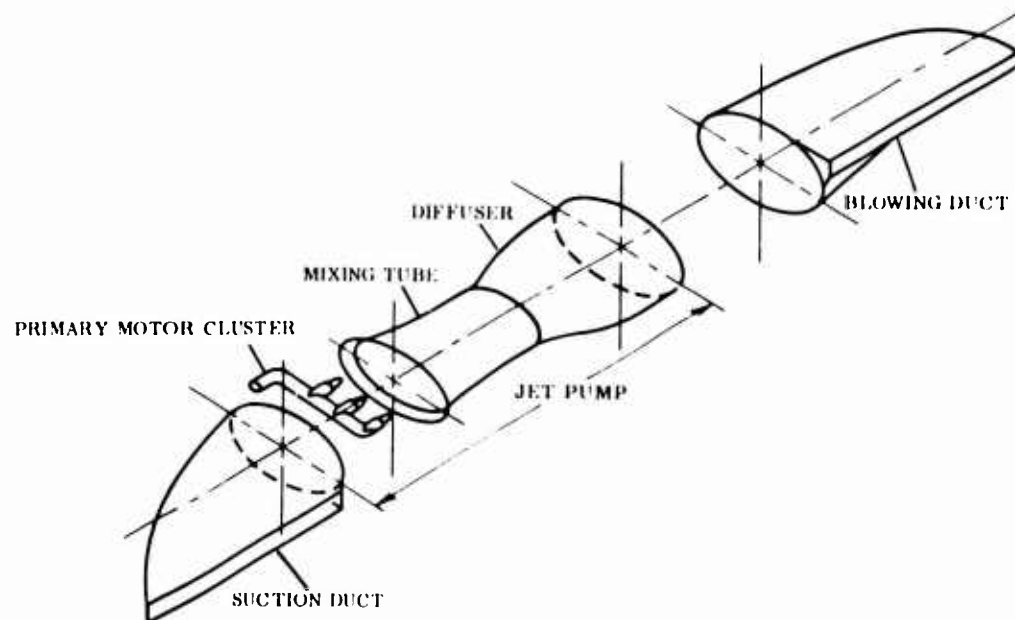


Figure 7. Jet Pump and Ducts

## EXPERIMENTAL PROCEDURE

### INTRODUCTION

Prior analytical work on the BLC system concept had provided some general idea of the order of magnitude of the significant parameters. Based on these data, all areas of work were initiated shortly after receipt of contract. Simultaneous studies were started on aircraft aerodynamics; the internal aerodynamics and thermodynamics of the duct systems; the arrangement and selection of components for the operation and control of the BLC system; the predesign space layout of ducts, flaps, and ailerons for the wing; and the design and fabrication of the bench test setup, on which heavy emphasis was placed.

All of the work on the aircraft and the BLC system was dependent on the results of the bench tests. Therefore, the test work was given first priority. Other studies were carried on with the knowledge that test results might later require adjustment of analyses already under way. This was worthwhile in view of the potential time saving in case the original estimates proved to be accurate.

The inboard duct system was chosen as the representative test unit configuration to be built because (1) it was the largest, (2) the wing had no taper in this area, (3) the slow configurations are simpler for a flap than for ailerons, and (4) available wing space volume was less critical.

After two months' work on the program, it became apparent that the jet pump/duct problems were more complex than anticipated and would require more time and effort than had been allotted in the planning. Consequently, with the full concurrence of the Contracting Officer, program emphasis was changed to put all effort on the jet pumps and to defer other aspects of the study until there was assurance of achieving an adequate jet pump configuration with satisfactory performance. Without such a satisfactory pump, all other work would be purely academic, as far as this particular effort was concerned. The success of the entire concept depended on developing this satisfactory jet pump configuration.

## THE JET PUMPS

In its simplest form, the jet pump is a means of moving a fluid by injecting one high velocity fluid stream into a lower velocity secondary stream. Energy from the primary stream is transferred to the secondary. Jet pumps, historically, have been inefficient, but their appeal lies in their simplicity, reliability, low weight and absence of moving parts. The elements of a jet pump are shown schematically in the preceding Figure 4. Features deemed necessary for a satisfactory jet pump for the BLC system included the following:

1. High velocity primary jet equal to Mach 3 (5370 feet per second) at the exit of the primary motor nozzle.
2. High temperature burning in the primary motor chamber. 3300° Rankine was chosen as a design point which would give a good balance between desirable high temperature burning, fuel/air mixture requirements, and problems of heat containment.
3. Minimum consumption of primary compressed air and of fuel.
4. Minimum internal duct losses.
5. Maximum entrainment ratio.
6. Maximum efficiency.
7. Maximum transfer of energy from the primary to the secondary stream (complete mixing) with uniform flow patterns in cross section.
8. Reliable starting, control, and operation.
9. Ability to be throttled.

The particular application of the jet pumps to the BLC for the Caribou imposed some restrictions which detracted from an idealized configuration. These limitations included:

1. Space available in the wing (aft of the rear spar, forward of the flaps or ailerons, and between the upper and lower wing skins), which was limited, particularly in the outer half of the wing span and in the tail.
2. Parallel locations of the sucking and blowing slots, both of which opened aft, which required turning the airflow through 360° in three bends: one about 180° to enter the suction slot and two about 90° within the jet pump.
3. Mixing tube length and diffuser length, which were limited by available space.
4. Inlet conditions, which were dictated by the required slot shapes and the local airstream.

The development work for the pumps can be considered in two parts: (1) the primary motor and (2) the ducting. Although the work on both proceeded concurrently, it is more convenient to describe them separately.

#### PRIMARY MOTOR

The general configuration of the primary motor is shown in Figure 8, and it is shown schematically in Figure 9. Design criteria for the test pump primary motor were:

Primary air mass flow rate	$W_{PG}$	0.10 lb/sec
Fuel type - aviation gasoline		115/145 octane
Fuel/air ratio	$F$	0.041 to 1
Operating chamber pressure	$P_{cc}$	450 psia
Throttleable to		200 psia
Combustion temperature	$T_{cc}$	3300° Rankine

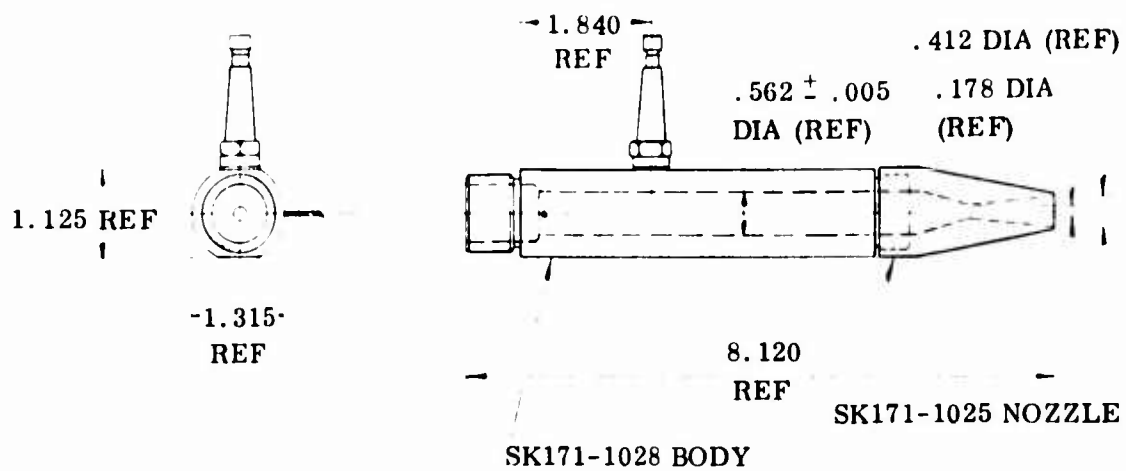


Figure 8. Motor Assembly - Type 1 (Material: Hastelloy X)

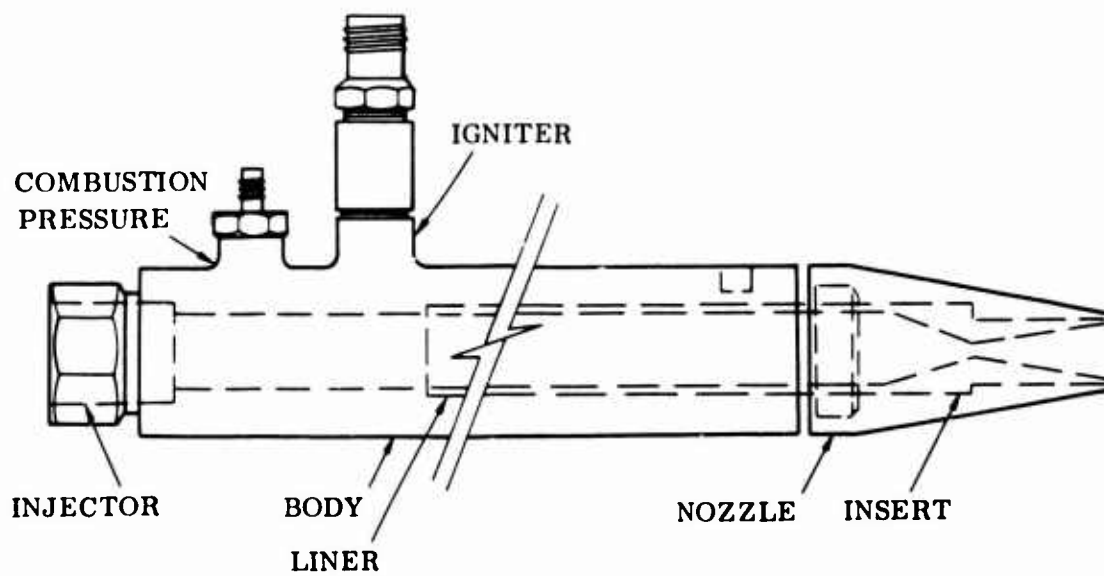


Figure 9. Jet Pump Primary Motor



Exit velocity	$V_{PJ}$	5370 ft/sec (Mach 3.0)
Exit temperature	$T_{PJ}$	1410° Rankine
Jet exit pressure	$P_{PJ}$	11.8 psia
Ignition - high energy electric spark		4.0 Joules @ 2000 volts at 1 cps

Dimensions for the primary motor were developed by using the methods Reference 4. This led to the design shown in Figure 8, which had a burning chamber 6 inches long by .562 inch in diameter. Air was introduced at the upstream end, and the downstream outlet was through a nozzle throat .178 inch in diameter with an exit divergence (included angle) of about 12° and a nozzle exit of .412 inch in diameter. The initial design called for the motor body and nozzle to be made of Hastelloy X material (manufactured by Haynes Stellite Co., Division of Union Carbide, Inc.). The igniter mounting hole was located about one-third of the length of the body from the upstream end. Wall thickness of approximately .38 inch was made somewhat heavier than would be required for later flight articles in order to obtain the advantages of ease of manufacture and flexibility for development changes.

Problems encountered in attaining satisfactory operation of the primary motor can be classified in three general categories:

1. Ignition
2. Mixture of the fuel and air
3. Temperatures

#### IGNITION

Proper ignition required that the motor be capable of immediate light-off at any chamber pressure up to the design operating pressure of 450 pounds per square inch absolute and that the igniter be able to provide an acceptable number of starts without replacement. The ignition system contained the two essential components: the exciter and the igniter. The exciter is an intermediate unit in the ignition system which transforms the low voltage electrical input current into a high energy, high voltage, low frequency current for induction into the

igniter. The igniter is the "spark plug" used to induce the ignition spark into the combustion chamber of the primary motor. Several versions of each were tried over the total period of testing. Best results were obtained with a Model PWA 364379-A exciter made by General Laboratories Associates, Inc., with type FHE-159-2 igniters made by Champion, and types YD-62X and YX-62X igniters made by AC Spark Plug Co. The exciter appeared to be satisfactory, but the igniters, which were designed for jet engine applications did not withstand the chamber temperatures. The electrode tips would turn off after one or two runs of 1 minute duration. No satisfactory igniter was found available during the period of experimental procedure.

#### MIXTURE OF FUEL AND AIR

Proper mixture of the fuel and air was very important for proper ignition and for sustained burning at a uniform rate at an acceptable temperature. First efforts were to operate at a fuel/air mass ratio of .041 to 1. However, it was found that the low temperature (about 40°F) of the incoming air required increasing the ratio to about .05 to 1. This incoming air was cool as a result of having been expanded from the storage containers. Motor designs capable of passing the cold incoming air around the burning chamber were conceived, but they would be expensive and were deemed to be beyond the intent of the contract. One of the advantages of the latter configuration is as follows: heating the air would provide cooling of the motor walls and also would increase the temperature of the fuel/air mixture prior to burning, and thereby would reduce the required fuel/air ratio and consequently reduce the burning temperature.

Many variations of fuel injection orifices were tried in the effort to assure that fuel and air were properly mixed and that fuel droplet size was small enough to result in complete burning. Spray patterns provided by small drilled holes and by various sizes and orientations of hypodermic needles were tested, but no definite trend of results indicated a preference for one arrangement over any other. The most beneficial technique consisted of providing a small mixing chamber immediately upstream of the burning chamber, into which the fuel and air were introduced and mixed in a highly turbulent area. The fuel/air mixture thus was rapidly expanded on entering the combustion chamber. The combination of some premixing followed by rapid expansion seemed to give the desired and necessary conditions of mixing and fuel particle size. Another concept tested was that of lengthening the burning chamber. Figure 10 shows such a device. The longer chamber did result in better performance which was indicated by easier starting and smoother operation.

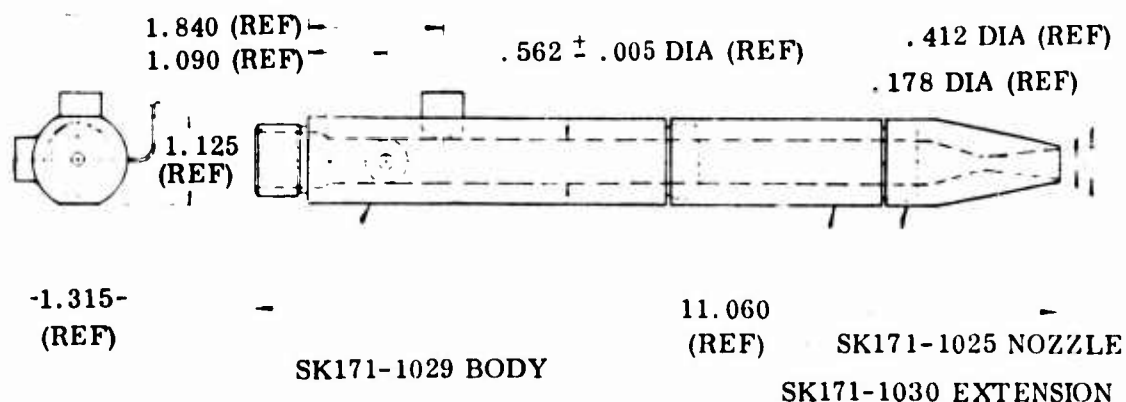


Figure 10. Primary Motor (Material: Hastelloy X)

#### TEMPERATURES

Temperatures presented the usual problem of compromise between the desire for higher thermodynamic efficiencies and for temperatures which can be tolerated by available materials. Several innovations were applied in the effort to contain or withstand the hot gases properly. The most successful innovations were to use zirconium oxide or titanium liners for the burning chamber and to use titanium metal or a Bendix proprietary material, "Chrome 30", for inserts in the nozzle throat. Less success was obtained from a sintered tungsten nozzle throat insert, which eroded excessively when operated for only 4 minutes. (Results on the tungsten insert were inconclusive, since only one unit was tested, and better endurance should be expected at the temperatures involved.) A zirconium oxide insert proved to be too brittle for the nozzle throat application. It rapidly cracked and crumbled owing to the combined effects of thermal shock and severe high frequency noise.

Burning chamber liners of zirconium oxide were marginally successful and gave considerable thermal protection for the motor walls (wall temperatures were reduced about 400°F when the zirconia insert was used), but the thermal shock and mechanical vibration resulted in rapid cracking, followed later by crumbling and erosion of the material. On the other hand, the titanium inserts showed no visible deterioration after more than 110 minutes of operation.

While no satisfactory solution was found to the problem of designing a primary motor to meet the desired criteria, sufficient operating time was obtained in small increments to permit exploration of the type of jet pump which was the primary goal of the program. This pump is described in the following paragraphs.

### JET PUMP DUCTING

The duct system chosen for test was one representative of the left hand inboard group (Figure 11). The major components of the system in the direction of flow of the airstream were:

1. A simulated suction inlet with a rectangular opening which faces aft.
2. A transition section whose converging cross section changes from a rectangle matching the inlet slot to a circle.

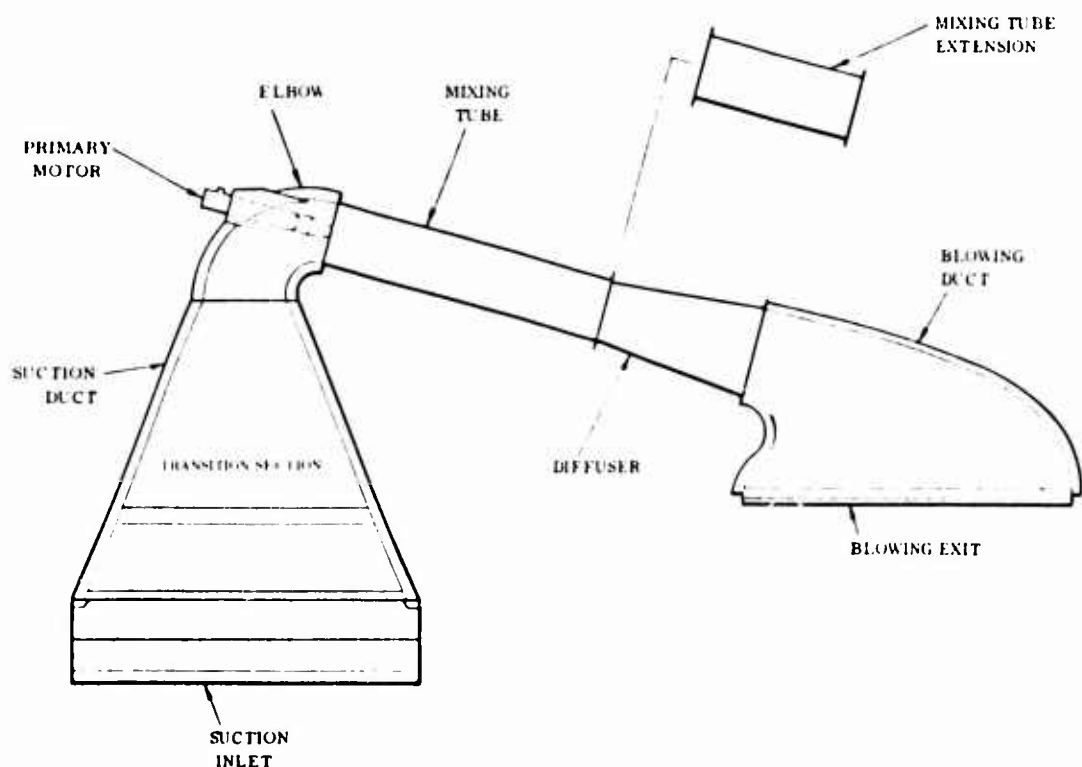


Figure 11. Duct System

3. A converging 105° elbow with a circular cross section as measured normal to the elbow centerline.
4. A right cylindrical mixing tube having a length to diameter ratio of 5-1/4 to 1.
5. A right circular conical diffuser with an included diffusion angle of 11°.
6. An exit turning segment of the blowing duct whose cross section changes through a 75° angle from a circle matching the diffuser outlet to a rectangle matching the outlet slot (the cross sectional area of the exit/turning segment, as measured normal to the predicted centerline of airflow, which increases linearly with length along the centerline).
7. A rectangular simulated blowing exit.

As shown in Figure 11, a mixing tube extension was designed which could be inserted between the mixing tube and the diffuser. The extension had a length to diameter ratio of 2-3/4 to 1, which, when installed, was a mixing chamber with an overall ratio of 8 to 1.

Preliminary estimates had indicated that the following design values should be used:

- |                   |                                      |  |
|-------------------|--------------------------------------|--|
| $C_{Q_S}$         | = 0.052                              | - Suction air volume flow coefficient                  |
| $C_{Q_B}$         | = $(1 + \frac{1}{m}) C_{Q_S} = .053$ | - Blowing air volume flow coefficient                  |
| $C_\mu$           | = 0.35                               | - Blowing air momentum coefficient                     |
| $\frac{V_J}{V_o}$ | = 3.3                                | - Velocity ratio of the blowing air to the free stream |
| $V_J$             | = 191.5 ft/sec                       | - Velocity of the blowing air                          |

$V_o$	$= 58.0 \text{ ft/sec}$	- Free stream velocity (= to the aircraft forward speed)
$m$	$= \frac{W_{SJ}}{W_{PJ}} = 70.0$	- Entrainment ratio
$W_S$	$= 7.0 \text{ lb/sec}$	- Suction air weight flow
$W_{PJ}$	$= 0.10 \text{ lb/sec}$	- Primary jet motor hot gas weight flow
$W_B$	$= W_{SJ} + W_{PJ} = 7.1 \text{ lb/sec}$	= Blowing air weight flow
$(s/c)_S$	$= 0.01957$	- Ratio of suction slot width to wing chord
$(s/c)_B$	$= 0.0171$	- Ratio of blowing slot width to wing chord
$A_E$	$= (s/c)_S \times \frac{S_S}{4} = 0.596 \text{ ft}^2$	- Area of the entrance (suction) slot
$A_M$	$= \frac{\pi}{4} D_M^2 = 0.148 \text{ ft}^2$	- Mixing tube (constant area) cross sectional area
$A_{Di_B}$	$= 0.35 \text{ ft}^2$	- Diffuser exit area (= blowing duct inlet area)
$A_{Si_B}$	$= (s/c)_B \times \frac{S_B}{4} = 0.521 \text{ ft}^2$	- Area of the exit (blowing) slot
$\frac{S_S}{S_B}$	$= 1.0$	- Ratio of the areas of the segments of the wing affected by the suction and blowing BLC

$$S_S = S_B = 121.8 \text{ ft}^2$$

- Reference areas of the wing segments related to the particular suction and blowing slots, respectively. The area is equal to the chord times the span of the related slot.

Using the above design values, the test duct was developed and fabricated. Portions of the system which involved compound curves were made from glass fiber reinforced plastic. These were the inlet transition section, the converging 105° elbow and the diverging exit turning segment. They were formed on plaster molds and oven cured. The plaster forms and method of lay up of the glass fiber are shown in Figures 12 through 15.

Entrance and exit slots were fabricated from aluminum bar stock, shaped to simulate the configuration as it would appear in the aircraft. The mixer chamber and the chamber extension were made from aluminum tube, machined inside to give a true and smooth surface. The diffuser was made from aluminum sheet rolled to form the desired cone. Aluminum flanges were welded to the ends of the mixer tube, extension, and diffuser. Later, an additional diffuser section was made of molded, glass fiber reinforced plastic (Figure 16). The new diffuser used the same inlet and outlet end dimensions but was longer (11-1/2 inches) and employed a smaller diffusion angle (7° instead of 11°). The new diffuser also incorporated a gradual, faired transition from the mixing section to the diffusion angle. This configuration was developed in an effort to reduce flow separation which had been observed at the walls of the diffuser.

The complete assembly of the test duct system is shown in Figure 17.

To support the tests of airflow measurement, a bellmouth inlet was made from glass fiber reinforced plastic. It was designed to fit at the inlet to the mixing chamber. The final article is seen in Figure 18.

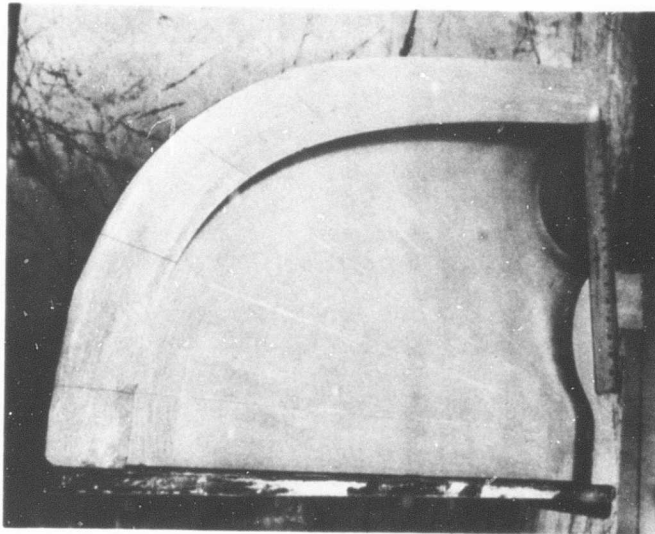


Figure 12. Plaster Mold for Suction Duct

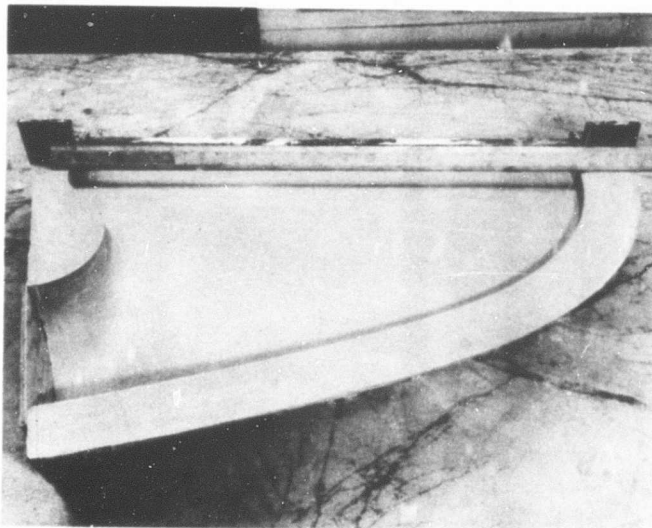


Figure 13. Plaster Mold for Blowing Duct



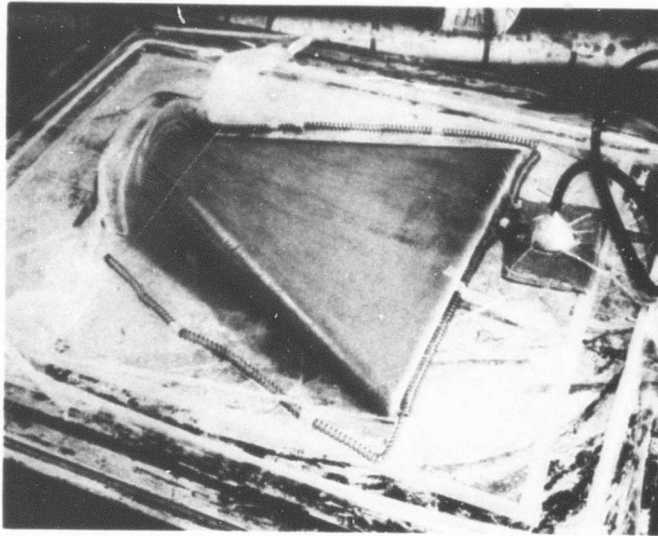


Figure 14. Plaster Mold for Elbow

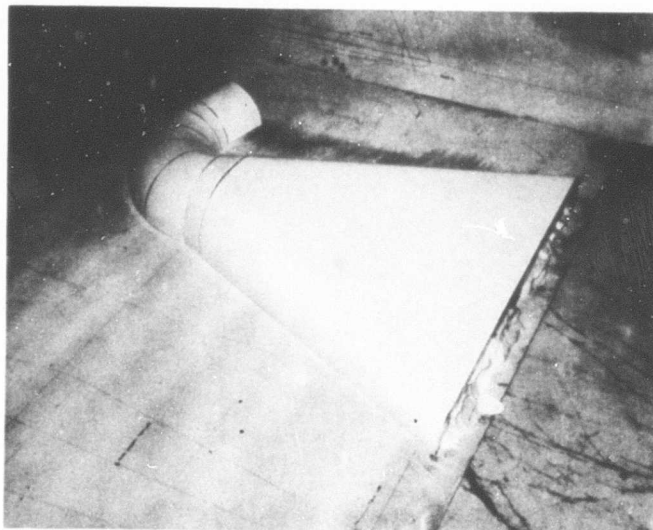


Figure 15. Plaster Forming Mold for Duct

Figure 16. Diffuser With  $7^\circ$  Angle

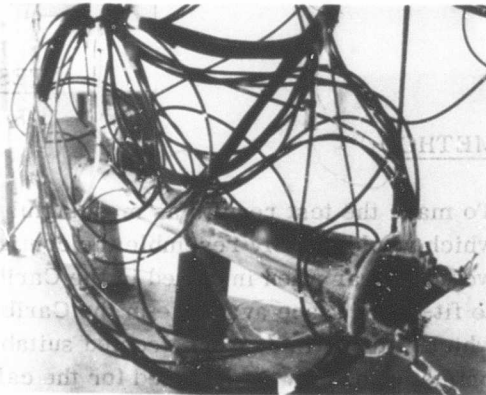


Figure 17. Assembly of Test Duct

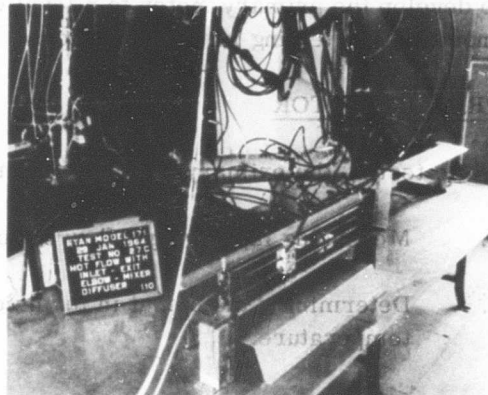
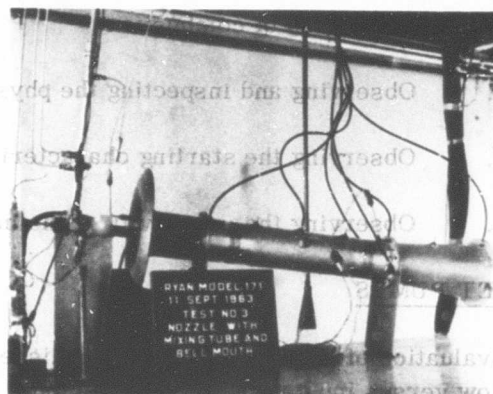


Figure 18. View of Bellmouth



## TESTS

### METHOD

To make the test results as meaningful as possible, a test setup was planned which would closely resemble the configuration of one of the duct systems as it would appear when installed in the Caribou aircraft. The duct system was made to fit in the space available in the Caribou wing and was fabricated of materials which, at the time, were deemed suitable for the aircraft installation. The primary nozzle was designed for the calculated required primary air jet mass flow, velocity, and temperature. Work was scheduled so that the primary motor would be available to drive the jet pumps. Initial testing was therefore planned to develop the primary motor to a level where it would give sufficient performance to allow testing in the jet pumps.

### PRIMARY MOTOR

While testing the primary motor, the performance was evaluated by:

1. Measuring input weight flow of compressed air and fuel.
2. Determining the output in terms of exit gas weight flow, velocity and temperature.
3. Measuring temperatures of incoming air, combustion chamber, and metal parts of the motor.
4. Steadiness of combustion.
5. Observing and inspecting the physical durability of the components.
6. Observing the starting characteristics.
7. Observing the sensitivity of the motor to changes in input conditions.

### JET PUMPS

Evaluation of jet pumps was accomplished in terms of total output air weight flow versus inputs to the primary motor. One series of tests was run using

the primary motor merely as a nozzle to direct a stream of unheated air. Such tests are referred to hereafter as "cold flow" tests. Cold flow tests served to establish a criterion relative to the use of hot gas jets. The purpose of this criterion was to establish a base from which to determine the gains achieved when hot gases are used. For future reference, it was also necessary to know what decrement in pumping would occur in an aircraft installation, if a primary motor should fail to burn for any reason.

The cold flow tests were simpler to conduct than hot tests and presented the opportunity to optimize the test setup under conditions which were simpler to control and to duplicate.

To evaluate losses in the jet pump, the various segments were tested in differing combinations. Figure 19 shows the components which were installed for each test run.

Weight flow characteristics were determined in terms of temperatures and pressures. Velocities were determined by two methods. One was based on static pressures and the other on total heads.

Methods used were conventional, consisting of pressure probes, gages, manometers, and thermocouples. A description of the instrumentation used is given in the following section.

A schematic drawing of the test setup is shown in Figure 20. Figure 21 is a diagram showing the locations of the pressure probes. The actual test setup is shown photographically in Figure 22.

The test arrangement included:

1. An air supply consisting of groups of 12 tanks, each at a pressure of 2500 psig. Manifolds and shut-off valves were also supplied for these tanks.
2. Air pressure regulators which reduced the 2500 psig to 700 psig.
3. An operator's air pressure regulating valve which served as a throttle.



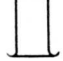
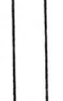
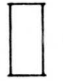



TEST RUN NUMBER	NOZZLE		SUCTON DUCT 	ELBOW 	BELLMOUTH 	MIXING TUBE 	EXTENSION 	11" DIFFUSER 	7" DIFFUSER 	BLOWING DUCT 
	COLD	HOT								
1 thru 7		X								
8	X				X	X		X		
9	X				X	X				
10	X				X	X	X			
11	X				X	X	X			
12	X				X	X	X			
13	X		X	X		X		X		X
14	X		X	X		X		X		X
15	X		X	X		X		X		
16	X			X		X				
17			(TEST VOIDED - NO DATA)							
18		X			X	X				
19		X			X	X				
20		X	X	X		X		X		
21 & 22			(TESTS VOIDED - NO DATA)							
23		X			X	X		X		
24		X		X		X		X		
25		X	X	X		X		X		
26		X	X	X		X		X		
27		X	X	X		X		X		X
29		X			X	X		X		X
30		X			X	X		X		X
31		X	X	X		X		X		X
32		X	X	X		X		X		X
33		X	X	X		X		X		X
34		X			X	X	X			
35		X			X	X			X	
36		X			X	X				

Figure 19. Configurations Tested



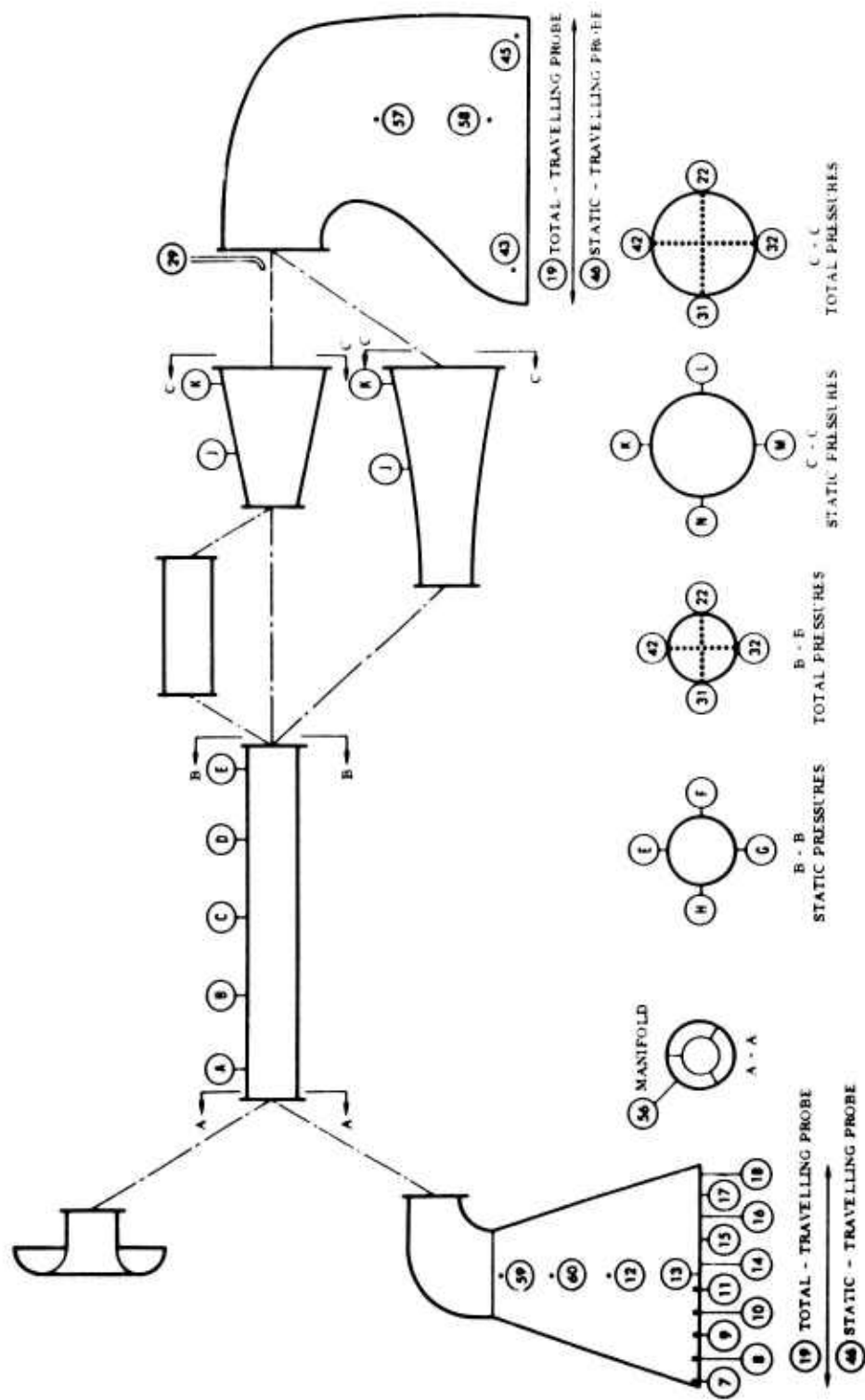


Figure 21. Schematic Drawing of Pressure Probe Location

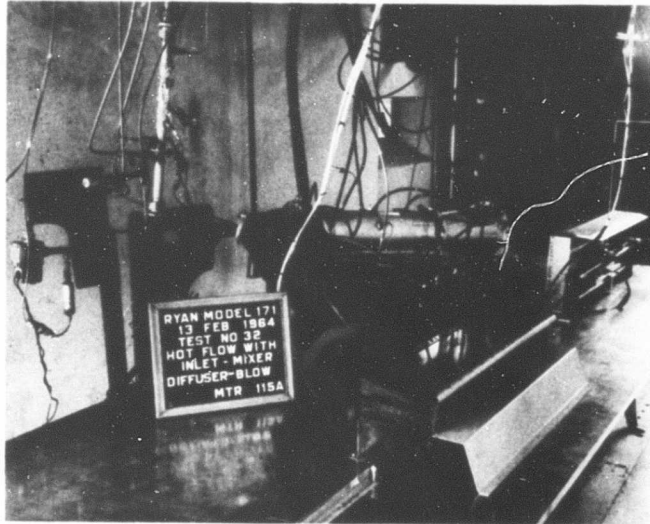


Figure 22. Final Arrangement for Cold Flow Tests

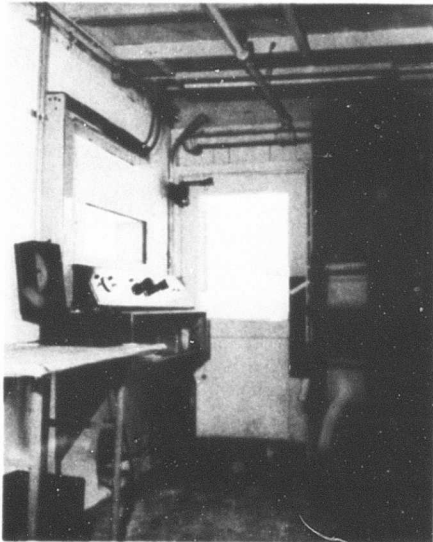


Figure 23. Operator's Control Panel

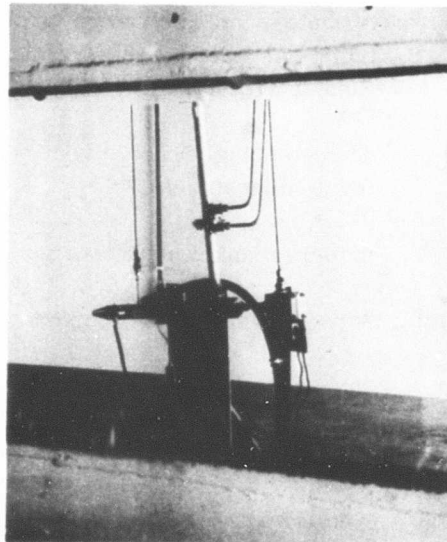


Figure 24. View of Primary Motor During Test



4. A solenoid-operated off-on air flow control valve.
5. A calibrated air-metering orifice.
6. Plumbing to connect the air supply to the valves, regulators, and orifice.
7. A calibrated glass fuel supply container.
8. An electric motor driven fuel pump capable of supplying up to 2 gallons per minute at 1000 psig.
9. A fuel pressure regulator adjusted to give a fuel supply pressure of 500 psig.
10. An operator's fuel flow control valve.
11. An off-on, solenoid-operated fuel valve.
12. Fuel plumbing to interconnect Items 7 through 11 with the test primary motor.
13. A photo-panel instrument group consisting of back lighted manometer tubes, pressure gages, a clock, and an identifying panel of slotted black flannel with white celluloid letters.
14. Two stepping switch direct reading recorders (one for high and one for low temperatures).
15. A four-channel pen recorder.
16. A two-channel pen recorder.
17. Pressure sensing probes.
18. Chromel/Alumel and iron/constantan thermocouples.
19. A 30-volt D.C. power supply to operate the ignition system, with necessary switches and wiring.

20. Noise pressure level measuring equipment.

The entire test setup was designed for the optimum accuracy at the least cost. Shown in Figure 23 is the operator's control panel. Figure 24 shows the primary motor in its test position.

#### DEVELOPMENT OF TESTS

The test program was conducted with an operational philosophy that the program was experimental research. In view of the limited overall budget, the instrumentation and test facility were primarily overhauled Contractor's equipment. However, in most cases, the equipment was satisfactory in performance and accuracy.

During the course of the test program, 36 tests were scheduled with an average of +3 runs per test. The minimum run time considered to be sufficient for data collection was 1 minute, with 4 data points at 15-second intervals. Three tests were cancelled or the data voided because of the erratic behavior of the primary motor. The program was conducted in three phases: (1) development of the primary motor, (2) cold flow jet pump performance test, and (3) hot flow jet pump performance test.

The development of the primary motor reached the experimental prototype stage. The jet pump performance showed that entrainment ratios of 30 could be obtained in cold flow and that hot flows could produce entrainment ratios of 47. These values were obtained, however, with ideal inlet and exit conditions. The data obtained revealed that values of energy generated, mass flows, exit velocities, pressure ratios, and efficiencies are subject to the many variables and are in many cases unpredictable. Figures 25 through 30 show these traits on the most stable conditions achieved during the tests. The data presented in this report are a minor portion of the total data collected and have been selected on a basis of highest quality available. In addition to the performance data of the primary motor and jet pumps, noise level measurements were taken, and the overall level is in excess of 140 decibels.

#### EXPERIMENTAL RESULTS

The experimental analysis of the duct system began with the instrumentation checkout. Nine runs were made using compressed air exhausting through the primary motor as the driving medium. Each of the nine runs was made

with different duct configurations so that the efficiency and instrumentation accuracy could be determined for each. After the motor was developed to a point where reliable data could be obtained, eighteen hot runs were made using the same configurations as in the cold runs.

The cold runs, (see Tables II, III, IV, and V) with compressed air, indicating an improvement of the pumping as the mixing tube length was extended if a diffuser was used. For the cold tests, it was noted that an increase in the mixing tube length without a diffuser had little or no effect on the pumping quantity. Separation of the flow in the diffuser occurred on all tests, and the increased mixing tube length failed to overcome this problem.

General trends obtained from the cold flow data indicate that improvement in pumping can be accomplished either by increasing the mixing tube length with an accompanying diffuser or by decreasing the angle and increasing the length of the diffuser. The entrainment ratios for all of the cold runs indicate an improvement as the primary energy level is decreased. This decrease indicates that an increase in mixing tube length is required for the higher primary jet velocities. The entrainment ratio for a primary flow rate of 0.006 pound per second was .229 with a duct configuration consisting of a bellmouth, mixing tube, tube extensions, and an 11° diffuser. The maximum entrainment ratio for a cold jet occurred at a very low energy level and was found to be 28/1 for the duct configuration of bellmouth, mixing tube, tube extension, and 11° diffuser. The quantity of secondary air pumped showed an exponentially decaying increase as the primary energy was increased with a shift upward in the general trend as the effective mixing length was increased. These curves indicate that at some energy level, the quantity of induced flow will not increase with an increase in primary jet energy unless duct geometry is altered.

A total of 18 hot runs was made (see Tables I, VI, VII, VIII, and IX) and the primary combustion gases were used as the driving source. In a few of the hot runs, test runs numbers 22 through 28, it was found upon reduction of data that incomplete combustion had occurred so that the data could not be directly related to the other tests. The difficulty in correlating these data was due to the difficulty in determining the actual quantity of fuel burned and, in turn, the resulting primary jet energy. The cause of the incomplete combustion resulted from the injected fuel pattern. The fuel injection was being developed simultaneously with the jet pump tests and was changed on jet pump test run 29.

The hot flow data revealed the same general trends as the cold flow except that equivalent induced flows occurred at a higher primary jet energy level. This higher energy level required for the same induced flow can be primarily attributed to mixing tube length, since the tube length is a function of the primary jet velocity. When the cold and hot jet velocities were compared, it was found that the hot jet was approximately three times that of the cold for the same primary flow energy level. This increase in velocity and accompanying decrease in mixing were revealed in the total pressure profile at the exit. The profile of the hot jet tests showed a much higher velocity core, which indicated that a considerable portion of the primary jet was not mixed.

By increasing the mixing tube length and by using the 11° diffuser, the hot jet produced a 5-percent increase in secondary weight flow. The flow separation in the diffuser was noted on all of the runs. After reexamining the flow in the mixing tube, it was decided that, to prevent diffuser separation, the diffuser angle would have to be reduced. A diffuser with a diverging angle of 4° was decided upon. The diffuser was then tested and was found to give an improvement in the velocity profile; separation was prevented at the higher flows even though the primary jet was misaligned. This diffuser showed higher secondary flow for any given primary energy level when compared with the 11° diffuser and mixing tube extension.

The entrainment ratio for the design point of 0.100 pound per second total primary flow was 32.5 to 1 when a bellmouth mixing tube and 4° diffuser were used. The maximum induced flow occurred with the same duct configuration and was 3.5 pounds per second for a primary flow of 0.10. This flow rate of 3.5 pounds per second with the new diffuser and without the tube extension gave approximately a 6-percent increase over the 11° diffuser with the mixing tube extension.

Through use of computer programs, several correlations were made of all data points. The data were compared with theoretical or predicted values as well as with other test data.

TABLE I							
SUMMARY OF PRIMARY MOTOR PERFORMANCE							
RUN NO	TIME SEC	$W_a$ LB/SEC	$W_f$ LB/SEC	$T_{cc_a}$ °R	$T_{PJ}$ °R	$V_{PJ}$ FT/SEC	$P_{PJ}$ PSI
18	160	.0864	.0048	3761	1622	5711	10.92
34	60	.0555	.0039	4348	1850	6172	6.50
34A	60	.0986	.0058	3885	1653	5834	10.42
34B	150	.0986	.0059	3950	1681	5883	10.42
34C	165	.1516	.0046	2501	1064	4681	12.09
35	75	.0650	.0046	4332	1843	6160	7.34
35A	75	.0650	.0045	4313	1835	6147	7.35
35B	105	.0956	.0069	4403	1873	6211	10.86
36	75	.0607	.0038	4066	1730	5969	7.00
36A	60	.0506	.0013	2288	973	4477	5.85
36B	75	.1016	.0066	4133	1759	6017	11.91
36C	60	.0939	.0041	3207	1364	5301	9.66
AVERAGE FOR 12 RUNS							
Avg.	93.3	.0853	.0047	3766	1437	5711	9.19

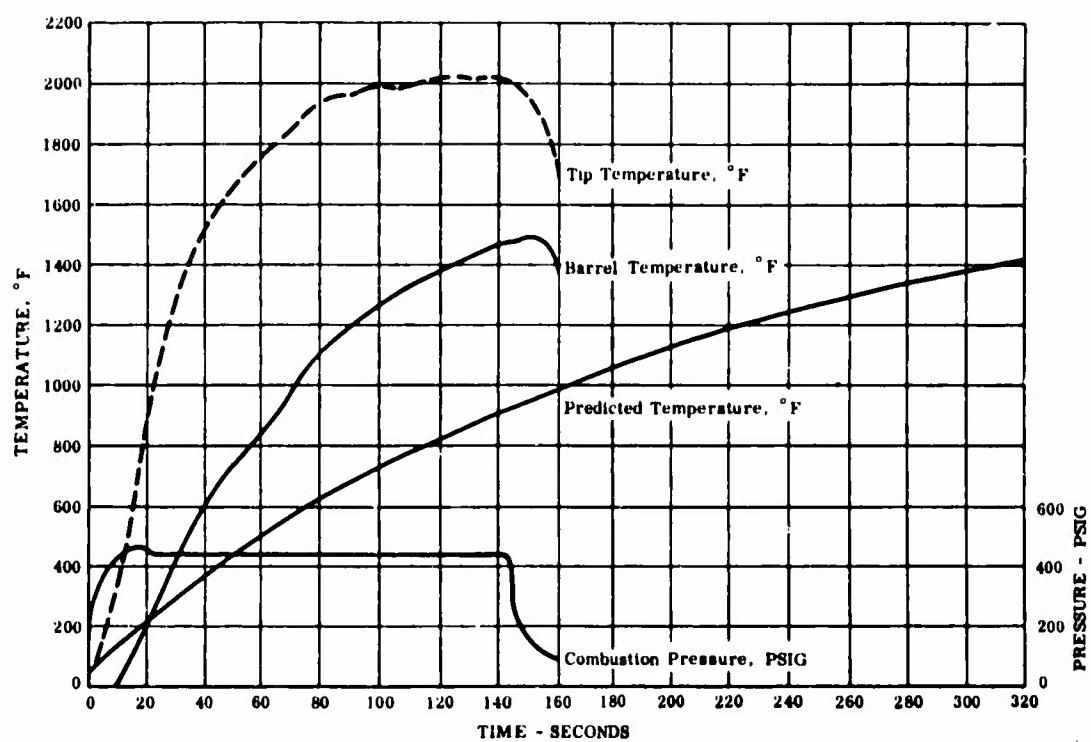


Figure 25. Primary Motor Performance - Run 18

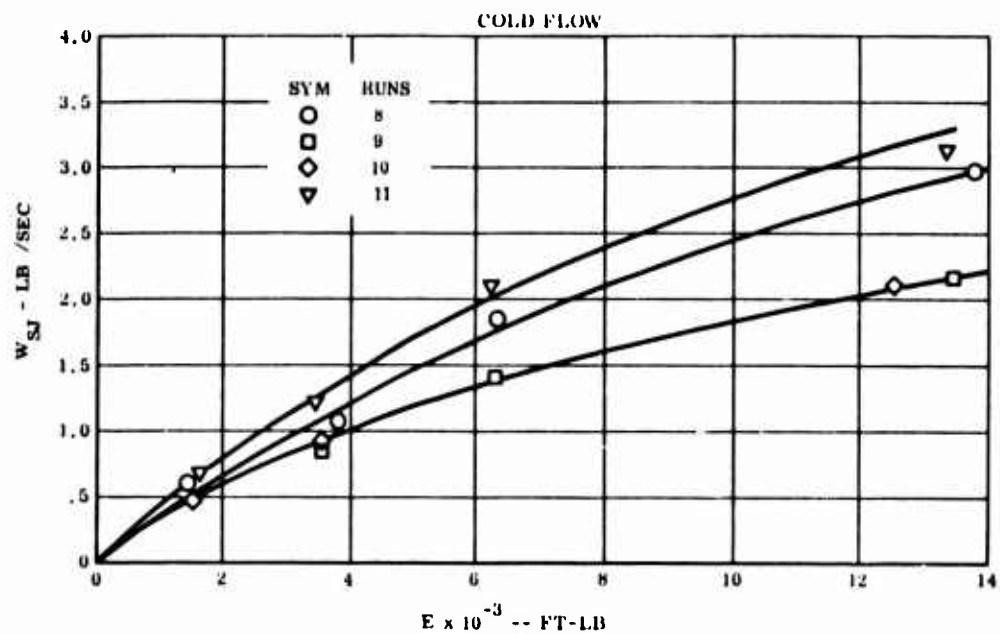


Figure 26. Kinetic Energy Values - Cold Flow

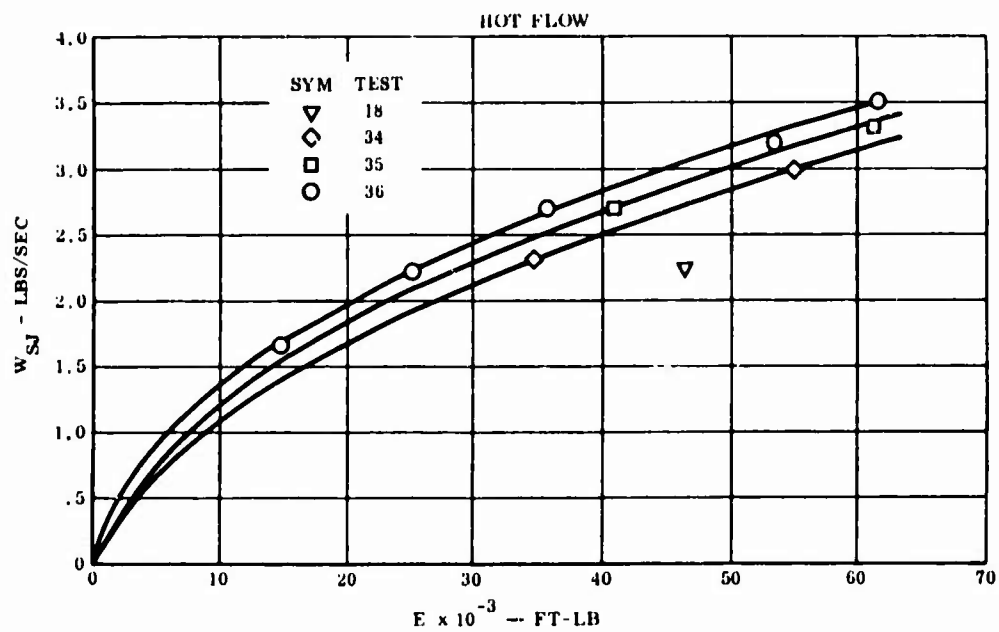


Figure 27. Kinetic Energy Values - Hot Flow

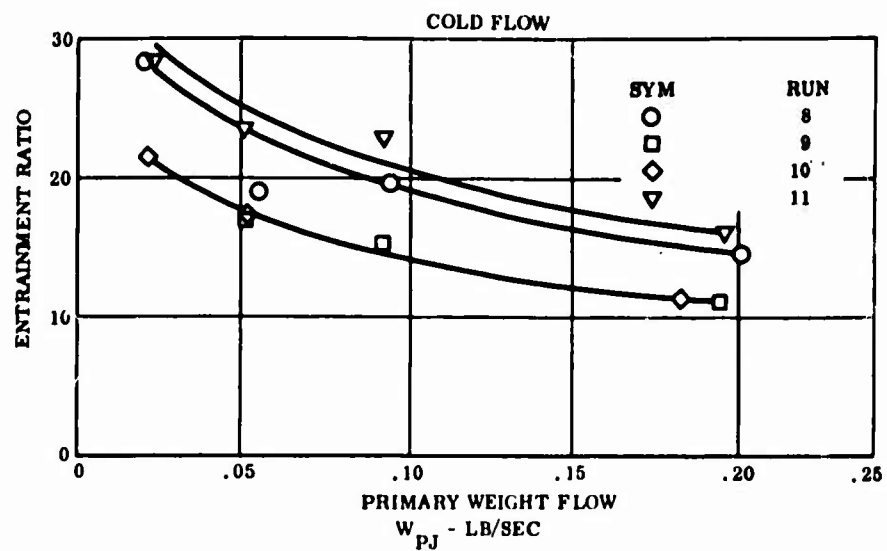


Figure 28. Entrainment Ratio Versus Primary Weight Flow - Cold Flow

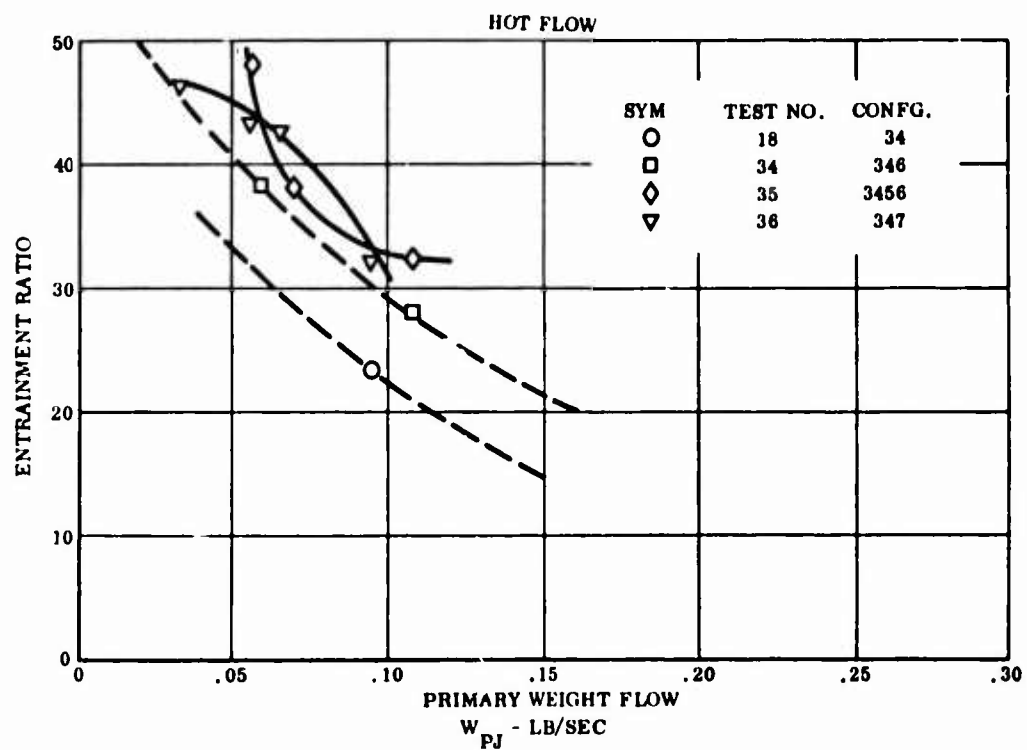


Figure 29. Entrainment Ratio Versus Primary Weight Flow - Hot Flow



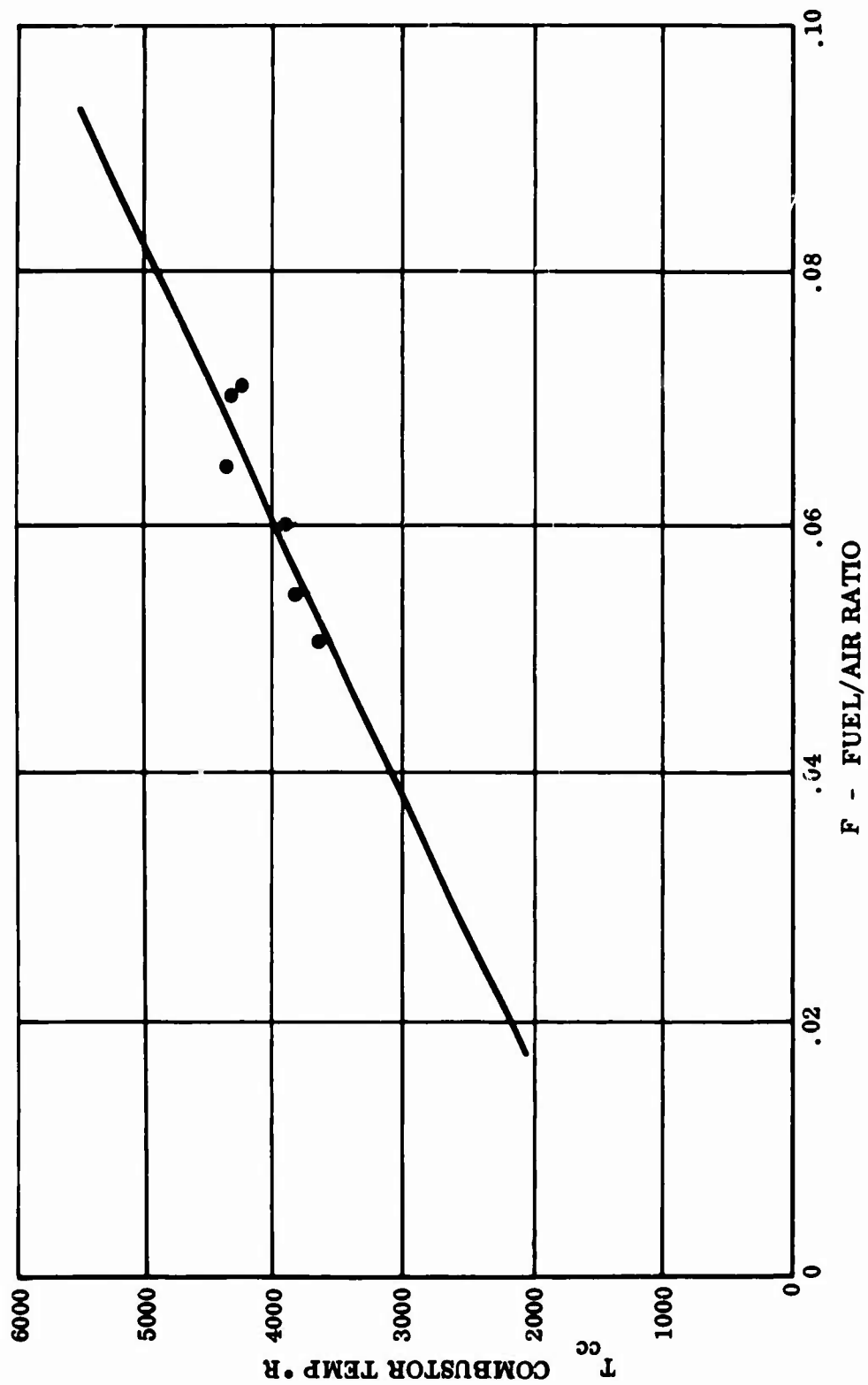


Figure 30. Fuel/Air Ratio Versus Combustor Temperature - Primary Motor

TABLE II  
SUMMARY OF SELECTED DATA - TEST NO. 8

COLD FLOW																			
Configuration Ballmash, Mixing Tube and 11" Diffuser																			
Primary Motor Performance																			
RTN	T SEC	W <sub>0</sub>	W <sub>1</sub>	W <sub>PJ</sub>	F	T <sub>exA</sub>	T <sub>ec</sub>	E <sub>Tec</sub>	DPPT	T <sub>H</sub>	P <sub>PJ</sub>	V <sub>i</sub>	V <sub>PJ</sub>	T <sub>PJ</sub>	T <sub>PJ</sub>	E <sub>T PJ</sub>			
4	60	0.2012	0.	0.2012	0.	546.0	559.3	0.901	28.41	12.33	0.548	979.9	2101.4	214.5	219.6	1.004			
4A	90	0.0942	0.	0.0942	0.	486.0	582.0	0.943	5.79	4.00	2.901	972.1	2004.6	211.1	219.2	1.004			
9B	120	0.0556	0.	0.0556	0.	499.0	456.9	1.002	2.02	1.90	2.135	975.1	2000.9	212.4	197.5	0.999			
Jet Pump Performance																			
RTN	T SEC	A <sub>0</sub>	V <sub>1</sub>	W <sub>PJ</sub>	m <sub>1</sub>	m <sub>2</sub>	E <sub>m</sub>	A <sub>0</sub>	V <sub>0</sub>	W <sub>0</sub>	C <sub>p</sub>	C <sub>0</sub>	C <sub>0</sub>	ρ <sub>m</sub>	V <sub>m</sub>	W <sub>m</sub>	T <sub>m</sub>	P <sub>0</sub>	T <sub>JP</sub>
4	60	0.07290	272.9	2.944	15.632	17.947	0.830	0.07472	94.5	10.10	4.00	0.0230	0.0154	0.07370	162.2	2.782	538.0	14.000	16.29
4A	90	0.07487	164.9	1.947	19.602	24.114	0.811	0.07599	50.2	4.16	4.00	0.0200	0.0097	0.07500	89.6	2.371	535.0	14.003	6.34
9B	120	0.07545	95.4	1.067	19.194	15.285	0.804	0.07607	29.2	0.94	4.00	0.0047	0.0045	0.07503	42.6	1.130	536.0	14.000	1.41

TABLE III  
SUMMARY OF SELECTED DATA - TEST NO. 9

COLD FLOW																			
Configuration Bellmouth, Mixing Tube																			
Primary Motor Performance																			
RUN	T SEC	W <sub>a</sub>	W <sub>f</sub>	W <sub>PJ</sub>	F	T <sub>CC A</sub>	T <sub>CC</sub>	E <sub>T CC</sub>	DPPT	T <sub>R</sub>	P <sub>PJ</sub>	V <sub>i</sub>	V <sub>PJ</sub>	T <sub>PJ</sub>	T <sub>PJ</sub>	E <sub>T PJ</sub>			
60	6.0	0.194*	0.	0.194*	0.	507.1	545.9	0.496	24.75	11.91	9.294	942.9	2107.6	215.8	221.5	1.027			
9A	90	0.0920	0.	0.0920	0.	504.0	571.9	0.441	5.52	4.57	3.932	979.9	2101.4	214.5	222.0	1.035			
9B	120	0.0511	0.	0.0511	0.	506.0	491.2	1.030	1.70	1.46	2.025	941.9	2105.5	215.3	208.2	0.954*			
Jet Pump Performance																			
RUN	T SEC	P <sub>SI</sub>	V <sub>i</sub>	W <sub>SI</sub>	W <sub>j</sub>	m	E <sub>m</sub>	P <sub>B</sub>	V <sub>B</sub>	Q <sub>B</sub>	Q <sub>0</sub>	C <sub>μ</sub>	C <sub>Q S</sub>	P <sub>M</sub>	V <sub>M</sub>	W <sub>M</sub>	T <sub>M</sub>	P <sub>S</sub>	T <sub>JP</sub>
60	6.0	0.0744*	194.1	2.144	11.026	12.031	0.916	0.07421	61.7	4.63	4.00	0.0231	0.0100	0.07622	224.7	2.538	520.0	14.644	17.5*
9A	90	0.07339	125.2	1.403	15.245	16.365	0.937	0.07703	39.2	1.94	4.00	0.0092	0.0064	0.07626	140.6	1.544	520.0	14.631	6.94
9B	120	0.07362	272.4	2.973	24.446	24.494	0.99*	0.0562*	104.1	9.4*	4.00	0.0474	0.0127	0.05594	157.4	3.042	715.3	14.925	14.97

TABLE IV  
SUMMARY OF SELECTED DATA - TEST NO. 10

COLD FLOW																			
Configuration: Bellmouth, Mixing Tube and Mixing Tube Extension																			
Primary Motor Performance																			
RTN	T SEP	W <sub>s</sub>	W <sub>t</sub>	W <sub>pj</sub>	F	T <sub>ccA</sub>	T <sub>cc</sub>	E <sub>Tcc</sub>	DPPT	T <sub>R</sub>	P <sub>PJ</sub>	V <sub>i</sub>	V <sub>PJ</sub>	T <sub>PJ</sub>	T <sub>PJ</sub>	E <sub>T PJ</sub>			
10	60	0.1428	0	0.128	0	508.0	573.0	0.443	21.75	11.04	7.414	941.9	2105.5	213.3	222.7	1.034			
10B	90	0.0519	0	0.0519	0	502.0	519.4	0.946	1.76	1.71	2.115	974.0	2097.2	213.6	211.3	0.949			
10C	120	0.0222	0	0.0222	0	505.0	561.4	0.499	0.32	0.14	0.940	940.9	2103.4	214.9	220.3	1.025			
Jet Pump Performance																			
RTN	T SEP	E <sub>qj</sub>	V <sub>i</sub>	W <sub>qj</sub>	m <sub>1</sub>	m <sub>2</sub>	E <sub>m</sub>	P <sub>R<sub>1</sub></sub>	V <sub>R<sub>1</sub></sub>	Q <sub>R<sub>1</sub></sub>	Q <sub>0</sub>	C <sub>p</sub>	C <sub>q</sub>	E <sub>q</sub>	V <sub>M</sub>	W <sub>M</sub>	T <sub>M</sub>	P <sub>s<sub>0D</sub></sub>	T <sub>JP</sub>
10	60	0.07471	190.8	2.114	11.540	11.902	0.973	0.0747	5.4	4.00	4.00	0.0200	0.0093	0.07626	204.5	2.356	520.0	14.491	15.27
10B	90	0.07598	79.4	0.497	17.276	16.904	1.022	0.07652	23.1	0.63	4.00	0.0032	0.0034	0.07626	42.2	0.929	520.0	14.491	2.37
10C	120	0.07614	42.4	0.471	21.674	-0.544	-39.440	0.07626	0.3	0.00	4.00	0.0000	-0.0001	0.07626	0.9	0.010	520.0	14.491	0.00

TABLE V  
SUMMARY OF SELECTED DATA - TEST NO. 11

TABLE 5 SUMMARY OF SELECTED DATA - TEST NO. 11 COLD FLOW Configuration Bellmouth, Mixing Tube Extension and 11" Diffuser																
Primary Motor Performance																
RUN	T SEC	$P_{S1}$	$W_b$	$W_f$	$W_{PJ}$	F	$T_{ccA}$	$T_{cc}$	$E_{Tcc}$	DPPT	$T_R$	$P_{PJ}$	$V_i$	$V_{PJ}$	$T_{PJ}$	$E_{T_{PJ}}$
1	60	0.1854	0	0.1864	0	0.1864	502.0	608.5	0.828	24.91	11.88	9.602	974.0	2087.2	213.6	1.969
11A	96	0.0820	0	0.0820	0	0.0820	500.0	551.2	0.907	5.52	4.94	3.061	976.0	2083.0	212.9	1.930
11B	120	0.0510	0	0.0510	0	0.0510	500.0	505.6	0.899	1.70						

Jet Pump Performance

RUN	T SEC	$P_{S1}$	$W_b$	$W_{SJ}$	$V_i$	$V_{SJ}$	$W_{bA}$	$V_{bA}$	$Q_b$	$Q_o$	$C_p$	$C_{Q5}$	$P_M$	$V_M$	$W_M$	$T_M$	$P_{S_{TD}}$	$T_{PJ}$
1	60	0.07242	283.3	3.144	16.108	17.542	0.814	0.07633	90.2	9.88	4.00	0.0483	0.0147	0.07408	138.5	1.623	523.0	14.708
11A	96	0.07437	191.5	2.110	22.840	26.250	0.874	0.07610	82.6	4.84	4.00	0.0322	0.0103	0.07408	94.6	2.507	523.0	14.708
11B	120	0.07547	107.7	1.204	23.401	23.639	0.994	0.07594	31.5	1.17	4.00	0.0046	0.0052	0.07408	47.4	1.257	523.0	14.708

TABLE VI  
SUMMARY OF SELECTED DATA - TEST NO. 18

TABLE 6 SUMMARY OF SELECTED DATA - TEST NO. 18 HOT FLOW Configuration Bellmouth and Mixing Tube																			
Primary Motor Performance																			
RUN	T SEC	$W_b$	$W_{PJ}$	F	$T_{ccA}$	$T_{cc}$	$E_{T_{cc}}$	DPPT	$T_R$	$P_{PJ}$	$V_i$	$V_{PJ}$	$T_{PJ}$	$E_{T_{PJ}}$					
1*	160	0.0464	0.0044	0.0222	3761.0	4355.0	0.944	4.87	15.49	10.821	2676.9	5711.5	1822.3	1689.9	1.042				
Jet Pump Performance																			
RUN	T SEC	$P_{S1}$	$V_i$	$W_{SJ}$	$m_b$	$m$	$E_B$	$P_{B_A}$	$V_{B_y}$	$Q_{B_A}$	$Q_o$	$C_p$	$C_{Q_5}$	$P_M$	$V_M$	$W_M$	$T_M$	$P_{S_{TD}}$	$T_{PJ}$
1*	160	0.37964	205.5	1.242	24.587	25.019	0.943	0.05418	53.3	5.84	4.00	0.0292	0.0096	0.05347	306.2	2.373	737.7	14.727	22.36

TABLE VII  
SUMMARY OF SELECTED DATA - TEST NO. 34

NOT FLOW																			
Configuration Ballinash Wharf 11' Diffuser																			
Primary Motor Performance																			
RUN	T SEC	$W_a$	$W_s$	$W_{PJ}$	$F$	$T_{crA}$	$T_{cr}$	$E_{cc}$	DPPM	$T_R$	$P_{PJ}$	$V_s$	$V_{PJ}$	$T_{PJ}$	$T_{PJ}$	$E_{T_{PJ}}$			
34	60	0.0535	0.0039	0.0584	0.0769	434.1	375.2	1.15	2.01	10.29	6.506	2878.3	6172.1	1650.4	1671.2	0.980			
34A	60	0.0997	0.0051	0.1044	0.0594	348.2	3121.4	1.243	6.34	18.34	10.42	2720.6	5534.6	1653.6	1440.4	0.871			
34B	130	0.0997	0.0051	0.1042	0.0806	3850.3	3121.4	1.264	6.34	18.52	10.42	2743.5	5412.2	1681.2	1450.2	0.843			
34C	162	0.1316	0.0047	0.136	0.0366	2501.5	1677.6	1.332	14.94	22.32	12.09	2143.2	4661.5	1864.6	496.3	0.942			
34V	60	0.1316	0.0037	0.135	0.0241	2134.9	1999.4	1.137	14.94	26.62	12.09	2028.1	4349.6	915.7	437.5	0.912			
Jet Pump Performance																			
RUN	T SEC	$E_{cc}$	$V_s$	$W_{SJ}$	$W_{PJ}$	$W_{CJ}$	$E_{cc}$	$E_{cc}$	$V_s$	$S_{P_s}$	$Q_c$	$C_c$	$C_{C_s}$	$E_{C_s}$	$V_{C_s}$	$W_{C_s}$	$T_{C_s}$	$P_{C_s}$	$T_{PJ}$
34	60	0.07445	20.7	2.315	39.841	44.375	0.965	0.08294	74.2	5.39	4.06	0.0264	0.0100	0.0599	117.5	2.454	864.0	16.427	6.34
34A	60	0.07445	24.6	2.701	41.874	47.838	0.675	0.06417	67.9	6.14	4.06	0.0406	0.013	0.06744	133.1	3.151	547.7	14.770	12.34

TABLE VIII  
SUMMARY OF SELECTED DATA - TEST NO. 35

HOT FLOW																			
Configuration Bellmouth, Mixing Tube Extension and 1" Diffuser																			
Primary Motor Performance																			
RUN	T SEC	$W_a$	$W_i$	$W_{PJ}$	$\Gamma$	$T_{ccA}$	$T_{cc}$	$E_{Tcc}$	DPP	$T_R$	$P_{PJ}$	$V_i$	$V_{PJ}$	$T_{PJ}$	$T_{PJ}$	$E_{T_{PJ}}$			
3"	75	0.0050	0.0044	0.0095	0.0702	4332.0	3485.2	1.239	2.75	12.32	7.34	2873.0	6180.7	1843.6	1608.3	0.873			
35A	75	0.0050	0.0045	0.0092	0.0686	4313.1	3495.7	1.233	2.75	12.26	7.34	2868.7	6147.3	1835.5	1606.6	0.875			
35A1		0.0494	0.001*	0.0512	0.0365	2851.4	3113.5	0.916	1.59	6.66	5.107	2330.9	4896.2	1213.5	1232.3	1.015			
351		0.0494	0.0013	0.0527	0.0677	4244.6	2838.9	1.444	1.59	8.69	5.107	2863.4	6094.2	1806.3	1460.9	0.809			
35B	105	0.0936	0.0065	0.1025	0.0722	4403.1	3516.7	1.251	5.96	19.26	10.965	2896.4	8211.1	1873.8	1627.9	0.889			
Jet Pump Performance																			
RUN	T SEC	$E_{SP}$	$V_i$	$W_{SP}$	$m$	$m$	$E_{SP}$	$E_{SP}$	$V_{SP}$	$S_{SP}$	$q_c$	$C_p$	$C_{Q_S}$	$P_M$	$V_M$	$W_M$	$T_M$	$P_{S_D}$	$T_{PJ}$
3"	35	0.0741*	245.3	2.456	35.784	41.196	0.942	0.0566*	95.0	6.25	4.00	0.0411	0.0125	0.06275	133.9	2.933	435.6	14.827	12.13
35A	35A	0.0745*	227.9	2.517	47.755	51.964	0.921	0.06013	86.1	7.25	4.00	0.0362	0.0117	0.06604	120.9	2.786	606.0	14.927	10.39
35B	35B	0.0724	306.9	3.313	32.64*	34.122	0.951	0.06589	103.5	10.96	4.00	0.054*	0.0149	0.05991	171.5	3.586	646.0	14.827	19.04

TABLE IX  
SUMMARY OF SELECTED DATA - TEST NO. 36

HOT FLOW																
Configuration Bellmouth Mixing Tube 7.0" Diffuser																
Primary Motor Performance																
W	T SEC	$\gamma_p$	$\gamma_s$	$\gamma_{s2}$	$\gamma_{s3}$	$\gamma_{s4}$	$\gamma_{s5}$	$\gamma_{s6}$	$\gamma_{s7}$	$\gamma_{s8}$	$\gamma_{s9}$	$\gamma_{s10}$	$\gamma_{s11}$	$\gamma_{s12}$	$\gamma_{s13}$	$\gamma_{s14}$
W	7.2	0.0607	0.0034	0.0045	0.0029	0.0029	0.0029	0.0029	0.0029	0.0029	0.0029	0.0029	0.0029	0.0029	0.0029	0.0029
W	4	0.0596	0.0033	0.0044	0.0028	0.0028	0.0028	0.0028	0.0028	0.0028	0.0028	0.0028	0.0028	0.0028	0.0028	0.0028
W	7.5	0.0607	0.0034	0.0045	0.0029	0.0029	0.0029	0.0029	0.0029	0.0029	0.0029	0.0029	0.0029	0.0029	0.0029	0.0029
W	8.0	0.0607	0.0034	0.0045	0.0029	0.0029	0.0029	0.0029	0.0029	0.0029	0.0029	0.0029	0.0029	0.0029	0.0029	0.0029
Jet Pump Performance																
W	T SEC	$\gamma_p$	$\gamma_s$	$\gamma_{s2}$	$\gamma_{s3}$	$\gamma_{s4}$	$\gamma_{s5}$	$\gamma_{s6}$	$\gamma_{s7}$	$\gamma_{s8}$	$\gamma_{s9}$	$\gamma_{s10}$	$\gamma_{s11}$	$\gamma_{s12}$	$\gamma_{s13}$	$\gamma_{s14}$
W	7.2	0.0607	0.0034	0.0045	0.0029	0.0029	0.0029	0.0029	0.0029	0.0029	0.0029	0.0029	0.0029	0.0029	0.0029	0.0029
W	4	0.0596	0.0033	0.0044	0.0028	0.0028	0.0028	0.0028	0.0028	0.0028	0.0028	0.0028	0.0028	0.0028	0.0028	0.0028
W	7.5	0.0607	0.0034	0.0045	0.0029	0.0029	0.0029	0.0029	0.0029	0.0029	0.0029	0.0029	0.0029	0.0029	0.0029	0.0029
W	8.0	0.0607	0.0034	0.0045	0.0029	0.0029	0.0029	0.0029	0.0029	0.0029	0.0029	0.0029	0.0029	0.0029	0.0029	0.0029



### ACOUSTICAL MEASUREMENTS, BLC

Noise measurements (sound pressure levels, SPL) were made at a location 36 inches downstream and at an angle of 45° from the center of the primary jet exit. Both overall SPL and octave spectra were taken under three different nozzle configurations.

Equipment consisted of the General Radio Type 1551A Sound Level Meter and the General Radio Type 1550A Octave-Band Noise Analyzer, which were used to read out the signal from an Altec Model 21BR-180 Capacitor Microphone. The microphone was suspended in a horizontal orientation with the sensing head pointed upstream parallel to the jet axis. (See Figure 31.)

Operational performance of the primary nozzle varied considerably from one configuration to the next. Parameters such as fuel-air ratio, combustion chamber pressure, and temperature affected both jet pump energy and acoustical levels.

Therefore, differences in measured noise with and without duct elements may in part be attributed to variations in primary nozzle performance.

However, the shape of the acoustical spectrum curves clearly shows the effect of duct organ pipe resonances when compared with a bare nozzle spectrum.

The major portion of the BLC nozzle acoustical energy is concentrated in the upper two octaves, probably 75 percent or more above 4800 cycles per second. (See Figure 32.)

### NOISE LEVELS AND OCTAVE SPECTRA

The overall noise levels and octave spectra were obtained during operations as follows:

<u>RUN NO.</u>	<u>CONFIGURATION</u>	<u>MAX. O. A. LEVEL, db</u>
18	Mtr. 105 - Bellmouth & Mixer Tube	133
20	Mtr. 106 - Complete Ducts (except Blowing)	132
28	Mtr. 111 - Bare	137

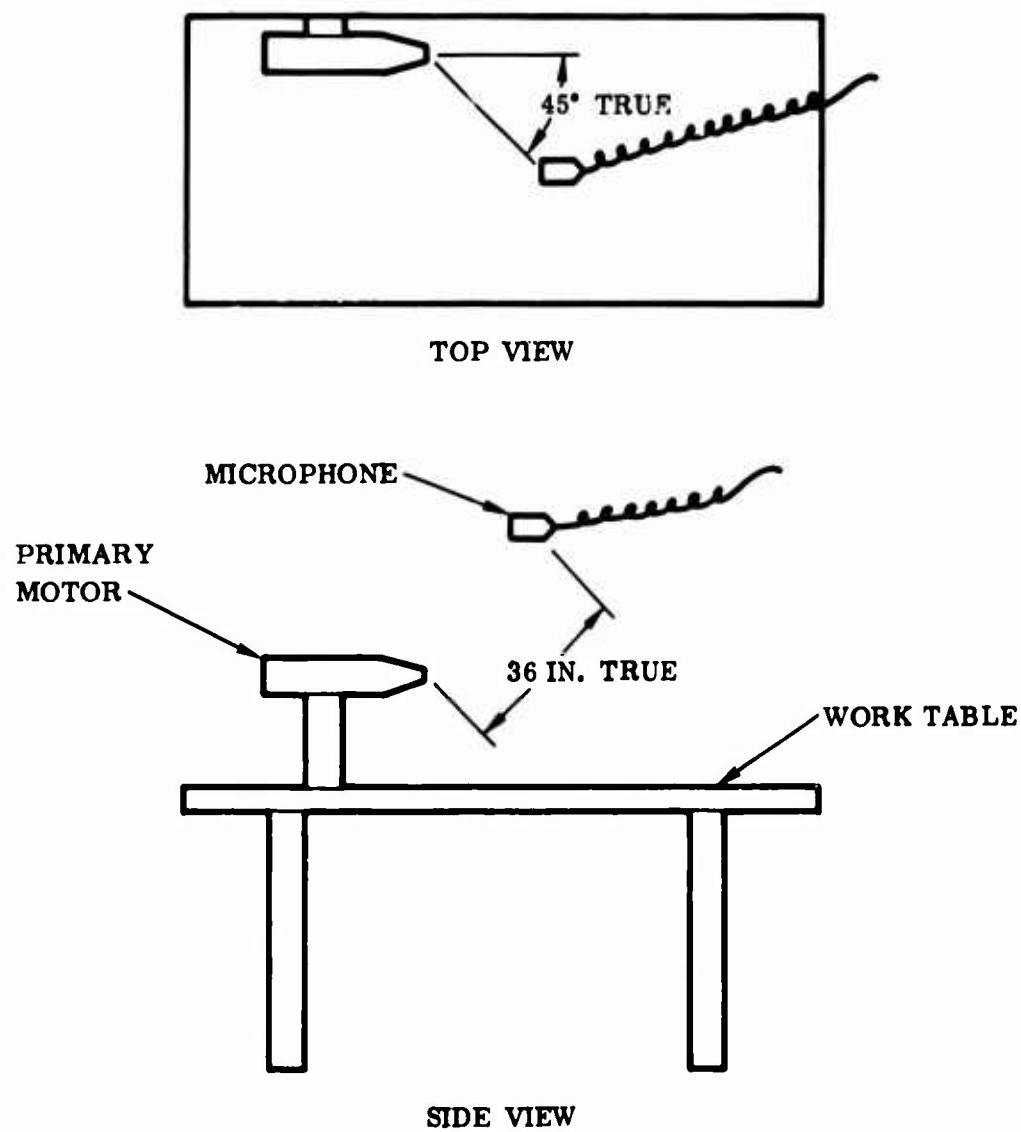


Figure 31. Location of Microphone With Respect to Primary Motor

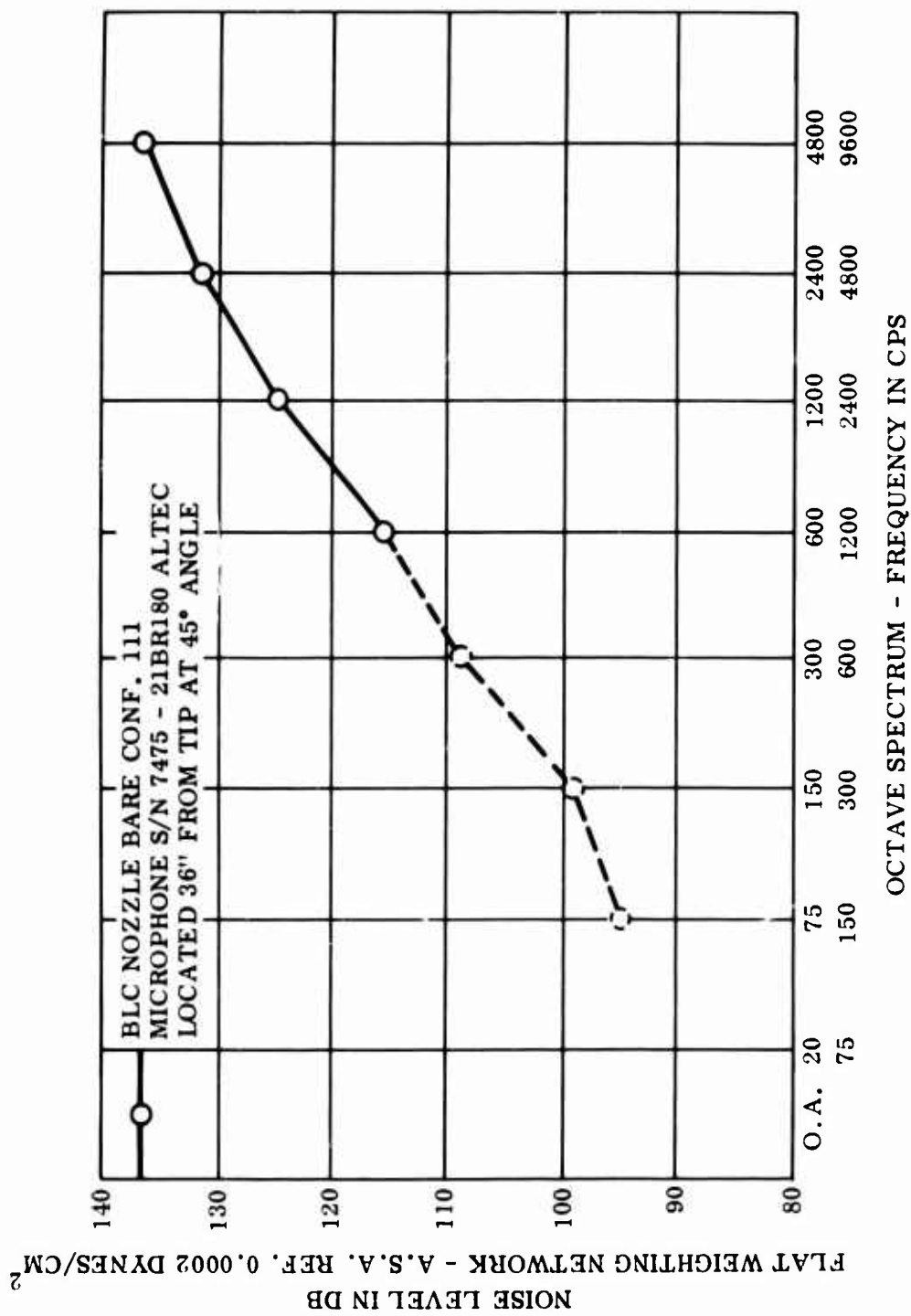


Figure 32. Noise Level Versus Frequency Spectrum

### INSTRUMENTATION

Instrumentation was conventional, and only well-known techniques were used. Measurements were made of temperatures, pressures, linear sizes, volumes, time, sound pressure levels, and frequencies. The variables measured, the method used, and the means of recording are shown in Table X.

Fuel flow rates were obtained by measuring fuel volume change against recorded time intervals. The measurements were taken during periods when flow was held stable and could be assumed to be essentially at a constant flow rate.

A redundant means of measuring fuel flow was provided by recording the differential pressures at (1) the fuel supply line just upstream of the primary motor and (2) the combustion chamber. The pressures were recorded on a two-channel Sanborn recorder.

Airflow rates were calculated from pressure and temperature data. Two methods were used in order to obtain a cross check. One was based on static pressures and the other on total pressures. Agreement was within instrument error limits.

Those temperatures which were subject to rapid and large changes were recorded on a four-channel hot wire recorder. Other temperatures were recorded on a direct reading recorder.

Figure 33 is a representative photograph of the photo-panel instruments.

Photography was used extensively to record conditions not conveniently subject to verbal description. For example, Figure 54 shows the conditions of a primary motor after failure.

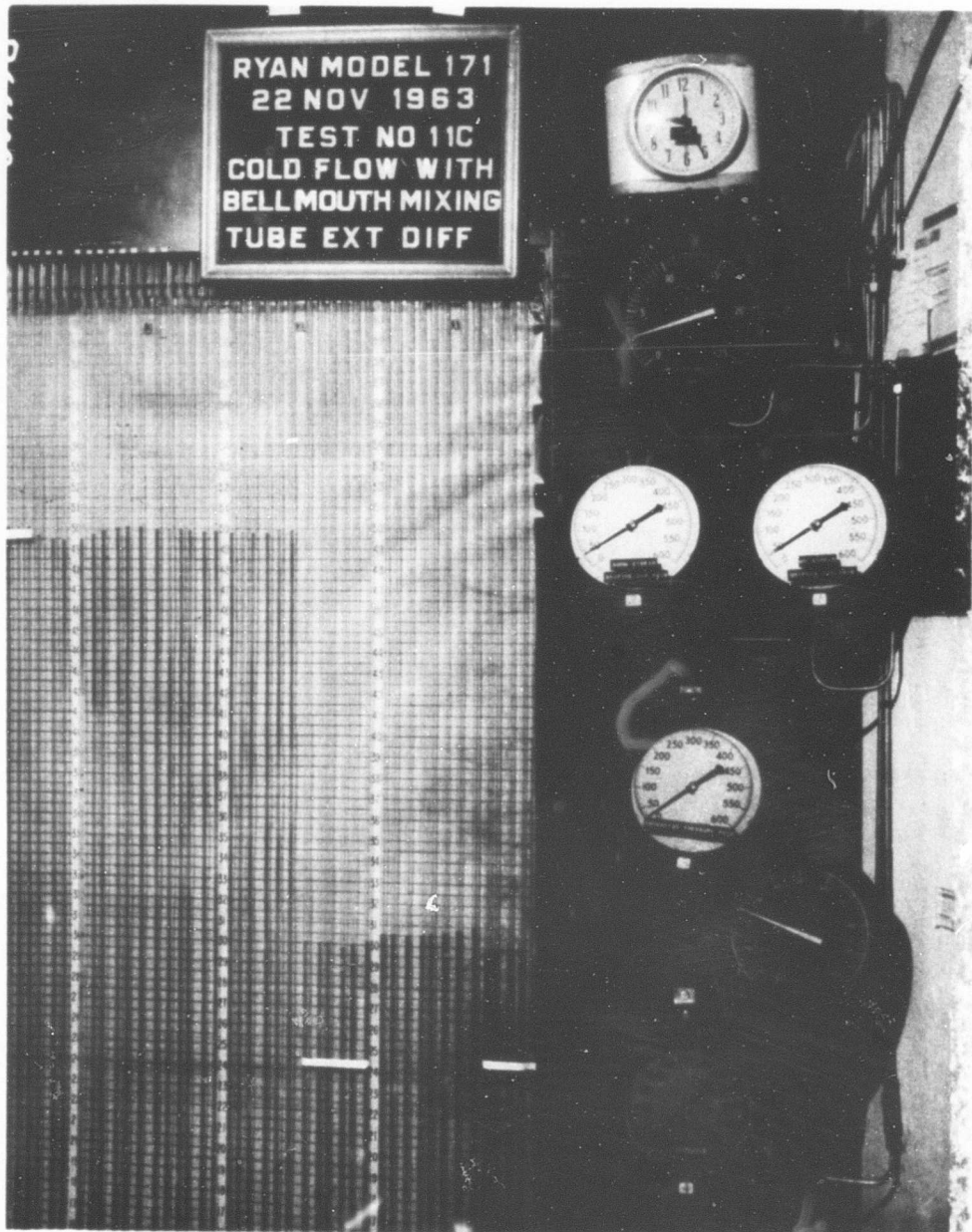


Figure 33. Photograph Record of Pressure Data

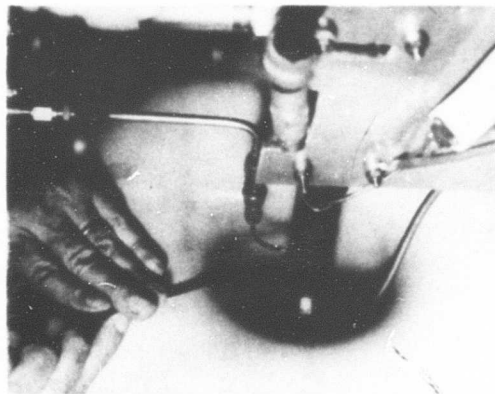
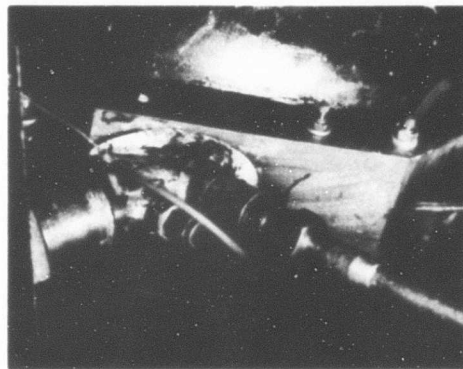
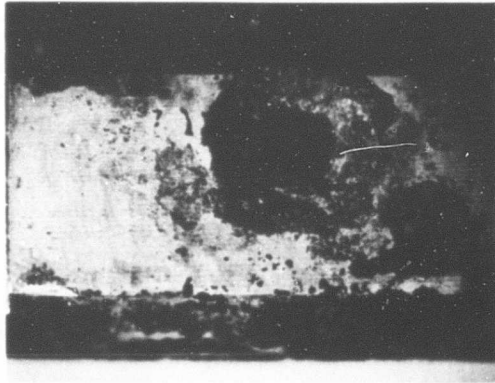


Figure 34. Primary Motor Failure

**TABLE X  
INSTRUMENTATION LIST**

Item	Variable	Symbol	Instrument	Recording Means
1.	Test unit static pressures - less than atmospheric		Flush probes connected to 60 in. manometers - fluid with 0.827 specific gravity	Photo Panel
2.	Test unit static pressures - atmospheric to 60 in. water		Flush probes connected to 60 in. manometers - fluid with 1.000 specific gravity	Photo Panel
3.	Test unit total pressures - atmospheric to 100 in. water		Total pressure probes connected to 60" manometers - fluid with 1.000 specific gravity	Photo Panel
4.	Air supply static pressure at supply tanks		Gage - 0 to 3000 psig	Hand Recorded
5.	Air supply static pressure upstream of metering orifice		Gage - 0 to 1000 psig	Photo Panel
6.	Air supply static pressure downstream of metering orifice		Gage - 0 to 600 psig	Photo Panel
7.	Secondary air total pressure at inlet to mixer tube		Total pressure probe connected to 60" manometer - fluid with 1.000 specific gravity	Photo Panel
8.	"Mixed" air total pressure at mixer/diffuser junction plane		Total	
9.	Differential pressure across air metering orifice		Gage - 0 to 25 psig	Photo Panel
10.	Combustion chamber pressure		Gage - 0 to 600 psig CEC pressure transducer	Photo Panel 2 Channel Sanborn Recorder
11.	Fuel supply pressure		Gage - 0 to 600 psig CEC pressure transducer	Photo Panel 2 Channel Sanborn Recorder
12.	Differential pressure from fuel supply to combustion chamber		Gage - 0 to 100 psig	Photo Panel
13.	Volume of fuel		Calibrated glass supply column	Hand Recorded
14.	Temperature - air supply upstream of metering orifice		Thermocouple - iron/constantan	Brown Recorder No. 1
15.	Temperature - air supply at inlet to motor		Thermocouple - iron/constantan	Brown Recorder No. 1
16.	Temperature of fuel supply		Thermometer	Hand Recorded
17.	Specific gravity of fuel		Hydrometer	Hand Recorded

TABLE X  
INSTRUMENTATION LIST (Cont'd)

Item	Variable	Symbol	Instrument	Recording Means
18.	Temperature - combustion chamber		Thermocouple - Chromel-Alumel	Brown Recorder No. 2
19.	Temperature - external surface of Primary Motor Body		Thermocouple - Chromel-Alumel	4 Channel Sanborn Recorder & Brown Recorder No. 2
20.	Temperature - nozzle tip		Thermocouple - Chromel-Alumel	4 Channel Sanborn Recorder & Brown Recorder No. 2
21.	Temperature - radiated heat in the Bellmouth opposite the nozzle tip		Thermocouple - Iron-constantan	Brown Recorder No. 1
22.	Temperature - secondary air at mixer inlet & 1/4 in. from duct wall		Thermocouple - Iron-constantan	Brown Recorder No. 1
23.	Temperature - mixed air stream at 50% point of mixer length & 1/4 in. from duct wall		Thermocouple - Iron-constantan	Brown Recorder No. 1
24.	Temperature - mixed air stream at 50% point of mixer length & on $Q_1$		Thermocouple - Iron-constantan	Brown Recorder No. 1
25.	Temperature - mixed air stream at mixer-diffuser junction plane & 1/4 in. from duct wall		Thermocouple - Iron-constantan	Brown Recorder No. 1
26.	Temperature - mixed air stream at mixer-diffuser junction plane & on $Q_1$		Thermocouple - Iron-constantan	Brown Recorder No. 1
27.	Temperature - air at diffuser outlet & 1/4 in. from duct wall		Thermocouple - Iron-constantan	Brown Recorder No. 1
28.	Temperature - air at diffuser outlet & on $Q_1$		Thermocouple - Iron-constantan	Brown Recorder No. 1
29.	Temperature - suction air slot adjacent to total pressure pickup on travelling rake		Thermocouple - Iron-constantan	Brown Recorder No. 1
30.	Temperature - flowing air slot adjacent to total pressure pickup on travelling rake		Thermocouple - Iron-constantan	Brown Recorder No. 1
31.	Noise - sound pressure at a point 3 ft. distant on a ray 45° off axis downstream from the nozzle exit		Microphone - connected to sound pressure spectrum analyzing meter	Hand Recorded
32.	Time		Clock w/ sweep second hand	Photo Panel



## REFERENCES

1. Wagner, F. G., The New Ryan BLC System for V/STOL, Ryan Report No. 61B083, Ryan Aeronautical Company, San Diego, California, March 1960, Revised April 1961.
2. Wagner, F. G., Therrien, C. J., and Urquhart, G. R., The Ryan System of BLC for the DeHavilland Caribou - Volume I - Proposal Summary, Ryan Report No. 62B045, Ryan Aeronautical Company, San Diego, California, April 1962, Revised February 1963.
3. Wagner, F. G., Therrien, C. J., and Urquhart, G. R., The Ryan System of BLC for the DeHavilland Caribou - Volume II - Technical, Ryan Report No. 62B046, Ryan Aeronautical Company, San Diego, California, April 1962, Revised February 1963.
4. Bogart, D., Okrent, D., and Turner, L. R., Thermodynamic Charts for the Computation of Fuel Quantity Required for Constant Pressure Combustion with Diluents, TN No. 1655, NASA Flight Propulsion Research Laboratory, Cleveland, Ohio, July 1948.
5. Grace, H. P., and Lapple, C. E., Discharge Coefficients of Small-Diameter Orifices and Flow Nozzles, American Society of Mechanical Engineers, New York, New York, July 1951.
6. Sutton-Wiley, G. P., Rocket Propulsion Elements, 1956.
7. Barrere, M., Rocket Propulsion, Elsevier, New York, New York, 1960.
8. Crocco, L., and Cheng, H. I., Theory of Combustion Instability in Liquid Propellant Rocket Motors, (Published for AGARD) by Butterworth Scientific Publications, London, England, 1956.
9. Brown, A., and Marco, S. M., Introduction of Heat Transfer, McGraw-Hill, Hightstown, New Jersey, 1951.
10. Eckert, E. R., and Drake, R. M. Jr., Introduction of the Transfer of Heat and Mass, McGraw-Hill, Hightstown, New Jersey, 1950.
11. A Theoretical Investigation on the Determination of Lift Coefficients in Two Dimensional Smoke Tunnels, Princeton University Engineering Dept. Report No. 289, Princeton University, Princeton, New Jersey, Feb. 1955.

## DISTRIBUTION

US Army Materiel Command	4
US Army Aviation Materiel Command	6
US Army Forces Southern Command	1
Chief of R&D, DA	1
Secretary of Defense, DOD	1
US Army R&D Group (Europe)	2
US Army Aviation Materiel Laboratories	13
US Army Limited War Laboratory	1
US Army Human Engineering Laboratories	1
US Army Research Office-Durham	1
Plastics Technical Evaluation Center	1
US Army Engineer Waterways Experiment Station	1
US Army Test and Evaluation Command	1
US Army Electronics Command	2
US Army Combat Developments Command, Fort Belvoir	2
US Army Combat Developments Command Experimentation Command	3
US Army Combat Developments Command Transportation Agency	1
US Army War College	1
US Army Command and General Staff College	1
US Army Aviation School	1
US Army Tank-Automotive Command	2
US Army Armor and Engineer Board	1
US Army Aviation Test Board	2
US Army Transportation Engineering Agency	1
US Army Aviation Test Activity, Edwards AFB	2
Air Force Flight Test Center, Edwards AFB	2
US Army Field Office, AFSC, Andrews AFB	1
Air Force Avionics Laboratory, Wright-Patterson AFB	1
Air Force Flight Dynamics Laboratory, Wright-Patterson AFB	1
Systems Engineering Group, Wright-Patterson AFB	3
Naval Ship Engineering Center	1
Naval Air Systems Command, DN	7
Office of Naval Research	4
Marine Corps Liaison Officer, US Army Transportation School	1
Lewis Research Center, NASA	1
Manned Spacecraft Center, NASA	1
NASA Scientific and Technical Information Facility	2
Ames Research Center, NASA	1
AFSC, NASA, Langley AFB	1
NAFEC Library (FAA)	2

US Army Aviation Human Research Unit	2
US Army Board for Aviation Accident Research	1
Bureau of Safety, Civil Aeronautics Board	2
US Naval Aviation Safety Center, Norfolk	2
US Naval Air Station, Norfolk	1
Federal Aviation Agency, Washington, DC	1
Civil Aeromedical Institute, FAA	2
US Army Medical R&D Command	1
Defense Documentation Center	20

## APPENDIX I - THEORETICAL DEVELOPMENT OF BOUNDARY LAYER CONTROL JET PUMP

### INTRODUCTION

A correlation of experimental data and a theoretical approach are made and utilized in the analyses of a BLC jet pump system as applied to the YCV-2B airplane. The method of analysis draws prominently from H. P. Helmbold's University of Wichita Reports 147 and 294, and the SAE Aerospace Applied Thermodynamics Manual (Reference 2, page 384).

The analyses assume incompressible turbulent flow in a smooth duct for the most part. However, compressibility effects are considered in the duct system where high dynamic pressures are evidenced. The airflow requirements dependent upon the BLC systems are  $C_{QB}$ ,  $C_{QS}$ , and  $C_\mu$ , which are the air volume flow coefficients for blowing and suction, and the blowing momentum coefficient, respectively.

The entrainment ratio and suction to blowing wing area ratio are established by an iterative process. Initially, values are selected to satisfy certain desirable aerodynamic characteristics. An elliptical spanwise lift distribution is desired. Therefore, an approximate wing area ratio may be selected which results in the desired air volume flow coefficient to yield the proper section lift coefficients.

The selection of the desired entrainment ratio is based upon the geometry of the duct system and the secondary to primary jet velocity ratio. The selected entrainment ratio should result in an acceptable pump efficiency and duct temperature for the BLC system.

The constant diameter mixing tube is more favorable than a constant pressure system for a number of reasons. One reason is that at higher velocity ratios, the constant diameter mixing tube exhibits markedly lower pressure losses. Secondly, the constant diameter tube is also much simpler in design. The constant pressure mixing tube is superior only at the lower velocity ratios of secondary jet velocity to primary jet velocity.

## DISCUSSION

The jet pump selected as the driving system is contingent upon a number of significant factors. A sound analysis and comparison may be found in Reference 1 (see page 87). The multiple ducting system with individual nozzles has been selected as the best system for this airplane based on the data in the referenced report.

In the application on any BLC system, the primary purpose is to design the system to achieve a desired lift coefficient ( $C_L$ ). To this end, certain air volume flow coefficients and blowing momentum coefficients must be satisfied. The correlation between the air flow coefficients and the lift coefficients is discussed in a separate section of this report.

The following theoretical method of analysis was developed to predict the BLC pump system performance. The analysis is based on the conservation of mass, energy, and total momentum. Basic assumptions made in order to facilitate the theoretical development are:

1. The flow is turbulent, incompressible, and one-dimensional.
2. The ejector walls are perfectly insulated.
3. The primary and secondary fluids are perfect gases.
4. The gas constants of the primary and secondary fluids are not the same but are constants.
5. The flow is considered to be adiabatic to the exit of the primary nozzle and the entrance of the mixing tube. The pressure losses due to friction and geometry are considered; they are discussed in the paragraph titled "Suction Duct Characteristics" of this appendix.
6. The primary and secondary fluids are completely mixed at the end of mixing tube.

The purpose of this analysis is to develop equations which can be used to calculate the pressure rise of the induced secondary stream, the momentum of the primary jet, and the state of the combined primary and secondary stream and the dimension of the ejector. Figure 11 describes the jet pump system considered in this study.

The air volume flow coefficients and the blowing momentum coefficients have the following relationships. The air volume flow coefficients are related by the ratio of wing areas and the entrainment ratio as illustrated by the following equation:

$$C_{Q_B} = \left[ \frac{S_S}{S_B} \right] \left[ 1 + \frac{1}{m} C_{Q_S} \right] \quad (1)$$

$S_S$  and  $S_B$  are the wing areas under the influence of the suction and blowing respectively. Each area is determined by the product of the spanwise length of the particular slot multiplied by the average wing chord between the inboard and outboard ends of the slot. The blowing momentum coefficient is found by the following procedure:

$$\text{Blowing momentum} = W_J V_J = C_{\mu} q_o S_B \quad (2)$$

$$\text{or } C_{\mu} = \frac{W_J V_J}{\frac{1}{2} \rho_o V_o^2 S_B g} = \frac{2 V_J^2 \rho_J A_{B_{St}}}{S_B \rho_o V_o^2} = \frac{2 Q_J \rho_J V_J}{S_B \rho_o V_o^2} \quad (3)$$

Utilizing the basic mass flow equation,

$$\begin{aligned} W_M &= W_M = W_B = V_J \rho_J A_{B_{St}} g = V_J \rho_J b_B s_B g \\ &= V_o \rho_o C_{Q_B} b_B s_B g \end{aligned} \quad (4)$$

or converting to volume flow,

$$Q_J = \frac{\rho_o}{\rho_J} A_B = \frac{\rho_o}{\rho_J} C_{Q_B} S_B V_o = V_J s_B b_B \quad (5)$$

From Equation (4) or Equation (5),

$$\frac{V_J}{V_o} = \frac{\rho_o C_{Q_B} S_B}{\rho_J s_B b_B} = \frac{\rho_o C_{Q_B}}{\rho_J (s/c)_B} \quad (6)$$

$$V_J = \frac{V_o \rho_o C_{Q_B}}{\rho_J (s/c)_B} \quad (7)$$

To determine the blowing jet density ( $\rho_J$ )

$$\rho_J = \rho_o \frac{T_S^o}{T_J} \quad (8)$$

$$T_B = T_J = T_B^o - \frac{V_J^2}{2g Jc_p} \quad (9)$$

$$T_B^o = \frac{T_S^o}{1 + \frac{1}{m}} + \frac{T_{PJ}^o}{m + 1} \quad (10)$$

$$\therefore T_J = \frac{T_S^o}{1 + \frac{1}{m}} + \frac{T_{PJ}^o}{m + 1} - \frac{V_J^2}{2g Jc_p} \quad (9a)$$

Substituting Equation (7) for  $V_J^2$ ,

$$T_J = \frac{T_S^o}{1 + \frac{1}{m}} + \frac{T_{PJ}^o}{1 + m} - \frac{\rho_o^2}{\rho_J^2} C_{Q_B}^2 \frac{V_o^2}{(s/c)_B^2 2g Jc_p} \quad (9b)$$

Substituting Equation (9b) into Equation (8),

$$\rho_J = \rho_o \frac{T_S^o}{\frac{T_S^o}{1 + \frac{1}{m}} + \frac{T_{PJ}^o}{1 + m} - \frac{\rho_o^2 V_o^2 C_{QB}^2}{\rho_J^2 (s/c)_B^2 2g Jc_p}} \quad (8a)$$

Simplifying Equation (8a), the density equation reduces to a quadratic equation:

$$\rho_J^2 = \frac{(m+1)^2 \rho_o T_S^o \rho_J}{\left[ m^2 (m+1) T_S^o + m (m+1) T_{PJ}^o \right]} - \frac{(m+1)^2 \rho_o V_o^2 C_{QB}^2}{2g Jc_p (s/c)_B^2 \left[ m^2 (m+1) T_S^o + m (m+1) T_{PJ}^o \right]} = 0 \quad (8b)$$

Substituting Equation (5) into Equation (3),

$$C_\mu = \frac{2 \rho_J V_J}{S_B \rho_o V_o^2} \cdot \frac{\rho_o}{\rho_J} C_{QB} S_B V_o = \frac{2 V_J C_{QB}}{V_o} \quad (11)$$

or

$$\frac{V_J}{V_o} = \frac{C_\mu}{2 C_{QB}} \quad (11a)$$



Substituting from Equation (6),

$$C_{\mu} = 2 C_{Q_B} \frac{\rho_o}{\rho_J} \frac{C_{Q_B}}{(s/c)_B} = \frac{2 C_{Q_B}^2 \rho_o}{(s/c)_B \rho_J} \quad (12)$$

Again utilizing Equation (6),

$$C_{\mu} = 2 \left( \frac{V_J}{V_o} \right)^2 \frac{\rho_J}{\rho_o} (s/c)_B = 2 (s/c)_B q_J / q_o \quad (13)$$

Regrouping Equation (13) gives

$$(s/c)_B = \frac{2 \rho_o C_{Q_B}^2}{\rho_J C_{\mu}} = \frac{\rho_o}{\rho_J} \cdot \frac{C_{\mu}}{2} \cdot \left( \frac{V_o}{V_J} \right)^2 \quad (14)$$

The wing area ratio ( $S_S/S_B$ ) is selected to give the  $C_{Q_B}$  and  $C_{Q_S}$  which will develop the wing lift coefficients  $C_L$  desired. Equation (1) is employed for this purpose

Utilizing Equation (6), the velocity ratio ( $V_J/V_o$ ) may be found. To accomplish this, however, the slot width to wing chord ratio must be arbitrarily selected within the geometrical restrictions of the wing structure. This procedure may be reversed in that a proper velocity ratio may be selected to give a practical  $(S/C)_B$ . In any event, it is desirable that the maximum  $(S/C)_B$  ratio is attained.

The entrance conditions ( $V_E$  and  $\rho_E$ ) may be determined in a similar manner.

The mass flow relationship is

$$W_E = W_S = V_E \rho_E g s_S b_S = V_o b_S c_S \rho_o g \quad (15)$$

or

$$Q_E = \frac{\rho_o}{\rho_E} Q_S \quad (16)$$

$$Q_E = V_E s_S b_S = V_E (s/c)_S s_S = \frac{\rho_o}{\rho_E} C_{Q_S} s_S V_o \quad (17)$$

Rearranging Equation (17),

$$\frac{V_E}{V_o} = \frac{\rho_o}{\rho_E} \cdot \frac{C_{Q_S}}{(s/c)_S} \cdot \frac{s_S}{s_S} \cdot \frac{\rho_o}{\rho_E} \cdot \frac{1}{(s/c)_S} \left[ \frac{C_{Q_B}}{(s_S/s_B) \left(1 + \frac{1}{m}\right)} \right] \quad (18)$$

or

$$V_E = \frac{\rho_o}{\rho_E} \cdot \frac{C_{Q_S}}{(s/c)_S} \cdot V_o = \frac{\rho_o V_o}{\rho_E (s/c)_S} \left[ \frac{C_{Q_B}}{(s_S/s_B) \left(1 + \frac{1}{m}\right)} \right] \quad (19)$$

or

$$(s/c)_S = \frac{\rho_o V_o}{\rho_E V_E} \left[ \frac{C_{Q_B}}{(s_S/s_B) \left(1 + \frac{1}{m}\right)} \right] \quad (20)$$

To solve for  $\rho_E$ ,

$$\rho_E = \frac{P_E}{g R T_E} \quad (21)$$

$$P_E = P_o - \frac{\rho_E}{2} V_E^2 - \Delta P_{T_E} \quad (22)$$

$$T_E = \frac{\rho_E}{\rho_o} T_o \quad (23)$$

$$\Delta P_{T_E} = -c_{p_{tE}} q_E = -c_{p_{tE}} \frac{\rho_E}{2} V_E^2 \quad (24)$$

Note: The loss coefficient  $(-c_{p_{tE}})$  includes the effects of energy loss in the boundary layer, turning loss over the cusp, and suction slot throat loss.

Substituting  $V_E$  and  $\Delta P_{T_E}$  into Equation (22),

$$P_E = P_o - \frac{\rho_E}{2} \left[ \frac{\rho_o}{\rho_E} \frac{C_{QS}}{(s/c)_S} V_o \right]^2 - \left[ -c_{p_{tE}} \cdot \frac{\rho_E}{2} \cdot \frac{\rho_o^2}{\rho_E^2} \frac{C_{QS}^2}{(s/c)_S^2} \cdot V_o^2 \right] \quad (25)$$

Simplification leads to

$$P_E = P_o - \frac{\rho_o^2 V_o^2 C_{QS}^2}{2 (s/c)_S^2 \rho_E} \left[ 1 - c_{p_{tE}} \right] \quad (26)$$

Now, returning to Equation (21),

$$\rho_E = \frac{P_o - \frac{\rho_o^2 V_o^2 C_{QS}^2}{2 \rho_E (s/c)_S^2} [1 - c_{p_{tE}}]}{g R \frac{\rho_E}{\rho_o} T_o} \quad (27)$$

Simplifying Equation (27) into a cubic form,

$$\rho_E^3 - \frac{\rho_o P_o \rho_E}{g R T_o} + \frac{\rho_o^3}{2 g R T_o} \left[ \frac{V_o^2 C_{QS}^2}{(s/c)_S^2} \right] [1 - c_{p_{tE}}] = 0 \quad (28)$$

To simplify the solution of the cubic equation, let

$$\rho' = \frac{\rho_o P_o}{g R T_o} \quad (29)$$

and

$$\rho'' = \frac{\rho_o^3}{g R T_o} \left[ \frac{V_o^2 C_{QS}^2}{(s/c)_S^2} \right] [1 - c_{p_{tE}}] \quad (30)$$

$$\therefore \rho_E^3 - \rho' \rho_E + \rho'' = 0 \quad (31)$$

Employing the standard solution for a cubic equation of this form, the equation has the following solutions:

$$\rho_{E_1} = 2 \sqrt{\rho'} \cos \frac{\xi}{3} \quad (31-1)$$

$$\rho_{E_2} = 2\sqrt{\rho} \cos \left( 60^\circ - \frac{\zeta}{3} \right) \quad (31-2)$$

$$\rho_{E_3} = 2\sqrt{\rho} \cos \left( 60^\circ + \frac{\zeta}{3} \right) \quad (31-3)$$

where

$$\zeta = \cos^{-1} \frac{\dot{\rho}}{\rho \sqrt{\rho}} \quad (31-A)$$

For the case of the blowing slot, the velocity ratio ( $V_E/V_Q$ ) can be found by an arbitrary selection of  $(s/c)_S$ . The reverse operation is also applicable as was the case for the suction slot.

Going to Equation (8), the blowing momentum coefficient ( $C_\mu$ ) may be found by using the solutions for  $V_J/V_O$  and  $C_{Q_B}$ .

The entrainment ratio ( $m$ ) introduced earlier in the discussion relates the primary jet mass flow to the induced secondary mass flow by

$$m = \frac{W_S}{W_{PJ}} \quad (32)$$

#### SUCTION DUCT CHARACTERISTICS

The pressure drop or losses incurred in the suction duct consider the entrance losses, turn losses, and frictional losses. The entrance losses ( $\Delta P_{T_E}$ ) have been considered in the previous discussion. It should be noted that the impulse loss of the suction air through its  $180^\circ$  turn against the wing airflow direction is accounted for as an aerodynamic drag increase,

$$\Delta C_{D_S} = 2 \frac{S_S}{S} C_{Q_S} \quad (33)$$

The two fundamental causes of pressure loss in a fully turbulent flow through any duct system are skin friction and flow separation. The losses are roughly proportional to the dynamic pressure of the airflow. Since the dynamic pressure is a function of the square of the flow velocity, the maintenance of a low air velocity would be a prime design factor for duct systems. For a given mass flow, proper duct sizing would control airflow velocity.

In straight ducts of constant cross section, skin friction is the major cause of pressure loss. However, this loss is small compared to the loss which occurs owing to flow separation from the duct walls. Separation is normally caused by two major factors. First, a deceleration of airflow, as in a diffuser, causes a rapid pressure rise causing an adverse pressure gradient. Separation in a duct for this reason is a function of the velocity of flow adjacent to the duct wall, since the presence of thick boundary layers of slow moving air is conducive to separation. Conversely, a decreasing pressure gradient, such as is found in a nozzle, tends to prevent separation.

Another factor which gives cause for separation is a change in flow direction such as occurs in duct bends. Also, any surface irregularities that cause a local disturbance adjacent to the duct wall increase the possibility of separation.

The frictional loss is given by

$$\Delta P_{t_{FS}} = \lambda_o \frac{b_S}{r'} q_{DS} \quad (34)$$

The loss coefficient is a function of the Reynolds number and is given by

$$\lambda_o' = 0.05594 \sqrt[4]{R'_e} \quad (35)$$

The Reynolds number ( $R'_e$ ) can be found by

$$R'_e = \frac{V_{DS} D_H}{\nu} \quad (36)$$

or

$$R'_e = \frac{V_{DS} D_H \rho}{\mu} \quad (36A)$$

or

$$R'_e = \frac{4 W_S}{\mu P_W} \quad (36B)$$

In computing the losses, an equivalent suction duct velocity ( $V_{DS}$ ) and a composite loss coefficient ( $\lambda_0'$ ) may be used. This method is valid for incompressible flow. However, in the case of compressible flow, a more exacting solution is required. The following method is recommended.

The analysis utilizes the principle of conservation of mass and also assumes an adiabatic process. In computing the dynamic pressure for a section, the properties of the smaller area of the duct segment in question are employed. In the special case of nozzles and diffusers, the mean conditions are utilized for computing the hydraulic diameter.

A weight function

$$\frac{W \sqrt{T_t}}{A P_t} \quad (37)$$

can be found. This is normally equated to

$$m \frac{P}{P_t} = \frac{W \sqrt{T_t}}{A P_t} = Mg \left( \frac{\gamma}{R} \right)^{1/2} \left( 1 + \frac{\gamma - 1}{2} M^2 \right)^{-\frac{\gamma + 1}{2(\gamma - 1)}} \quad (38)$$

(See Ref. 7)

From Equation (38), the Mach number (M) can be found. Now, utilizing the equation

$$\frac{q}{P_t} = \frac{\gamma M^2}{2} \left[ 1 + \frac{\gamma - 1}{2} M^2 \right]^{-\frac{\gamma}{\gamma + 1}} \quad (39)$$

the dynamic pressure  $q$  can be found. The pressure loss is then given by

$$\Delta P_{t_{FS}} = \lambda'_{o_1} q_1 \quad (40)$$

For the subsequent section, the total pressure  $P_t$  is decreased by the loss ( $\Delta P_{t_{FS}}$ ) of the preceding section. This new total pressure, plus an area change,

if applicable, is used to calculate a new mass flow function  $\left( \frac{W\sqrt{T}}{A P_t} \right)$

The turn losses are computed in a similar manner. The turn loss coefficient  $\Phi_T$  is a function of Reynolds Number, radius ratio, and aspect ratio. The coefficients may be found in Reference 4. The dynamic pressure used is the same as that used to calculate the friction losses. The turn loss ( $\Delta P_{t_{TS}}$ ) is given by

$$\Delta P_{t_{TS}} = \Phi_T q \quad (41)$$

The pressure loss coefficients for friction and turn loss may be added for each respective section to find the total pressure loss. It should be noted that the turn loss coefficient should be modified if the cross-sectional area varies in the bend.

The total pressure loss in the suction system is

$$\Delta P_{t_S} = \Delta P_{t_E} + \Delta P_{t_{TS}} + \Delta P_{t_{FS}} \quad (42)$$



### PRIMARY JET STATION

The station plane at which the primary nozzle is located is identified as Station I. This station also marks the end of the suction duct and the inlet of the mixing tubes. The static pressure  $P_I$  at this station is given by

$$P_I = P_o - \Delta P_{t_S} - \frac{1}{2} \rho_{SJ} V_{SJ}^2 \quad (43)$$

or

$$P_I = P_{t_I} - \frac{1}{2} \rho_{SJ} V_{SJ}^2 \quad (44)$$

Therefore,

$$P_{t_I} = P_o - \Delta P_{t_S} \quad (45)$$

The standard nozzle equation is

$$V_{PJ} = \left\{ 2 g J c_p T_{p_o} \left[ 1 - \left( \frac{P_I}{P_{p_o}} \right)^{\frac{k-1}{k}} \right] + V_i^2 \right\}^{1/2} \quad (46)$$

The enthalpy change due to the primary jet is given by

$$\Delta h = V_{PJ}^2 / 2 g J \quad (47)$$

The primary jet temperature is given by

$$T_{PJ} = T_{p_o} - \frac{V_{PJ}^2}{2 g J c_p} \quad (48)$$

or

$$T_{PJ} = \frac{2 g J c_p T_{p_o} - V_{PJ}^2}{2 g J c_p} \quad (48a)$$

Substituting Equation (46) into (48a) and reducing gives

$$T_{PJ} = T_{p_o} \left[ \left( \frac{P_I}{P_{p_o}} \right)^{\frac{k-1}{k}} - \frac{V_i^2}{2 g J c_p} \right] \quad (49)$$

The primary jet density is found by

$$\rho_{PJ} = \frac{P_I}{g R T_{PJ}} \quad (50)$$

Substituting for  $T_{PJ}$  from Equation (49)

$$\rho_{PJ} = \frac{P_I P_o^{\frac{k-1}{k}}}{g R T_{p_o} P_I^{\frac{k-1}{k}}} = \frac{P_I^{1/K} P_o^{\frac{k-1}{k}}}{g R T_o} \quad (51)$$

The secondary jet velocity may be found by utilizing Equation (38) and determining the Mach number. Multiplying the Mach number by the speed of sound for this condition determines the desired velocity. The speed of sound may be found by

$$V_{SOUND} = \sqrt{k g R T} \quad (52)$$

Therefore,

$$V_{SJ} = M V_{\text{SOUND}} \quad (53)$$

The ratio of secondary jet velocity to primary jet velocity is designated by  $\alpha$  and written as

$$\alpha = \frac{V_{SJ}}{V_{PJ}} \quad (54)$$

The secondary jet density can be found from the relationship

$$\rho_{SJ} = \frac{P_I}{g R_{SJ}} \quad (55)$$

Substituting for  $P_I$  from Equation (43) and for  $T_{SJ}$  from the relationship

$$T_{SJ} = T_{SJ}^o - \frac{V_{SJ}^2}{2 g J c_p} \quad (56)$$

Equation (55) becomes

$$\rho_{SJ} = \frac{P_{tI}}{g R_{SJ} T_{SJ}^o - \left( \frac{J c_p}{2 J c_p} \right) V_{SJ}^2} \quad (57)$$

The preceding equations for Station I are either directly or indirectly a function of the static pressure  $P_I$ .  $P_I$ , in turn, is a function of the secondary jet velocity and density. Therefore, a simultaneous solution of three equations in three unknowns is in order. The three equations are:

$$P_I = P_o - \Delta P_{tS} - \frac{1}{2} \rho_{SJ} V_{SJ}^2 \quad (45)$$

$$V_{SJ} = \alpha \sqrt{2 g J c_p T_{P_o} \left[ 1 - \left( \frac{P_2}{P_o} \right)^{\frac{k-1}{k}} \right] + V_i^2} \quad (58)$$

$$\rho_{SJ} = \frac{P_o - \Delta P_{t_s}}{g R T_{SJ}^o - \left( \frac{J c_p - R}{2 J c_p} \right) V_{SJ}^2} \quad (59)$$

An algebraic solution of these equations results in a complex exponential equation of various orders of  $P_I^{k-1/K}$ . Therefore, the solution of this set of equations is accomplished by an iterative process.

The initial step in the iteration process is to assume a series of static pressures  $P_I$  for a given velocity ratio ( $\alpha$ ). For each assumed  $P_I$ , a corresponding  $V_{PJ}$ ,  $V_{SJ}$ , and  $\rho_{SJ}$  is determined. The secondary jet dynamic pressure

$$q_{SJ} = \frac{1}{2} \rho_{SJ} V_{SJ}^2 \quad (59-1)$$

is calculated and subtracted from the total secondary pressure

$$P_{t_{SJ}} = (P_o - \Delta P_{t_s}) \quad (59-2)$$

This value is the resulting static pressure, designated  $P_I^*$ , for the assumed static pressure  $P_I$ . A graph of assumed  $P_I$  versus calculated  $P_I^*$  is superimposed on a graph of  $P_I$  and  $P_I^*$  versus ( $\alpha$ ). The intersection of the two curves gives the point at which  $P_I = P_I^*$  for a given velocity ratio ( $\alpha$ ). This is a solution for the above equations.

Using the obtained values of  $P_I$ , the other parameters at Station I are calculated as a function of the velocity ratio ( $\alpha$ ).

### MIXING TUBE - DIFFUSER STATION

The station which defines the end of the mixing tube and the beginning of the blowing diffuser is identified as Station M. There are six unknown parameters which must be determined for Station M. These are:

1. Density,  $\rho_M$
2. Static pressure,  $P_M$
3. Total pressure,  $P_{tM}$
4. Static Temperature,  $T_M$
5. Velocity,  $V_M$
6. Ideal Mixer efficiency,  $\eta_i$

There are eight independent equations applicable to the solution for the six unknown parameters. These equations are:

$$1. \quad P_M = R g T_M \rho_M \quad (\text{Ideal Gas Law}) \quad (60)$$

$$2. \quad T_M = T_B^o - \frac{V_M^2}{2 g J C_p} \quad (61)$$

$$3. \quad P_{tM} = P_M + \frac{1}{2} \rho_M V_M^2 \quad \left. \begin{array}{l} (62) \\ (63) \end{array} \right\} \quad (\text{Enthalpy Relationships})$$

$$4. \quad P_{tM} = 2 g J h_{tM} \rho_M \quad (63)$$

$$5. \quad \rho_{PJ} V_{PJ} A_{PJ} + \rho_{SJ} V_{SJ} A_{SJ} = \rho_M V_M A_M \quad (\text{Conservation of Mass}) \quad (64)$$

$$6. \quad P_I A_M + \rho_{PJ} V_{PJ}^2 A_{PJ} + \rho_{SJ} V_{SJ}^2 A_{SJ} = P_M A_M + \rho_M V_M^2 A_M$$

(Conservation of Momentum) (65)

$$7. \quad \Delta P_{tEXAV.} = \frac{\rho_M \left( \eta_E J \Delta h_{I_{PJ}} - \frac{\Delta P_{tS}}{\rho_{SJ}} \cdot m \right)}{m + 1} \quad \text{where } \eta_E = \xi \eta_i$$

(66)

(See page 80 for derivation)

$$8. \quad \eta_i = \frac{A_{SJ} V_M \left( P_{TM} - P_{tI} \right) + A_{PJ} V_M \left( P_{tM} - P_o \right)}{A_{PJ} V_{PJ} \left( \frac{\rho_{PJ} V_{PJ}^2}{2} - \frac{\rho_{SJ} V_{SJ}^2}{2} \right)}$$

(67)

(see pages 83, 84, and 85 for derivation)

The solution of these equations again becomes complex because of their non-linearity. The problem lends itself to a numerical solution utilizing a finite difference or relaxation method.

To simplify the foregoing analysis, the following assumptions are made. In the following analysis, only the initial and final conditions are discussed. Theoretically, only at an infinite length of mixing can a uniform stream be attained. However, once a reasonable finite length is reached, the mixing process tends to approach the ideal uniform state asymptotically. Therefore, an analysis of the ideal state at some finite length yields a reasonable approximation.

To simplify the ideal efficiency, Equation (67), it is assumed that the entrance losses are negligible or of minor consequence. It is also assumed that  $\rho_M$ ,  $\rho_{SJ}$ ,  $\rho_{PJ}$ , and  $\rho_J$  are essentially equal. The derivation of the simplified form of Equation (67) can be found on pages 83, 84, and 85.

$$\eta_i = \left( \frac{\alpha + \phi}{1 + \alpha} \right) \left( \frac{2 + \phi (1 + \alpha)}{(1 + \phi)^2} \right)$$

(67a)

By utilizing the same assumptions, Equation (66) may now be simplified to

$$\Delta P_{t_{EX_{AV.}}} = \frac{\rho_J \eta_E^J \Delta h_{I_{PJ}} - \Delta P_{t_S}^m}{m + 1} \quad (66a)$$

The excess pressure available at Station M can also be related as

$$\Delta P_{t_{EX_{AV.}}} = P_{t_M} - P_o \quad (68)$$

or

$$P_{t_M} = \Delta P_{t_{EX_{AV.}}} + P_o$$

Next, combining Equations (62) and (65), an equation for the static pressure  $P_M$  at station M may be written as

$$P_M = 2 P_{t_M} - P_I - \frac{\phi \rho_{PJ} V_{PJ}^2 + \rho_{SJ} V_{SJ}^2}{1 + \phi} \quad (69)$$

Now, utilizing Equations (60) through (65), the remaining unknown parameters at Station M can be determined.

It should be noted that the ideal efficiency ( $\eta_i$ ) is modified by experimental data found in Reference 2. The experimental data are presented in a graph relating theoretical efficiency to experimental efficiency and plotted as  $\eta_E/\eta_i = \xi$  versus the velocity ratio ( $\alpha$ ).

#### BLOWING DIFFUSER

The diffuser or diverging channel is a means of converting a velocity head to a pressure head. For maximum efficiency, the flow should be symmetrical and the diffuser expansion angle maintained at less than 15°. Nonadherence to either of these conditions can cause separation in the flow and consequently an increase in pressure loss. The optimum expansion angle is a function of area ratio, surface roughness, and Reynolds number.

The pressure loss in a straight wall conical diffuser may be expressed as the sum of the friction loss and the expansion loss.

$$\Delta P_{t_{D_B}} = \left[ C K_t + \frac{4 f L}{D_M} \right] q_{D_B} \quad (70)$$

For diffuser angles of less than  $30^\circ$ , the contraction loss coefficient is zero. Therefore, the contribution to the diffuser loss by contraction ( $C K_t q_{D_B}$ ) is neglected in this analysis.

The friction factor ( $f$ ) for smooth pipes can be found in Reference 4. For a given relative roughness factor, the friction factor is a function of Reynolds number. An empirical equation which gives accurate results up to Reynolds numbers of  $5 \times 10^6$  is

$$f = \frac{.046}{R_e^{0.2}} \quad (71)$$

The dynamic pressure required to compute the losses is found in the manner similar to the method employed in the suction duct analysis. The weight flow function

$$\frac{W \sqrt{T_t}}{A P_t}$$

is calculated. By using Equation (38), the Mach number  $M$  may be found and used in the solution of Equation (39). This will give the desired dynamic pressure. In the case of the diffuser, the Station  $M$  parameters are employed for the analysis.

The blowing duct is analyzed in the same manner as the suction duct utilizing Equations (34), (35), (37), (38), (39), (40), and (41). An additional loss is the jet loss ( $\Delta P_{t_J}$ ).

$$\Delta P_{t_J} = \frac{1}{2} \rho_J V_J^2 \quad (72)$$



The total blowing system pressure loss is

$$\Delta P_{t_B} = \Delta P_{t_J} + \Delta P_{t_{T_B}} + \Delta P_{t_{F_B}} + \Delta P_{t_{D_B}} \quad (73)$$

Now, the total excess pressure for the jet pump system is

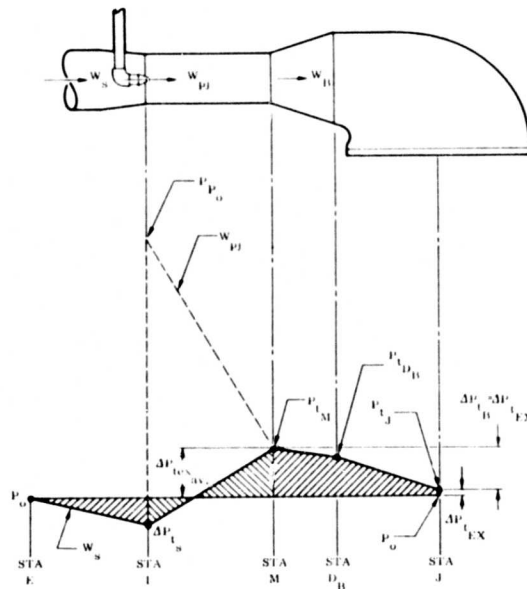
$$\Delta P_{t_{EX}} = \Delta P_{t_{EX_{AV}}} - \Delta P_{t_B} \quad (74)$$

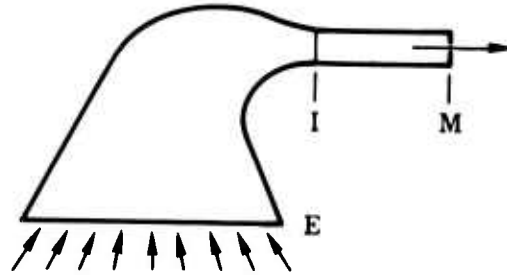
### TOTAL EXCESS PRESSURE AVAILABLE

#### Derivation of Method I

The total excess pressure available is found at Station M (mixing tube exit) and is designated as  $\Delta P_{t_{EX_{AV}}}$ .

the following schematics are presented in conjunction with the analysis. (See below and on page 81.)





$$\Delta h W_{PJ} \eta_E J = \frac{W_S}{\rho_J g} \Delta P_{t_S} + \frac{W_S}{\rho_J g} \Delta P_{t_{EX_{AV}}} + \frac{W_{PJ}}{\rho_J g} \Delta P_{t_{EX_{AV}}} \quad (75)$$

or

$$\Delta h W_{PJ} \eta_E J = \frac{1}{\rho_J g} \left[ W_J \Delta P_{t_S} + W_B \Delta P_{t_{EX_{AV}}} \right]$$

or

$$\Delta h \eta_E J = \frac{1}{\rho_J g} \left[ m \Delta P_{t_S} + (m + 1) \Delta P_{t_{EX_{AV}}} \right]$$

$$\therefore \Delta P_{t_{EX_{AV}}} = \frac{\Delta h \eta_E J \rho_J g - m \Delta P_{t_S}}{m + 1} \quad (76)$$

### Derivation of Method II

The total excess available pressure may also be derived by the following method.

Total avail. = excess available + loss

$$\left(h_{I_{PJ}} - h_o\right) = \left(h_{M_{SJ}} - h_o\right) + \left(h_{M_{PJ}} - h_o\right) + \left(h_{I_{SJ}} - h_o\right)$$

$$\Delta h_{I_{PJ}} = \Delta h_{M_{SJ}} + \Delta h_{M_{PJ}} + \Delta h_{I_{SJ}}$$

$$W \Delta h_{I_{PJ}} = W_{SJ} \Delta h_{M_{SJ}} + W_{PJ} \Delta h_{M_{PJ}} + W_{SJ} \Delta h_{I_{SJ}}$$

$$= \frac{\Delta P_{t_{M_{SJ}}} W_{SJ}}{\rho_M J} + \frac{\Delta P_{t_{M_{PJ}}} W_{PJ}}{\rho_M} + \frac{\Delta P_{t_{I_{SJ}}} W_{SJ}}{\rho_{SJ}}$$

$$J W_{PJ} \Delta h_{I_{PJ}} = \frac{\Delta P_{t_{M_{SJ}}} W_{SJ}}{\rho_M} + \frac{\Delta P_{t_{M_{PJ}}} W_{PJ}}{\rho_M} + \frac{\Delta P_{t_{I_{SJ}}} W_{SJ}}{\rho_{SJ}}$$

Assuming complete mixing,

$$\Delta P_{t_{M_{SJ}}} = \Delta P_{t_{M_{PJ}}} = \Delta P_{t_M}$$

$$\therefore J W_{PJ} \Delta h_{I_{PJ}} = \frac{\Delta P_{t_M}}{\rho_M} [W_{SJ} + W_{PJ}] + \frac{\Delta P_{t_{I_{SJ}}} W_{SJ}}{\rho_{SJ}}$$

$$J W_{PJ} \Delta h_{I_{PJ}} = \frac{\Delta P_{t_M} W_M}{\rho_M} + \frac{\Delta P_{t_{I_{SJ}}} W_{SJ}}{\rho_{SJ}}$$

Dividing by  $W_{PJ}$

$$J\Delta h_{I_{PJ}} = \frac{\Delta P_{t_M}}{\rho_M} (1 + m) + \frac{\Delta P_{t_{I_{SJ}}}^m}{\rho_{SJ}}$$

$$\therefore \Delta P_{t_M} = \Delta P_{t_{EX_{AV}}} + \frac{\rho_M \left( J\Delta h_{I_{PJ}} - \frac{\Delta P_{t_{I_{SJ}}}^m}{\rho_{SJ}} \right)}{m + 1}$$

#### IDEAL EFFICIENCY - Derivation of

Assuming  $\rho_M \neq \rho_J \neq \rho_{SJ} \neq \rho_{PJ}$

The useful power available is given by

$$\eta_i N_o = A_{SJ} V_M (P_{t_M} - P_{t_I}) + A_{PJ} V_M (P_{t_M} - P_o)$$

The impelling power is given by

$$N_o = \Delta h W_{PJ} J$$

$$= A_{PJ} V_{PJ} \left[ \frac{\rho_{PJ}}{2} V_{PJ}^2 - \frac{\rho_{SJ}}{2} V_{SJ}^2 \right]$$

$$\therefore \eta_i = \frac{A_{SJ} V_M (P_{t_M} - P_{t_I}) + A_{PJ} V_M (P_{t_M} - P_o)}{A_{PJ} V_{PJ} \left[ \frac{\rho_{PJ}}{2} V_{PJ}^2 - \frac{\rho_{SJ}}{2} V_{SJ}^2 \right]}$$

For simplification of the analysis, assume

$$P_{t_I} = P_o \quad (\text{No losses in suction})$$

$$\therefore \rho_{PJ} = \rho_{SJ} = \rho$$

Now,

$$\begin{aligned} \eta_i &= \frac{A_{SJ} V_M (P_{t_M} - P_{t_I}) + A_{PJ} V_M (P_{t_M} - P_{t_I})}{A_{PJ} V_{PJ} \left[ \frac{\rho}{2} V_{PJ}^2 - \frac{\rho}{2} V_{SJ}^2 \right]} \\ &= \frac{(A_{SJ} + A_{PJ}) (P_{t_M} - P_{t_I}) V_M}{A_{PJ} V_{PJ} \rho (V_{PJ}^2 - V_{SJ}^2)} \\ &= \frac{V_M A_M (P_{t_M} - P_{t_I})}{A_{PJ} V_{PJ} \rho (V_{PJ}^2 - V_{SJ}^2)} \end{aligned}$$

and, since

$$P_{t_M} = P_M + \frac{1}{2} \rho V_M^2$$

and

$$P_{t_I} = P_I + \frac{1}{2} \rho V_{SJ}^2$$

but

$$\rho_M = \rho_{SJ}$$

$$\therefore P_{t_M} - P_{t_I} = P_M - P_I + \rho \frac{V_M^2 - V_{SJ}^2}{2}$$

Now,

$$\eta_i = \frac{V_M A_M \left( P_M - P_I + \rho \frac{V_M^2 - V_{SJ}^2}{2} \right)}{A_{PJ} V_{PJ} \rho \frac{V_{PJ}^2 - V_{SJ}^2}{2}}$$

Since the densities are assumed to be equal, the continuity may be written as

$$Q = A_{PJ} V_{PJ} + A_{SJ} V_{SJ} = A_M V_M = (A_{PJ} + A_{SJ}) V_M$$

Dividing by  $A_{SJ} V_{PJ}$  and letting

$$\alpha = V_{SJ}/V_{PJ}$$

$$\beta = V_M/V_{PJ}$$

$$\phi = A_{PJ}/A_{SJ}$$

then

$$\frac{Q}{A_{SJ} V_{PJ}} = \phi + \alpha = (\phi + 1) \beta$$

$$\beta = \frac{\phi + \alpha}{\phi + 1}$$

From the momentum equation,

$$(P_M - P_I) A_M = \rho \left( V_{PJ}^2 A_{PJ} + V_{SJ}^2 A_{SJ} \right) - \rho V_M^2 A_M$$

Dividing by  $\rho V_{PJ}^2 A_{SJ}$ ,

$$\frac{P_M - P_I}{\rho V_{PJ}^2} (1 + \phi) = \phi + \alpha^2 - \beta^2 (1 + \phi)$$

Utilizing the equation

$$\beta = \frac{\alpha + \phi}{1 + \phi}$$

we get

$$\frac{P_M - P_I}{\rho V_{PJ}^2} = \frac{\phi + \alpha^2}{1 + \phi} - \left( \frac{\alpha + \phi}{1 + \phi} \right)^2 = \left( \frac{1 - \alpha}{1 + \phi} \right)^2 \phi$$

or

$$P_M - P_I = \rho V_{PJ}^2 \phi \left( \frac{1 - \alpha}{1 + \phi} \right)^2$$

Substituting into the ideal efficiency equation, expanding, collecting, and factoring, the equation reduces to

$$\eta_i = \left( \frac{\alpha + \phi}{1 + \phi} \right) \left[ \frac{2 + \phi (1 + \alpha)}{(1 + \alpha)^2} \right]$$

#### REFERENCES RELATED TO APPENDIX I

1. Kruger, W., Calculations and Experimental Investigations on the Feed Power Requirements of Airplanes with Boundary Layer Control, TM1167, NACA, Washington, D. C., September 1947.
2. Helmbold, H. B., Luessen, G., and Heinrich, A. M., An Experimental Comparison of Constant-Pressure and Constant-Diameter Jet Pumps, Engineering Report No. 147, University of Wichita, Wichita, Kansas, July 1954.
3. Helmbold, H. B., Contributions to Jet Pump Theory, Engineering Report No. 294, University of Wichita, Wichita, Kansas, September 1957.
4. Aerospace Applied Thermodynamics Manual, Society of Automotive Engineers, New York, New York, February 1960.



## APPENDIX II - DIGITAL COMPUTER PROGRAMS

In an effort to take full advantage of all applicable Ryan capabilities in the pursuit of technical research and development of a BLC system for the YCV-2B aircraft, three IBM 704 digital computer programs were initiated. These programs increased the overall analysis by enabling a broader scope of the problem areas to be investigated.

The following text presents these methods in the state existing at the end of contractual work.

### PRIMARY MOTOR PERFORMANCE

This program is basically a data reduction technique utilizing test data to analyze the primary motor performance. The program is limited to the following conditions:

1. Universal gas constant  $R = 53.92 \frac{\text{ft-lb}}{\text{lb-}^\circ\text{R}}$  (for the combustion mixture)
2. Fuel mixture of gasoline and air
3. Specific heat ratio  $k = 1.295$  (for the combustion mixture)

The inputs for this program were the following recorded data from test runs of a motor:

1. Duration of test run
2. Atmospheric pressure
3. Upstream air pressure and temperature
4. Downstream air pressure
5. Combustion chamber pressure

6. Incremental fuel height on sight gage
7. Nozzle throat area and diameter
8. Nozzle exit area

The program will compute and print the following information:

1. Density correction factor  $\sigma\Delta p$
2. Air mass flow
3. Fuel mass flow
4. Fuel to air ratio
5. Corrected combustion chamber temperature
6. Nozzle mass flow
7. Combustion chamber temperature by continuity equation
8. Combustion chamber temperature error
9. Exit pressure
10. Throat velocity
11. Exit velocity
12. Exit temperature
13. Exit temperature using continuity equation
14. Exit temperature error

The following equations are employed in the analysis.

1.  $P_A = P_{\text{gage}} + P_{\text{ATM}}$  gage pressure to absolute pressure
2.  $T_A = T_{\text{gage}} + 460$  gage temperature to absolute temperature
3.  $\Delta P = P_1 - P_2$  differential pressure
4.  $W_a = 3.916 \times 10^{-2} \sqrt{\frac{\Delta P P_1}{T_A}}$  air mass flow
5.  $\omega = .0522 \Delta h$  fuel weight
6.  $W_f = \frac{\omega}{\Delta t}$  fuel weight flow
7.  $F = W_f / W_a$  fuel to air mixture ratio
8.  $\Delta T_{\text{cc}} = -263750 F^2 + 72100 F + 54$  temperature rise due to ideal constant pressure as a function of initial temperature except if  $f = 0$ ,  $\Delta T_{\text{cc}} = 0$
9.  $T_{\text{cc}A} = \Delta T_{\text{cc}} + T_A$  total combustion chamber temperature
10.  $W_{\text{PJ}} = W_f + W_a$  nozzle mass flow
11.  $T_{\text{cc}}' = \frac{.1735 P_{\text{cc}A}^2 D_{\text{ACT}}^4}{W_{\text{PJ}}^2}$  combustion chamber temperature by continuity equation

$$12. \quad \left( \frac{A_t}{A_x} \right)^2 = 19.8 \left( \frac{P_x}{P_{ccA}} \right)^{1.545} - 19.8 \left( \frac{P_x}{P_{ccA}} \right)^{1.773} \quad \text{reduced form of classical nozzle equation}$$

$$13. \quad V_t = 43.65 \sqrt{T_{ccA}} \quad \text{throat velocity}$$

$$14. \quad V_x = 123.5 \sqrt{T_{ccA} \left[ 1 - \left( \frac{P_x}{P_{ccA}} \right)^{0.288} \right]} \quad \text{exit velocity}$$

$$15. \quad T_x = T_{ccA} \left( \frac{P_x}{P_{ccA}} \right)^{0.228} \quad \text{exit temperature}$$

$$16. \quad T_x' = \frac{A_x V_x P_x}{53.92 W_{PJ}} \quad \text{exit temperature using continuity equation}$$

$$17. \quad T_R = \frac{W_{PJ} V_x}{g} + (P_x - P_{ATM}) A_x \quad \text{primary motor thrust}$$

#### INPUT DATA FOR COMPUTER PROGRAM

1.  $\Delta t$ , sec, time
2.  $P_{ATM}$ , psia, atmospheric pressure
3.  $T_A$ , °F, upstream air temperature
4.  $P_1$ , psig, upstream air pressure
5.  $P_2$ , psig, downstream air pressure

6.  $P_{cc}$ , psig, combustion chamber pressure
7.  $A_t$ , in.<sup>2</sup>, nozzle throat area, actual
8.  $A_{PJ}$ , in.<sup>2</sup>, nozzle exit area
9.  $D_{ACT}$ , in., actual throat diameter
10.  $\Delta h$ , in., sight gage fuel height

#### ANALYSIS AND PRINTED OUTPUT

1.  $P_{1A} = P_1 + P_{ATM}$

2.  $P_{ccA} = P_{cc} + P_{ATM}$

3.  $T_{AA} = T_A + 460$

4.  $\Delta P = P_1 - P_2 = P_{1A} - P_{2A}$

5. 
$$\frac{\Delta P \times P_{1A}}{T_{AA}} \quad \text{(PRINTED)}$$

6. 
$$W_a = 3.916 \times 10^{-2} \sqrt{\frac{\Delta P \times P_{1A}}{T_{AA}}} \quad \text{(PRINTED)}$$

7.  $\omega = 0.0522 \Delta h$

8.  $W_f = \omega / \Delta t \quad \text{(PRINTED)}$

9.  $F = W_f / W_a \quad \text{(PRINTED)}$

$$10. \quad \Delta T_{cc} = -263750 F^2 + 72100 F + 54 \text{ for } \Delta h \neq 0 = 0 \text{ for } \Delta h = 0$$

$$11. \quad T_{cc_A} = \Delta T_{cc} + T_{A_A} \quad (\text{PRINTED})$$

$$12. \quad W_{PJ} = W_f + W_a \quad (\text{PRINTED})$$

$$13. \quad T'_{cc} = .1735 P_{cc_A}^2 D_{ACT}^4 / W_{PJ}^2 \quad (\text{PRINTED})$$

$$14. \quad \text{ERROR} = T_{cc_A} / T'_{cc} \quad (\text{PRINTED})$$

$$15. \quad \text{Solution of } P_{PJ} \text{ in}$$

$$\left( \frac{A_t}{A_{PJ}} \right)^2 = 19.8 \left( \frac{P_{PJ}}{P_{cc_A}} \right)^{1.545} - 19.8 \left( \frac{P_{PJ}}{P_{cc_A}} \right)^{1.773} \quad (\text{PRINTED})$$

$$16. \quad V_t = 43.65 \sqrt{T_{cc_A}} \quad (\text{PRINTED})$$

$$17. \quad V_{PJ} = 123.5 \sqrt{T_{cc_A}} \sqrt{1 - \left( \frac{P_{PJ}}{P_{cc_A}} \right)^{0.228}} \quad (\text{PRINTED})$$

$$18. \quad T_{PJ} = T_{cc_A} \left( \frac{P_{PJ}}{P_{cc_A}} \right)^{.228} \quad (\text{PRINTED})$$

$$19. \quad T'_{PJ} = \frac{53.92 W_{PJ}}{A_{PJ} V_{PJ} P_{PJ}} \quad (\text{PRINTED})$$

$$20. \quad \text{ERROR} = T_{PJ}' / T_{PJ} \quad (\text{PRINTED})$$

$$21. \quad T_R = \frac{W_{PJ} V_{PJ}}{g} + (P_{PJ} - P_{ATM}) A_{PJ} \quad (\text{PRINTED})$$

#### COMPUTER PROGRAM WRITE-UP

Since the computer output machines are limited to alphanumeric outputs, all in upper case letters, it is not always feasible to use exactly the same symbols as are used in the text of this report and its appendices. The programming language below is therefore keyed to the List of Symbols in the body of the report by showing the equivalent symbol in the right-hand column.

<u>Programming Language</u>			<u>Symbol Equivalent</u>
1.	RI	read-in area	Not Applicable
2.	RS	storage area	Not Applicable
3.	ERR	array containing names of parameters for error identification	Not Applicable
4.	CASE 1, CASE 2, case no.		Not Applicable
5.	DELT		$\Delta t$
6.	PATM		$P_{ATM}$
7.	TA		$T_A$
8.	P1		$P_1$
9.	P2		$P_2$
10.	PCC		$P_{cc}$

		<u>Symbol Equivalent</u>
11.	AT	$A_t$
12.	AX	$A_{PJ}$
13.	DACT	$D_{ACT}$
14.	DELH	$\Delta h$
15.	WA	$W_a$
16.	WF	$W_f$
17.	WN	$W_{PJ}$
18.	W	$\omega$
19.	F	$F$
20.	TCCA	$T_{cc_A}$
21.	TCCP	$T'_{cc}$
22.	ETCC	$E_{T_{cc}}$
23.	PX	$P_{PJ}$
24.	VT	$V_t$
25.	VX	$V_{PJ}$
26.	TX	$T_{PJ}$
27.	TXP	$T'_{PJ}$
28.	ETX	$E_{T_{PJ}}$
29.	PIA	$P_{1_A}$



		<u>Symbol Equivalent</u>
30.	PCCA	$P_{cc_A}$
31.	TAA	$T_{A_A}$
32.	DELP	$\Delta P$
33.	DPPT	DPPT
34.	DTCC	$\Delta T_{cc}$
35.	PXCC	$P_{PJ/P_{cc_A}}$
36.	DATE 1, DATE 2, date	Not Applicable
37.	I6P refers to the ith ( $i = I6P + 1$ ) group per page	Not Applicable
38.	N no. of cases	Not Applicable

#### Numerical Methods

1. Algebraic solutions of definitive equation
2. Iteration process for  $P_{PJ}/P_{cc_A}$  to tolerance of 0.0000001

#### Program Description

1. Arithmetic mode: Single precession
2. Programming mode: FORTRAN II
3. Table sizes: RI (12), RS (26), ERR (14)
4. Program size: 569<sub>10</sub>
5. Calling sequence: Does not apply

6. Order of programming: In order of definitive equations
7. Program usage: a) Main routine and subroutine, b) standard data card, c) input data (one card per case)
8. Tape usage: Tape 2 - input data, tape 3 - output
9. Subroutine usage: FORTRAN subroutine plus DSEP, CTAPE, TPRINT, and ENDFIL.

#### Limitations

1. Program restrictions: None
2. Error Stops: None. If error occurs, message is printed out, and next case is taken.

#### Time Estimate

1. Computer:  $64 + 5.5 N$  seconds
2. Personnel:
  - a) Process input:  $0.5 N$  minutes
  - b) Run routine:  $64 + 5.5 N$  seconds
  - c) Process output: 2 minutes

#### Output Format

1. See printed output of sample case (pages 98 through 101)

#### Input Format

2. See sample input form entitled "Primary Motor Performance" (Figure 35).

```

C      JOB NO. 1163      ROCKET MOTOR PERFORMANCE
C
C      DIMENSION RI(12),RS(27)
C
C      EQUIVALENCE (CASE1,RS( 1)),(CASE2,RS( 2)),( DFLT,RS( 3)),
1      ( PATM,RS( 4)),( TA,RS( 5)),( DFLH,RS( 6)),
2      ( P1,RS( 7)),( P2,RS( 8)),( PCC,RS( 9)),
3      ( AT,RS(10)),( AX,RS(11)),( DACT,RS(12))
C      EQUIVALENCE ( WA,RS(13)),( WF,RS(14)),( WN,RS(15)),
1      ( F,RS(16)),( TCCA,RS(17)),( TCCP,RS(18)),
2      ( ETCC,RS(19)),( DPPT,RS(20)),( TR,RS(21)),
3      ( PX,RS(22)),( VT,RS(23)),( VX,RS(24)),
4      ( TX,RS(25)),( TXP,RS(26)),( ETX,RS(27))
C
1 FORMAT (A6,A2)
2 FORMAT (7A6,10F6.0)
3 FORMAT (13H1JOB NO. 1163,35X,24HROCKET MOTOR PERFORMANCE,34X,6HDATA
1E ,A6,A2)
4 FORMAT (1H0,6X,4HCASE,8X,5HDEL T,3X,4HPATM,5X,2HTA,5X,5HDEL H,12X,
12HWA,6X,2HWF,6X,2HWN,7X,1HF,5X,4HTCCA,4X,5HTCC-P,3X,5HE-TCC,2X,6HD
2P=P/T,3X,2A6,1X,FA,1,FB,3,FB,1,FB,2,8X,4FB,4,2FB,1,FB,3,FB,2/1H0,3
3X,2HP1,6X,2HP2,6X,3HPCC,5X,2HAT,6X,2HAY,5X,4HDACT,13X,2HTR,6X,2HPX
4,6X,2HVT,6X,2HVX,6X,2HTX,5X,4HTX-P,4X,4HE-TX/1X,FB,2,FB,2,FB,1,3FA
5,4,8X,FB,2,FB,3,4FB,1,FA,3)
C
      CALL START
      CALL CTAPF
      CALL ENDFIL(DUMP)
F      DUMP
C
      RIT 2,1,DATE1,DATE2
S      90 STZ IGP
100 RIT 2,2,(RI(J),J=1,5),1H ,J=7,12),RI(6)
      DO 120 J=1,12
S      CLA RI(J)
S      TPL *110
S      TZF *120
S      110 STO RS(J)
120 CONTINUE
C
      WA = 99.9999
S      STO WF
S      STO WN
S      STO F
      ETCC = 999.999
S      STO PX
S      STO FTX
      DPPT = 9999.99
S      STO TR
      TCCA = 99999.9
S      STO TCCP
S      STO VT
S      STO VX
S      STO TX
S      STO TXP
C
S      CLA PATM
S      TZF *130
S      TMI *130
S      CLA P1

```

```

C      TZF *240
C      TMI *240
      P1A = P1+PATM
C      CLA P2
C      TZF *240
C      TMI *240
      DFLP = P1-P2
C      TZF *240
C      TMI *240
C      CLA PCC
C      TZF *240
C      TMI *240
      PCCA = PCC+PATM
      J = 1
C      TRA *140
130 J = 2
C 140 CLA TA
C      TZF *240
C      TMI *240
      TAA = TA+460.0
      GO TO (150,240).J
150 DPPT = DFLP*P1A/TAA
      WA = 0.03916*DPPT**0.5
C      CLA DFLH
C      TZF *160
C      TMI *240
160 W = 0.0522*DFLH
C      CLA DFLT
C      TZF *240
C      TMI *240
      WF = W/DFLT
      WN = WF+WA
      F = WF/WA
C      CLA DFLH
C      TNZ *166
C      STZ DTCC
C      TRA *167
166 DTCC = (-263750.0*F+72100.0)*F+54.0
167 ICCA = DTCC+TAA
C      CLA DACT
C      TZF *240
C      TMI *240
      ICCP = 0.1735*(PCCA*DACT*DACT/WN)*(PCCA*DACT*DACT/WN)
      ITCC = ICCA/ICCP
C      CLA ICCA
C      TZF *170
C      TMI *240
      ICCS = ICCA**0.5
C      TRA *180
C 170 STZ ICCS
180 VT = 43.65*ICCS
C      CLA AT
C      TZF *240
C      TMI *240
C      CLA AX
C      TZF *240
C      TMI *240
      TMP = (AT/AX)**2/19.8
      IL = 1
      ZI = TMP

```

```

190 Z = Z1**1.1475728*TMP
C 154 Z1
C 155
C 156 STO ABST
11 (ABST-1.0E-7) 230,230,200
200 IF (100-IL) 210,210,220
210 IF (ABST-5.0E-6) 230,230,240
220 Z1 = Z
11 = IL+1
IRA = 190
230 PXCC = 2**0.64724919
PX = PCCA*PXCC
TMP = PXCC**0.228
TX = TCCA*TMP
VX = 123.5*TCOS*(1.0-TMP)**0.5
TX = WN*VX/32.174049+AX*(PX-PATM)
TXP = AX*VX*PX/(53.92*WN)
C 157 CLA TX
C 158 TZF = 240
FTX = TXP/TX
C
C 240 CLA IGP
C 159 TNZ = 250
WOT 3,3,DATE1,DATE2
250 WOT 3,4,(RS(J),J=1,6),(RS(J),J=13,20),(RS(J),J=7,12),(RS(J),J=21,
1 27)
11 (IGP-7) 260,90,90
260 IGP = IGP+1
C 160 IRA = 100
C
END (0,1,1,1,0)

```

JOB NO. 1163    PRIMARY MOTOR PERFORMANCE    DATE 01/08/64

CASE	DEL T	PATM	TA	DEL H		
TEST RUN 18	120.0	14.745	42.0	11.10		
P1	P2	PCC	AT	AX	DACT	
494.60	489.83	447.4	0.0248	0.1333	0.1820	
WA	WF	WN	F	TCCA	TCC-P	E-TCC DP*P/T
0.0862	0.0048	0.0910	0.0560	3768.5	4912.0	0.767 4.84
TR	PX	VT	VX	TX	TX-P	E-TX
15.74	10.856	2679.6	5748.0	1602.3	1695.6	1.058



### BLC JET PUMP PERFORMANCE

This computer program is a technique to reduce jet pump test data quickly and accurately to meaningful performance data. The required inputs are temperatures, pressures, and geometrical parameters. A primary driving motor is also required. The program will compute densities, velocities, dynamic pressures, and mass flows at all significant stations of the jet pump. If a blowing duct is not utilized any positive integers for the blowing duct exit temperature and area should be placed to allow the program to run to completion. The blowing duct loss coefficient (K) can be zero. The static head at the end of the diffuser or mixing tube (whichever is applicable) can be negative. All other inputs must be positive. Inlet conditions are independent of whether a suction duct, bellmouth, or mixing tube is used. If an actual blowing duct is used, blowing momentum and suction volume flow coefficients are computed.

### INPUT DATA FOR COMPUTER

1.  $P_o$ , psi, ambient pressure
2.  $T_o$ , °R, ambient temperature
3.  $\Delta h_{SI}$ , in., inlet static head
4.  $A_I$ , ft<sup>2</sup>, inlet area
5.  $W_{PJ}$ , lb/sec, primary motor mass flow
6. K, —, loss coefficient, blowing duct
7.  $\Delta h_{SXD}$ , in., static head at exit to diffuser or mixing tube
8.  $T_{WXD}$ , °R, wall temperature at exit to diffuser or mixing tube
9.  $T_{CLXD}$ , °R, centerline temperature at exit to diffuser or mixing tube



10.  $\Delta h_{TXD}$ , in. , dynamic exit head, diffuser or mixing tube
11.  $A_{XD}$ ,  $\text{ft}^2$  exit area of diffuser or mixing tube
12.  $\rho_o$ ,  $\text{lb/ft}^3$ , freestream density
13.  $V_o$ ,  $\text{ft/sec.}$  , freestream velocity
14.  $T_{BX}$ ,  $^{\circ}\text{R}$ , blowing exit temperature
15.  $A_{BX}$ ,  $\text{ft}^2$ , blowing exit area
16.  $(s/c)_B$ , —, blowing slot width to wing chord
17.  $S_B/S_S$ , —, wing area ratio, blowing to suction

#### OUTPUT AND ANALYSIS

1.  $\rho_{SI} = \frac{2.699 P_o}{T_o}$ ,  $\text{lb/ft}^3$ , static inlet density
2.  $V_I = C \sqrt{\frac{276.84 \Delta h_{SI}}{\rho_{SI}}}$ ,  $\text{ft/sec}$ , inlet velocity
3.  $W_{SJ} = \rho_{SI} V_I A_I$ ,  $\text{lb/sec}$ , secondary or entrained flow
4.  $m_1 = \frac{W_{SJ}}{W_{PJ}}$ , , entrainment ratio based on inlet duct and primary motor

5.  $m_2 = \frac{W_{MD} - W_{PJ}}{W_{PJ}}$ , entrainment ratio based on mixing duct-diffuser and primary motor
6.  $E_m = \frac{m_1}{m_2}$ , error
7.  $\rho_{BX} = \frac{P_{t_{BX}} + \sqrt{P_{t_{BX}}^2 - \frac{3.316 T_{BX} W_{BX}^2}{A_{BX}^2}}}{106.70 T_{BX}}$ , lb/ft<sup>3</sup>, density at exit to blowing duct
8.  $V_{BX} = \frac{W_{BX}}{\rho_{BX} A_{BX}}$ , ft/sec, velocity at exit to blowing duct
9.  $q_{BX} = \frac{\rho_{BX} V_{BX}^2}{64.3481}$ , lb/ft<sup>2</sup>, dynamic pressure at exit to blowing duct
10.  $q_o = 0.5 \rho_o V_o^2$ , lb/ft<sup>2</sup>, freestream dynamic pressure
11.  $C_\mu = 2 (s/c)_B q_J / q_o$ , blowing momentum coefficient
12.  $C_{QS} = (S_B / S_S) \left( \frac{1}{1 + \frac{1}{m}} \right) \left( \frac{V_J}{V_o} \right) \left( \frac{P_J}{\rho_o} \right) (s/c)_B$ , suction air volume coefficient
13.  $\rho_{MD} = \frac{2.699 P_{SXD}}{T_{MD}}$ , lb/ft<sup>3</sup>, density at end of mixing tube
14.  $V_{MD} = \sqrt{\frac{(334.752 \Delta h_{t_{XD}} + .827 \Delta h_{SXD})}{\rho_{MD}}}$ , ft/sec, velocity at end of mixing tube

15.  $W_{MD} = \rho_{MD} V_{MD} A_{XD}$ , lb/sec, mass flow at end of mixing tube
16.  $T_{MD} = T_{WXD} + .33 \left( T_{C_{LXD}} - T_{WXD} \right)$ , OR, average temperature at end of mixing tube
17.  $P_{SXD} = P_{AMB} - .02986 \Delta h_{SXD}$ , psi, static pressure at end of mixing tube or diffuser depending on input  $\Delta h_{SXD}$
18.  $T_{JP} = \frac{W_{MD} V_{MD}}{g} + 144 \left( P_{SXD} - P_{ATM} \right) A_{XD}$ , lb, jet pump thrust
19.  $q_J = q_{BX}$ , lb/ft<sup>2</sup>, blowing exit dynamic pressure
20.  $q_{MD} = \frac{\rho_{MD} V_{MD}^2}{64.3481}$ , lb/ft<sup>2</sup>, dynamic pressure at end of mixing tube
21.  $P_{t_{XD}} = 144 P_{SXD} + q_{MD}$ , lb/ft<sup>2</sup>, total pressure at end of diffuser
22.  $P_{t_{BX}} = P_{t_{XD}} - K q_{MD}$ , lb/ft<sup>2</sup>, total pressure at end of diffuser

#### COMPUTER PROGRAM WRITE-UP

Since the computer output machines are limited to alphanumeric outputs, all in upper case letters, it is not always feasible to use exactly the same symbols as are used in the test of this report and its appendices. The programming language below is therefore keyed to the List of Symbols in the body of the report by showing the equivalent symbol in the right-hand column.

<u>Programming Language</u>			<u>Equivalent Symbol</u>
1.	RI	read in area	Not Applicable
2.	RS	storage area	Not Applicable
3.	CASE	case no.	Not Applicable
4.	PAMB		$P_o$
5.	TAMB		$T_o$
6.	TWXD		$T_{WXD}$
7.	TCLXD		$T_{CLXD}$
8.	TBX		$T_{BX}$
9.	WN		$W_{PJ}$
10.	AI		$A_I$
11.	AXD		$A_{XD}$
12.	ABX		$A_{BX}$
13.	RH $\bar{O}O$		$\rho_o$
14.	VO		$V_o$
15.	DHSI		$\Delta h_{SI}$
16.	DHTXD		$\Delta h_{TXD}$
17.	DHSXD		$\Delta h_{SXD}$
18.	FK		K
19.	SCB		$(s/c)_B$

<u>Programming Language</u>		<u>Equivalent Symbol</u>
20.	SBSS	$s_B/s_S$
21.	RHOSI	$\rho_{SI}$
22.	VI	$v_I$
23.	WSS	$w_{SJ}$
24.	FM1	$m_1$
25.	FM2	$m_2$
26.	EM	$E_m$
27.	RHOBX	$\rho_{BX}$
28.	VBX	$v_{BX}$
29.	QBX	$q_{BX}$
30.	QO	$q_o$
31.	CMU	$C_\mu$
32.	CQS	$C_{QS}$
33.	RHOMD	$\rho_{MD}$
34.	VMD	$v_{MD}$

Programming LanguageEquivalent Symbol

35.	WMD	$W_{MD}$
36.	TMD	$T_{MD}$
37.	PSXD	$P_{SXD}$
38.	PTXB	$P_{t_{BX}}$
39.	PTXD	$P_{t_{xDi}}$
40.	QMD	$q_{MD}$
41.	DATE 1, DATE 2    date	Not Applicable
42.	I6P      refers to the ith ( $i = I6P + 1$ ) group per page	Not Applicable
43.	N          no. of cases	Not Applicable

Numerical Methods

1. Algebraic solution of definitive equations

Program Description

1. Arithmetic mode: Single precession
2. Programming mode: FORTRAN II
3. Table sizes: RI (18) , RS (43)
4. Program size:  $547_{10}$
5. Calling sequence: Does not apply
6. Order of programming: In order of definitive equations

7. Program usage: a) Main routine and subroutine, b) standard data card, c) input data (two cards per case)
8. Tape usage: Tape 2 - input data  
Tape 3 - output data
9. Subroutine usage: FORTRAN subroutine plus DSEP, CTAPE, TPRINT, and ENDFIL.

#### Limitations

1. Program restrictions: None
2. Error stops: None

#### Time Estimate

1. Computer:  $63 + 6.5 N$  seconds
2. Personnel:
  - a) Process input: N minutes
  - b) Run routine:  $63 + 6.5 N$  seconds
  - c) Process output: 2 minutes

#### Input/Output Formats

1. Input: See input form
2. Output: See output print out

#### OUTPUT

$$\rho_{SI} = \text{static inlet density, lb/ft}^3$$

$$V_I = \text{inlet velocity, ft/sec}$$

$W_{SJ}$  = secondary or entrained flow, lb/sec

$m_1$  = entrainment ratio based on inlet duct and nozzle data

$m_2$  = entrainment ratio based on mixing duct-diffuser and nozzle data

$E_M$  = error between  $M_1$  and  $M_2$  based on  $M_1/M_2$

$\rho_{BX}$  = density at exit to blowing duct, lb/ft<sup>3</sup>

$V_{BX}$  = velocity at exit to blowing duct, ft/sec

$q_{BX}$  = dynamic pressure at exit to blowing duct, lb/ft<sup>2</sup>

$q_o$  = freestream dynamic pressure, lb/ft<sup>2</sup>

$C_\mu$  = blowing momentum coefficient

$C_{QS}$  = suction air volume flow coefficient

$\rho_{MD}$  = density at end of mixing tube, lb/ft<sup>3</sup>

$V_{MD}$  = velocity at end of mixing tube, ft/sec

$W_{MD}$  = mass flow at end of mixing tube, lb/sec

$T_{MD}$  = temperature at end of mixing tube, °R

$P_{SXD}$  = static pressure at end of mixing tube or diffuser depending on  
input  $\Delta h_{SXD}$



## DISTRIBUTION OF LIFT, SHEAR, BENDING MOMENT AND TORSION

In the initial phases of work done in establishing computer techniques for analysis of the wing augmented with a jet pump BLC system, a program (Ryan digital program 1148) which calculated the distribution of the two-dimensional lift coefficients was written. This distribution was put into an existing program (Ryan digital program 1048) that utilized the finite step method of solution outlined in NACA TN 2011 to determine the spanwise distribution of lift, shear and bending moment of the three dimensional wing. The spanwise distribution of torsion and wing pitching moment are determined from the two-dimensional lift output of the 1148 program, plus use of chord-wise pressure distributions estimated from theoretical values presented in NACA Report 634 and experimental results shown in NACA Report 633 and Fairchild Report R246-006. The procedure for determining the torsion and pitching moment of the wing is similar to that presented in NACA RMA55D07. This procedure has been incorporated into the computer program. To eliminate additional time required for the complete analysis, the 1048 program and the 1148 program have been integrated into what hereafter is referred to as the 1148 program.

### Purpose of Computer Program 1148

There were four basic reasons for initiating the digital computer program 1148. They are:

1. To calculate two-dimensional lift coefficients for flapped airfoils under the influence of suction or blowing type boundary layer control.
2. To provide section lift characteristics as a function of spanwise location for a given wing geometry and flap configuration.
3. To provide section lift characteristics for input to program section calculating span loading by the finite-step method for determination of three-dimensional lift coefficient and shear and moment characteristics.
4. To provide a method of evaluating slipstream contribution to lift through the derivation of a pseudo two-dimensional effect of slipstream on lift.

## Definition of Terms

Section Lift:

$$C_{\ell_{TOT}} = C_{\ell_{\Gamma}} + C_{\ell_R}$$

$$C_{\ell_{\Gamma}} = \text{circulation lift}$$

$$C_{\ell_R} = \text{reaction lift}$$

and

$$C_{\ell_{\Gamma}} = C_{\ell_{P.F.}} + \Delta C_{\ell_S} + \Delta C_{\ell_B} + \Delta C_{\ell_{\Gamma_{S.S.}}}$$

$$C_{\ell_R} = \Delta C_{\ell_{R_B}} + \Delta C_{\ell_{R_{S.S.}}}$$

where

$$C_{\ell_{P.F.}} = \text{theoretical potential flow lift}$$

$$\Delta C_{\ell_S} = \text{suction induced circulation lift}$$

$$\Delta C_{\ell_B} = \text{blowing induced circulation lift}$$

$$\Delta C_{\ell_{\Gamma_{SS}}} = \text{slipstream induced circulation lift}$$

$$\Delta C_{\ell_{R_B}} = \text{blowing momentum reaction lift}$$

$$\Delta C_{\ell_{R_{SS}}} = \text{direct thrust lift}$$

**Geometry:**

$S$  = wing area

$S_B$  = wing area under influence of blowing flap

$S_S$  = wing area under influence of suction flap

$b$  = wing span

$\eta_\gamma$  = wing spanwise location as decimal fraction of wing semi-span

$t/c$  = airfoil thickness to chord ratio

$C_{f/c}$  = ratio of flap chord to airfoil chord

$s/c$  = ratio of BLC system slot width to airfoil chord

$\epsilon$  = wing twist angle

$i_\omega$  = incidence of wing root chord referenced to fuselage longitudinal axis

$\bar{c}$  = wing mean aerodynamic chord

$\delta_j$  = angle between upper surface of airfoil trailing edge and airfoil chord line

$D_P$  = propeller diameter

$X_3$  = distance between propeller disc and wing quarter chord location

$\eta_T$  = spanwise location of propeller centerline

## AERODYNAMICS AND BLC

$\alpha_g$  = angle between fuselage longitudinal axis and relative wing

$\alpha$  = section zero lift angle of attack

$C_{Q_S}$  = BLC suction system quantity airflow coefficient

$C_\mu$  = BLC blowing system momentum flow coefficient

$T$  = propeller thrust

$A_P$  = propeller disc area

$D_{SS}$  = slipstream diameter at wing quarter-chord

$T_C$  = thrust coefficient

$X_{SS}$  = distance between wing station under consideration and thrust centerline

$F_1, F_t/F_1, F_o/F_1$  = incorporated in program as tables of look-up. (See plots in Figures 36 and 37.)

$N_{SS}$  = exponent used in  $K'_{SS}$  equation

NUM = numerator of expression for A as used in  $K'_{SS}$  equation.

### Equations - Basic

$$1. \quad C_{l_{PF}} = k_t \times F_1 \times \left[ \sin \alpha + \frac{F_t}{F_1} \sin \delta_F + \frac{F_1}{F_o} \sin \delta_J \right]$$

where

$$k_t = 1 + \left( .7488 \frac{t}{c} \right) (1 + .00375 \delta_j)$$

$$2. \quad \Delta C_{l_S} = k_t \times k_S \times C_{Q_S}$$

where

$$\begin{aligned} k_S = & \left[ 7.16 + (18.6) (C_f/c) + (16.6) (C_f/c)^2 \right] \\ & - \left[ .0408 - (.114) (C_f/c) + (.1095) (C_f/c)^2 \right] \delta_F \\ & + \left[ 2.22 - (7.64) (C_f/c) + (7.23) (C_f/c)^2 \right] (10^{-4}) (\delta_F)^2 \end{aligned}$$

$$3. \quad \Delta C_{l_B} = C_{l_r} - C_{l_{PF}}$$

where

$$C_{l_r} = k_t \times F_1 \times \left[ \sin \alpha + \frac{F_T}{F_1} \sin \delta_F + \frac{F_O}{F_1} \sin \delta_j \right]$$

$$4. \quad \Delta C_{l_{r_{SS}}} = (C_{l_{PF}})_{\text{THRUST} \neq 0} - (C_{l_{PF}})_{\text{ZERO THRUST}}$$

where

$$(C_{l_{PF}})_{\text{THRUST} \neq 0} = K_{SS} C_{l_{PF}}$$

and

$K_{SS}$  = ratio of local slipstream dynamic pressure to free-stream dynamic pressure (calculation shown under secondary equations below)

$$5. \quad \Delta C_{l_{RB}} = C_{\mu_{te}} \sin \phi_2$$

where

$$C_{\mu_{te}} = .97 C_{\mu}$$

and

$$\phi_2 = \alpha_g + i_{\omega} + \epsilon + \delta_F + \delta_j$$

$$6. \quad \Delta C_{l_{SS}} = (\text{To be defined - See page 134})$$

At present, direct thrust lift is calculated on a three-dimensional basis from following equation:

$$\Delta C_{l_{SS}} = C_T' \frac{F}{T} \sin (\theta + \alpha_p) \text{ as presented in Ryan Report 62B046}$$

#### EQUATIONS - SECONDARY

$$\alpha = \alpha_g + i_{\omega} - \alpha_{o_l} + \epsilon$$

$$q_o = \frac{1}{2} \rho_o V_o^2$$

$$q_{SS} = q_o + \frac{T}{A_p}$$

$$T_C = \frac{T}{(2) q_o D_P^2}$$

$$D_{SS} = \left[ \frac{1+\alpha}{1+s} \right]^{1/2} (D_P)$$

where

$$\alpha = \frac{1}{2} \left[ \left( 1 + \frac{8 T_C}{\pi} \right)^{1/2} - 1 \right]$$

and

$$s = \alpha \left[ 1 + \frac{1}{\sqrt{\frac{D}{2 X_3} + 1}} \right]$$

$$\eta_{D_{SS}} = \frac{D_{SS}}{b/2}$$

$$X_{SS} = \left[ \eta_T - \eta_{SS} \right]$$

$$K'_{SS} = \frac{1}{1 + 10^N (A X_{SS})^{N+1}}$$

where

$$A = \frac{NUM}{\eta_{D_{SS}}}$$

and therefore N and NUM are chosen so as to produce the desired slipstream spanwise distribution.

$$K_{SS} = 1 + K'_{SS} (q_{SS}/q_o - 1)$$

## PROGRAM PHILOSOPHY

The program objectives were not completely defined at the start of programming. Results of concurrent investigations and analyses gave rise to the need for modifying the basic equations and increasing the scope of the program objectives.

In anticipation of such modifications and objective extensions, the program utilizes a matrix form for data input. The input matrix has been designated as the G -matrix. This matrix consists of 20 rows of 10 columns each. Of the 200 available locations, only 98 are committed currently. Therefore, further expansion of the program is possible.

The program is so written that various spanwise flap configurations may be studied. The method of defining flap parameters is explained under "Input Matrix".

In addition, control cards must be provided to establish the extent of investigations and to provide additional data where necessary. Control card coding is explained under "Control Cards".

## INPUT MATRIX

A copy of the input matrix form is included in this discussion (see Figure 36). Pertinent wing geometry and flight conditions are entered. All inputs must be in floating point notation, i. e. , must include the decimal point.

Those locations which defined the flap configuration are rows 3, 4, 5, 6, 7, 8, 11, and 12; all columns (1 through 10) in each of these rows are included. Therefore, it is possible to have as many as 10 distinct flaps per wing semispan.

## Restrictions

Flap must be listed in the input matrix in order from inboard flap at column 1 to outboard flap at column N where N is the number of flap areas required to extend the full semispan. Unflapped regions must also be accounted for so that the relationship

$$G(3, I) + G(4, I) = G(3, I + 1)$$

is maintained.



An exception to this rule is in the case of an inboard flap whose inboard edge is coincidental with the fuselage line. In such case,

$$G(3, 1) + G(4, 1) + G(14, 1) = G(3, 2)$$

In addition to containing geometry and flight parameters, the input matrix contains information for program logic commands.

These logic commands are contained in locations

$$G(14, 3) \text{ and } G(14, 4)$$

The value of  $G(14, 3)$  is dictated by the number of flap areas per semispan. If full span flaps are not utilized, unflapped areas must also be included, as stipulated in note (below).

The value of  $G(14, 4)$  is dictated by the number of spanwise points desired for the investigation within the following limits:

- If  $G(14, 4) = 1.0$ , no meaningful data will be obtained with program in current status.
- If  $1.0 < G(14, 4) \leq 10$ , each flap span will be divided into a number of equal parts as determined by the value of  $G(14, 4)$ .
- If  $G(14, 4) > 10$ , the entire wing semispan is divided into a number of equal parts, as determined by the value of  $G(14, 4)$ .

Section lift characteristics are calculated at each of these divisions.

Note:

For incorporation of the results of this program into the "Finite-Step Method For Calculation of Span Loading" program, the value of  $G(14, 4)$  cannot exceed 40.0.

## CONTROL CARDS

The control cards are used in this program to perform the following functions:

1. Supply annotation for output
2. Dictate disposition of results
3. Revise normal point routine.

The control cards (Figures 39, 40, 41, 42, and 43) utilize columns 1 through 3 of the input card.

Column 1 of the control card determines the nature of the card, as follows:

<u>No. in Column 1</u>	<u>Function</u>
1	Supplies comments to be printed on two-dimensional output. No coding required in columns 2 and 3
2	Performs commands as dictated by values in columns 2 and 3
3	Supplies comments to be printed on three-dimensional output
4	Supplies additional data required by three-dimensional program

<u>No. in Column 2</u> (Used only with 2 in Col. 1)	<u>Function</u>
0	Prints only changes to G-matrix for each case with results
1	Prints entire G-matrix for each case with results

Column 2 of control card:

1. Zero or blank indicates this is not end of a set of cases.
2. One indicates the end of a set of cases.

The two-dimensional program leaves two blank cards between each case of punched output. These cards must be removed before these cards can be used in the three-dimensional program.

<u>No. in Column 3</u> (Used only with 2 in Col. 1)	<u>Function</u>
0	Does not store two-dimensional output on tape
1	Stores two-dimensional output on tape for use as input to three-dimensional program

The number 2 in column 1 indicates control card. Column 3 of the control card has two alternatives:

1. A zero or blank indicates no punch-out for the three-dimensional program
2. A number 1 indicates punched cards for the three-dimensional program

The number 3 in column 1 indicates comment card for punched data. Comment must be in columns 2 - 25 if analysis is for parametric study of full span flaps  $\{G(14,3) = 1\}$ ; otherwise, columns 2 - 72 can be used  $\{G(14,3) > 1\}$ .

The number 4 in column 1 indicates that additional data cards are required, as specified by the three dimensional program.

#### DATA CARD

The data card for the three-dimensional program is not punched by the two-dimensional program and should be requested.

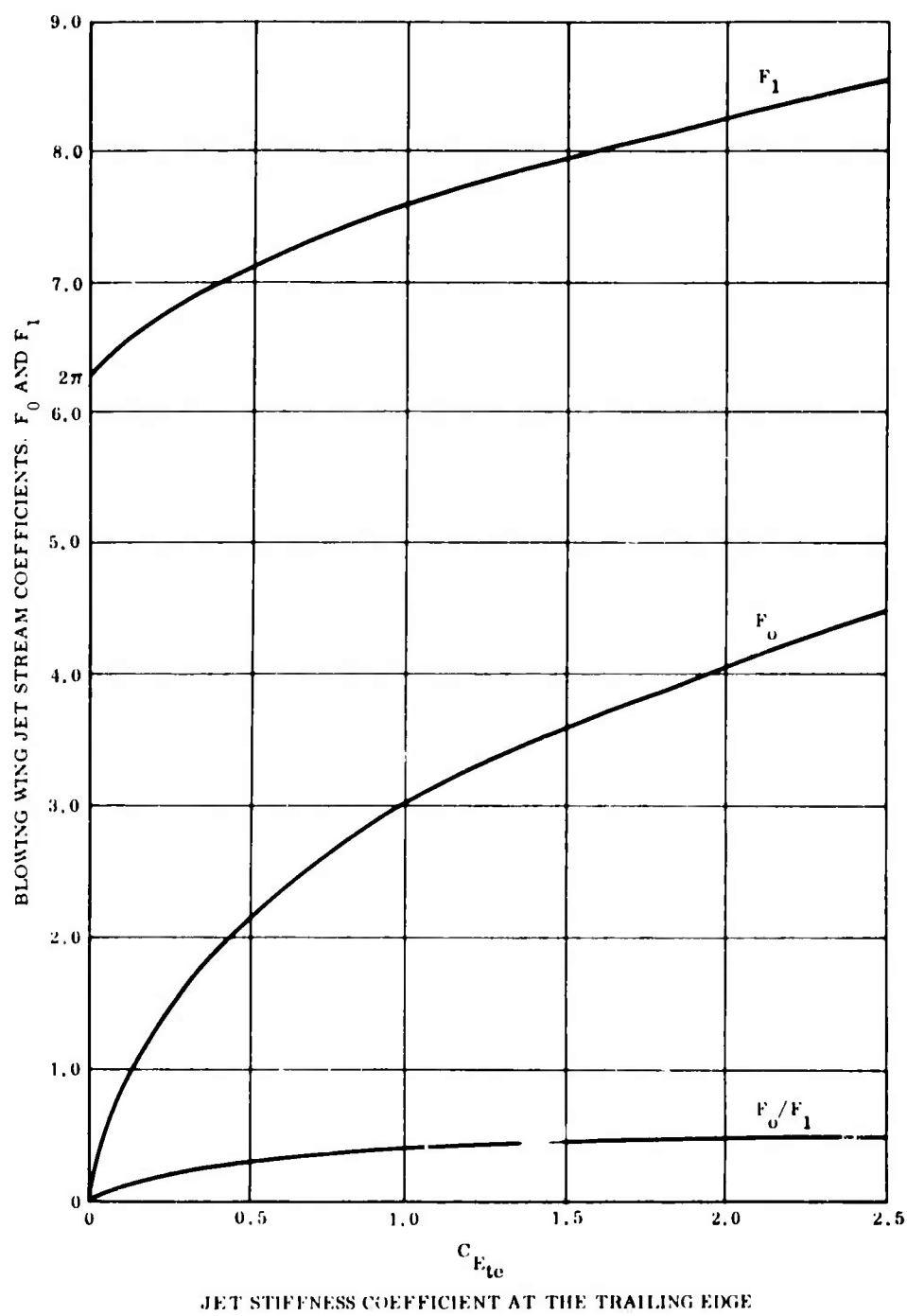


Figure 36. Blowing Wing Coefficient - Look-Up Values

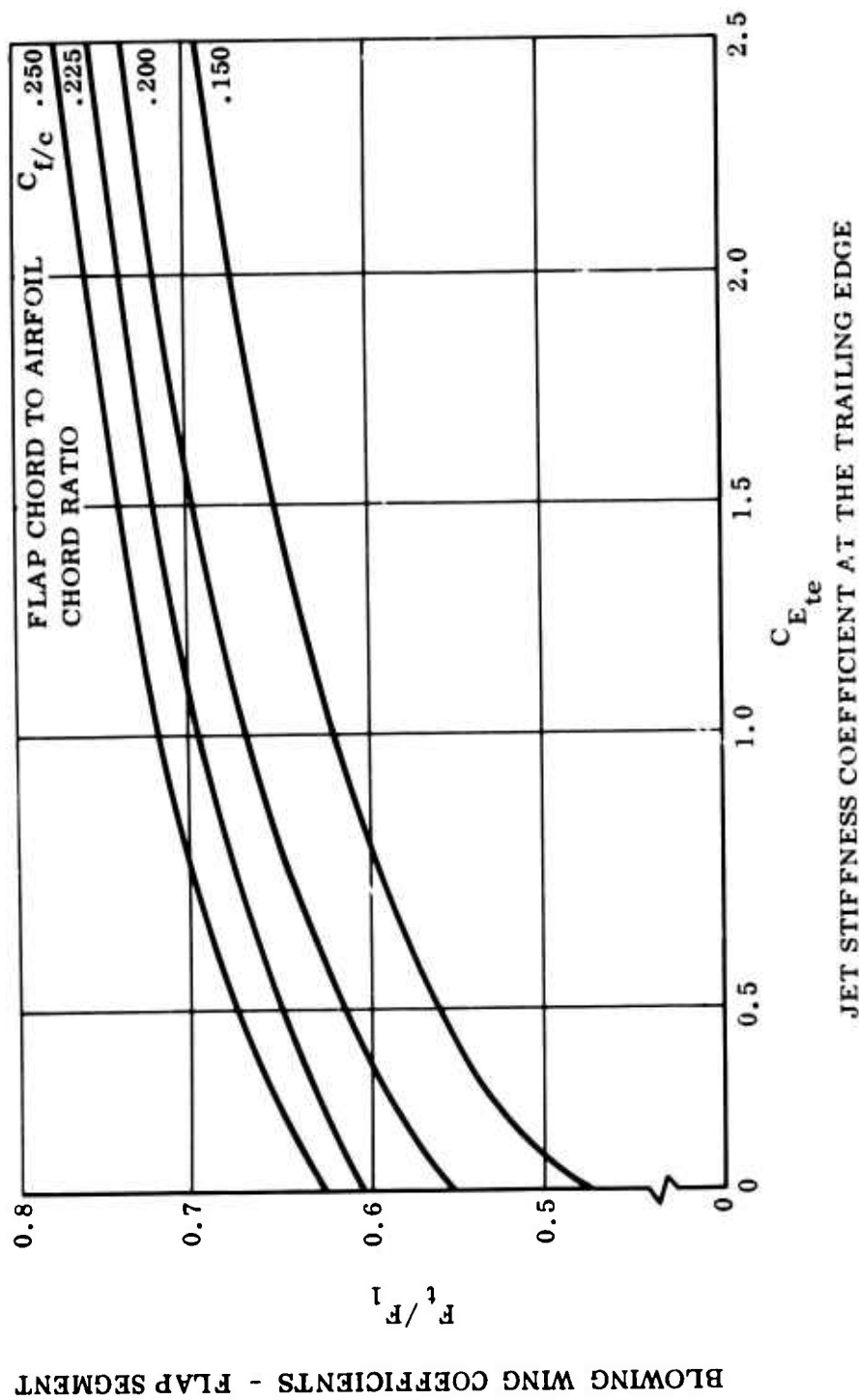


Figure 37. Blowing Wing Coefficient - Look-Up Values

BLC AIRFOIL LIFT DATA BASIC G-MATRIX

	1	2	3	4	5	6	7	8	9	10
1	$\alpha_g$ (deg)	$S_w$ (ft <sup>2</sup> )	b (ft)	AR	$i_w$ (deg)	$\bar{C}$ (ft)				
2	V <sub>FPS</sub>	$\rho$ slugs/ft <sup>3</sup>	thrust (lbs)	prop dia (ft)	X.3 (ft)	$\eta_T$	N <sub>SS</sub>	NUM. (AD <sub>SS</sub> )		
3	$\eta_1$	$\eta_2$	$\eta_3$	$\eta_4$	$\eta_5$	$\eta_6$	$\eta_7$	$\eta_8$	$\eta_9$	$\eta_{10}$
4	$\Delta\eta_1$	$\Delta\eta_2$	$\Delta\eta_3$	$\Delta\eta_4$	$\Delta\eta_5$	$\Delta\eta_6$	$\Delta\eta_7$	$\Delta\eta_8$	$\Delta\eta_9$	$\Delta\eta_{10}$
5	$\delta_{F_1}$ (deg)	$\delta_{F_2}$ (deg)	$\delta_{F_3}$ (deg)	$\delta_{F_4}$ (deg)	$\delta_{F_5}$ (deg)	$\delta_{F_6}$ (deg)	$\delta_{F_7}$ (deg)	$\delta_{F_8}$ (deg)	$\delta_{F_9}$ (deg)	$\delta_{F_{10}}$ (deg)
6	$C_{F/C_1}$	$C_{F/C_2}$	$C_{F/C_3}$	$C_{F/C_4}$	$C_{F/C_5}$	$C_{F/C_6}$	$C_{F/C_7}$	$C_{F/C_8}$	$C_{F/C_9}$	$C_{F/C_{10}}$
7	(S/C) <sub>1</sub>	(S/C) <sub>2</sub>	(S/C) <sub>3</sub>	(S/C) <sub>4</sub>	(S/C) <sub>5</sub>	(S/C) <sub>6</sub>	(S/C) <sub>7</sub>	(S/C) <sub>8</sub>	(S/C) <sub>9</sub>	(S/C) <sub>10</sub>
8	$S_{F_1}$ (ft <sup>2</sup> )	$S_{F_2}$ (ft <sup>2</sup> )	$S_{F_3}$ (ft <sup>2</sup> )	$S_{F_4}$ (ft <sup>2</sup> )	$S_{F_5}$ (ft <sup>2</sup> )	$S_{F_6}$ (ft <sup>2</sup> )	$S_{F_7}$ (ft <sup>2</sup> )	$S_{F_8}$ (ft <sup>2</sup> )	$S_{F_9}$ (ft <sup>2</sup> )	$S_{F_{10}}$ (ft <sup>2</sup> )
9										
10										
11	$C_{QS_1}$	$C_{QS_2}$	$C_{QS_3}$	$C_{QS_4}$	$C_{QS_5}$	$C_{QS_6}$	$C_{QS_7}$	$C_{QS_8}$	$C_{QS_9}$	$C_{QS_{10}}$
12	$C_{\mu_1}$	$C_{\mu_2}$	$C_{\mu_3}$	$C_{\mu_4}$	$C_{\mu_5}$	$C_{\mu_6}$	$C_{\mu_7}$	$C_{\mu_8}$	$C_{\mu_9}$	$C_{\mu_{10}}$
13										
14	$\eta_f$	S <sub>OBS</sub> (ft <sup>2</sup> )	Nu	# of incre.						
15										
16										
17										
18										
19										
20										

Figure 38. Input Matrix Format



# CONTROL CARD

1	2	3	4	5	6	7	8	9	10	11	12	13	14	15	16	17	18	19	20	21	22	23	24	25	26	27	28	29	30	31	32	33	34	35	36									
$\eta$ BREAK																		$(\tau b/2)$																				CARD 1						
																		2		9		.		7																				
																		(SLOPE)		(INTERCEPT)																								
$u/c$																		0 . 0		. 1 7 5																		CARD 2						
$\delta_j$																		0 . 0		1 6 . 0																		CARD 3						
$\sigma_{I=0}$																		0 . 0		- 3 . 0																		CARD 4						
$\epsilon$																		0 . 0		0 . 0																		CARD 5						
																		1 0 0 . 0																				CARD 6						
$u/c$																		- . 0 0 0 3 5 4 0 0 6 5 2 5		1 5 6 4 0 6 5 3																		CARD 7						
$\delta_j$																		. 0 1 5 6 4 7 2 2 6		1 5 . 5 3 5 2 7 7																		CARD 8						
$\sigma_{I=0}$																		- . 0 1 2 5 0 2 2 7 6		- 2 . 6 1 9 7 7 2 4																		CARD 9						
$\epsilon$																		- 0 . 0 4 6 9 4 1 6 7 9		1 . 3 9 4 1 6 7 9																		CARD 10						

The above card defines the wing geometry as it pertains to  $t/c$ ,  $\delta_j$ ,  $\alpha_{l=0}$ , and  $\epsilon$  as a function of wing span location. The card is added to the back of the basic deck.

$t/c$  = thickness/chord ratio

$\delta_j$  = trailing edge angle (upper surface  $\omega/R$  chord line)

$\alpha_{l=0}$  = section zero lift angle

$\epsilon$  = wing twist angle (referenced to root chord incidence angle)

Figure 40. Control Card



PAGE \_\_\_\_\_ OF \_\_\_\_\_  
DATE \_\_\_\_\_

(ANNOTATION FOR 2-D AND 3-D PROGRAM OUTPUT)

	MODEL	SYSTEM	NO. FLAP SETTING	CONFIGURATION	V = MPH	T = LBS.
1						
2						
3						
4						
5						
6						
7						
8						
9						
10						
11						
12						
13						
14						
15						
16						
17						
18						
19						
20						
21						
22						
23						
24						
25						
26						
27						
28						
29						
30						
31						
32						
33						
34						
35						
36						
37						
38						
39						
40						
41						
42						
43						
44						
45						
46						
47						
48						
49						
50						
51						
52						
53						
54						
55						
56						
57						
58						
59						
60						
61						
62						
63						
64						
65						
66						
67						
68						
69						
70						
71						
72						
73						
74						
75						
76						
77						
78						
79						
80						
81						
82						
83						
84						
85						
86						
87						
88						
89						
90						
91						
92						
93						
94						
95						
96						
97						
98						
99						
100						

THIS PORTION OF ANNOTATION IS  
SUPPLIED BY PROGRAM

- 3245 - D. MEX. 2/68

**Figure 41. Comment 2 Control Cards**

$\delta$	$C_{F/C}=.1$	$C_{F/C}=.2$	$C_{F/C}=.3$	$C_{F/C}=.4$	$C_{F/C}=.5$	$C_{F/C}=.6$	$C_{F/C}=.7$	$C_{F/C}=.8$	$C_{F/C}=.9$	$C_{F/C}=1.0$
0	.3	.48	.61	.70	.77	.835	.88	.93	.965	1.0
10	.295	.455	.57	.65	.725	.78	.84	.91	.95	
20	.26	.395	.50	.58	.655	.72	.79	.86	.93	
30	.21	.335	.44	.52	.570	.64	.72	.81	.91	
40	.19	.30	.375	.44	.485	.55	.63	.76	.88	
50	.182	.275	.325	.37	.420	.48	.58	.69	.87	
60	.175	.25	.30	.33	.37	.425	.53	.67	.86	
70	.168	.23	.285	.31	.335	.38	.49	.66	.852	
80	.161	.22	.27	.30	.315	.35	.46	.655	.846	
90	.155	.21	.26	.29	.310	.345	.45	.650	.843	1.0

Figure 42. Look-Up Card for Plain Flaps

$\frac{\alpha}{\delta}$	$C_{F/C}=.1$	.2	.3	.4	.5	.6	.7	.8	.9
0	.38	.525	.625	.7	.775	.835	.835	.93	.965
10	.35	.485	.57	.64	.71	.77	.83	.88	.94
20	.34	.455	.54	.61	.69	.75	.82	.87	.935
30	.315	.43	.505	.58	.65	.72	.785	.855	.93
40	.295	.40	.47	.535	.61	.68	.75	.83	.915
50	.275	.355	.41	.475	.54	.62	.69	.78	.875
60	.210	.29	.35	.415	.48	.56	.64	.735	.845
70	.180	.25	.31	.37	.43	.51	.59	.685	.81
80	.170	.23	.28	.335	.405	.47	.545	.65	.77
90	.160	.20	.25	.30	.37	.45	.535	.64	.75

Figure 45. Look-Up Card for Single Slotted Flaps

The following discussion presents the method of analysis used to obtain the wing torsion. This portion has been added subsequent to the original initiation of the computer program and does not necessarily represent the best procedure or method. Time limitations did not permit a full investigation of the span of possible methods which might be employed.

Look up card data have been provided for data used in the computer analysis. (See pages 140 and 141.) Terms peculiar to the computer program, their sources, and form have also been given. (See pages 133, 134, and 135.)

Let

$$C_M' = \left[ \text{Torsion Coefficient} \right] = \frac{\text{Torsion}}{qS\bar{c}} \quad \left( \frac{\text{ft-lb}}{\text{lb-ft}} \right)$$

$$= C_{M\Gamma}' + C_{M_{RSS}}' + C_{M_{RB}}'$$

$$C_M = \frac{\text{Running Torsion}}{qc^2} \quad \left( \frac{\text{ft-lb/ft}}{\text{lb/ft}^2 \text{ft}^2} \right) = \frac{\text{Running Torsion Coefficients}}$$

$$C_{M\Gamma}' = \frac{1}{2} \int_{\eta=1}^{\eta} \frac{c}{\bar{c}^2} C_{M\Gamma} d\eta = \frac{\overline{AR}^2}{2} \int_{\eta=1}^{\eta} \frac{c}{b^2} C_{M\Gamma} d\eta$$

$$CM_{\Gamma} = \left( C_{M_o} \right) + \left( \Delta C_{M_o} \right)_{\delta_F} + \left( \frac{C_M}{C_l} \right) C_l$$

$\left( C_{M_o} \right)$  - Aerodynamic pitching moment coefficient of local airfoil due to camber; measured relative to local airfoil aerodynamic center.

$\left( \Delta C_{M_o} \right)_{\delta_F}$  - Aerodynamic pitching moment coefficient of local airfoil due to flap deflection measured with respect to local airfoil aerodynamic center.

$$\left(\frac{C_M}{C_l}\right) = \frac{\partial C_M}{\partial C_l} - \text{Rate of change in moment coefficient with change in local lift coefficient measured about reference line specified for torsion computations}$$

$C_l$  - Local lift coefficient including effects of tip vortices.

$C_{M_o} \sim$  Zero lift moment coefficient of wing

$$C_{M_o} = \overline{AR}^2 \int_{\eta=1}^{\eta} \left(\frac{c}{b}\right)^2 \left[ \left(C_{M_o}\right) + \left(\Delta C_{M_o}\right)_{\delta_F} \right] d\eta \text{ for complete wing}$$

$$= 2 \left[ C_M' - \frac{AR}{2} \int \frac{c^2}{b^2} \left(\frac{C_M}{C_l}\right) (C_l) d\eta \right]$$

$C_M \sim$  Wing total pitching moment coefficient

$$C_M = 2 C_M' \text{ at } \eta = 0$$

$$C_M' = \frac{\overline{AR}^2}{2} \int_{\eta=1}^{\eta} \left\{ \left(\frac{c}{b}\right)^2 \left[ \left(C_{M_o}\right) + \left(\Delta C_{M_o}\right)_{\delta_F} \right] + \left(\frac{c}{b}\right) \left(\frac{C_l}{b}\right)_{3-D} \right\} d\eta$$

where

$$\left(\Delta C_{M_o}\right)_{\delta_F} = \left(C_{\eta_b}\right)_{\delta_F} \left\{ \left[ C_{M_{c/4}} / \left(C_{\eta_b}\right)_{\delta_F} \right] + \left[ \left(\frac{x_{a.c.}}{c}\right)_{\text{Local}} - .25 \right] \right\}$$

and

$$\left(C_{\eta b}\right)_{\delta_F} = \left(\Delta C_{l_r}\right)_{\delta_F, 2-D} \left[ \frac{\sqrt{(E - \sin \delta_F)^2 + 1 + E (\cos \delta_F - 1.0)^2}}{1 + E (\cos \delta_F - 1.0)} \right]$$

<u>TERM</u>	<u>SOURCE</u>	<u>FORM</u>
$\left(C_{m_o}\right)$	2-D Program Table of Look-Up	CMO [Slope (J, 14), Intercept (J, 15)]
$\left[\left(\frac{X_{a.c}}{c}\right)_{local} - .25\right]$	2-D Program Table of Look-Up	[Slope (J, 16), Intercept (J, 17)]
$\left[\left(C_{m_{c/4}}\right) / \left(C_{\eta b}\right)_{\delta_F}\right]$	2-D Program Table of Look-Up	[ ] = f (E, $\delta_F$ )
$\left(\Delta C_{l_r}\right)_{\delta_F, 2D}$	2-D Program Output	CLGAM (For condition ALPHA = 0.0)
E, $C_F/C$	2-D Program Input	G (6, -)
$\delta_F$	2-D Program Input	G (5, -)
C	2-D Program Table of Look-Up	CLOC Slope (J, 10), Intercept (J, 11)
b	2-D Program Input	G (1, 3)
l	2-D Program Table of Look-Up	Slope (J, 18), Intercept (J, 19)
AR	2-D Program Input	G (1, 4)

<u>TERM</u>	<u>SOURCE</u>	<u>FORM</u>
$\left(\frac{C C_l}{b}\right)_{3-D}$	3-D Program Output	CL * C/B (For 2-D Input Cond.)
$C_{l_R}$	2-D Program Output	CLR
$C'_{M_R} = C_{M_{R_{SS}}} + C'_{M_{R_B}}$		
$= \frac{AR^2}{2} \int_{\eta=1}^{\eta=0} \frac{c}{b} C_{l_R} \left\{ \frac{l}{b} + \frac{c}{b} \left[ \left( \frac{x_{ac}}{c} \right)_{local} - .25 - (.75 - E) \right] \right\} d\eta$		
$+ \frac{AR}{2} C'_T \frac{F}{T} \text{Cox} (\theta + \alpha_p) \frac{z}{b}$		
$C_{l_R} = C_{l_{R_B}} + C_{l_{R_{SS}}}$		
$C_{l_{R_B}} = 2\text{-D Program Output, CLR}$		
$C_{l_{R_{SS}}} = \frac{\Delta A}{A} C'_T \frac{F}{T} \text{Sin} (\theta + \alpha_p)$		

where

$$A = \frac{\pi D_{SS}^2}{4}$$

$$\Delta A = C_z dy \quad dy = d\eta \cdot \frac{b}{2}$$

$$C'_T = \frac{\eta T}{q_o S}$$

**q<sub>o</sub> = QFS in 2-D Program**

### S = G (1, 2) in 2-D Program

$$\frac{F}{T} = \text{FOVT in 2-D Program}$$

$\theta$  = THETAR in 2-D Program

$$\alpha_p = \text{ALFAPR in 2-D Program}$$

**Z = Input to 2-D Program**

**D<sub>SS</sub> = DSS in 2-D Program**

## PROCEDURE

**For each span station  $\eta$ :**

1. Determine type of flap by:
  - a. Suction flap if value other than zero for input G(11, -).
  - b. Blowing flap if value other than zero for input G(12, -).
  - c. No BLC if both G(11, -) and G(12, -) are either zero or blank. If no BLC, determine type of flap by G(9, 1) =
    - 0 for split flap
    - 1 for plain flap
    - 2 for single slotted flap
    - 3 for double slotted flap
2. Determine:
 

$D_{l\alpha}$ ,  $\alpha$  hypothetical for input to 3-D program for input condition



3. Set ALPHA = 0.0 and solve for

$$\text{CLGAM DF} = \text{CLGAM for ALPHA} = 0$$

$$\text{CLR DF} = \text{CLR for ALPHA} = 0$$

$$\text{CLRSS DF} = \text{CLRSS for ALPHA} = 0$$

4. Determine TORK 0 by

$$\text{TORK } 0 = \frac{\overline{\text{AR}}^2}{2} \left( \frac{c}{b} \right)^2 C_{m_0}$$

where

$$\text{AR} = \text{G}(1, 4)$$

$$b = \text{G}(1, 3)$$

$$c = f(\eta) = \text{CLOC} \left[ \text{Slope}(\text{J}, 10), \text{intercept}(\text{J}, 11) \right]$$

$$C_{m_0} = f(\eta) = \text{CMO} \left[ \text{Slope}(\text{J}, 14), \text{intercept}(\text{J}, 15) \right]$$

5. Determine TORK DF by:

$$\text{TORK DF} = \text{CLGAM DF} \left[ \frac{\sqrt{(E - \sin \delta_F)^2 + [1 + E (\cos \delta_F - 1.0)]^2}}{1 + E + (\cos \delta_F - 1.0)} \right]$$

$$* \frac{\overline{\text{AR}}^2}{2} \left( \frac{c}{b} \right)^2 * \left\{ \left[ \frac{C_{m_{c/4}}}{C_{\eta_b \delta_F}} \right] \right.$$

$$\left. + \left[ \left( \frac{X_{ac}}{c} \right)_{\text{Local}} - .25 \right] \right\}$$

Note: Store for 3-D Program print-out

6. Determine TORK RB by

$$\text{TORK RB} = \text{CLRDF} * \frac{\overline{\text{AR}}^2}{2} * \frac{c}{b} * \text{CLR DF} \\ * \left\{ \frac{l}{b} + \frac{c}{b} \left[ \left( \frac{X_{ac}}{c} \right)_{\text{Local}} - .25 \right] - (.75 - E) \right\}$$

Note: Store for 3-D Program print-out

7. Determine TORK RSS by:

$$\text{TORK RSS} = \frac{\overline{\text{AR}}^2}{2} * \frac{c}{b} * \text{CLRSS DF} \\ * \left\{ \frac{l}{b} + \frac{c}{b} \left[ \left( \frac{X_{ac}}{c} \right)_{\text{Local}} - .25 \right] - (.75 - E) \right\} \\ + \frac{\text{AR}}{2} C'_T \left( \frac{F}{T} \right) \cos (\theta + \alpha_p) \frac{z}{b}$$

Note: Store for 3-D Program print-out

8. Store for 3-D Program Usage

- a. Table:  $l = f(\eta)$  [Slope (J, 18), intercept (J, 19)]
- b.  $S = G(1, 2)$
- c.  $b = G(1, 3)$
- d. QFS

9. Using  $C_{l_\alpha}$  and  $\alpha_{\text{hypothetical}}$  from step 2 above, determine  $CL * C/B$  and other 3-D program outputs

10. Determine [LIFT TORK] by

$$[\text{LIFT TORK}] = \left(\frac{l}{b}\right) * [CL * (C/B)]$$

from 3-D Program

11. Determine TORK 0 COEFF by

$$\text{TORK 0 COEFF} = \int_{\eta=1.0}^{\eta} \text{TORK 0 } d\eta \quad (\text{See Figure 44.})$$

From 3-D Program

12. Determine TORK DF COEFF by

$$\text{TORK DF COEFF} = \int_{\eta=1.0}^{\eta} \text{TORK DF } d\eta$$

13. Determine TORK RB COEFF by

$$\text{TORK RB COEFF} = \int_{\eta=1.0}^{\eta} \text{TORK RB } d\eta$$

14. Determine TORK RSS COEFF by

$$\text{TORK RSS COEFF} = \int_{\eta=1.0}^{\eta} \text{TORK RSS } d\eta$$

15. Determine LIFT TORQ COEFF by

$$\text{LIFT TORK COEFF} = \int_{\eta=1.0}^{\eta} \text{LIFT TORK } d\eta$$

16. Determine TORSION by

$$\text{TORSION} = q S^2 / b * 12 * \sum \text{TORK COEFF}$$

17. T - GAM T = TORSION -  $\left[ \text{LIFT TORK COEFF} * q * (S^2/b) * 12 \right]$

$$18. \quad \text{GAM T/GAM L} = \frac{|\text{LIFT TORK COEFF}| \times \bar{C} \times 12}{C_L}$$

$$= \frac{|\text{LIFT TORK COEFF}| * \bar{C} * 12}{|\text{BIG CL} / (\text{B/CAV})| * \text{AR}}$$

<sup>6</sup>	<sup>8</sup>	<sup>8</sup>	<sup>8</sup>	<sup>8</sup>	<sup>8</sup>	<sup>8</sup>	<sup>4</sup>	<sup>8</sup>
2y/B	COEFF TORK O	COEFF TORK DF	COEFF TORK RB	COEFF TORK DSS	COEFF LIFT TORK	TORSION	T-GAM. T	GAM. T/ GAML IN.
						IN-LB	IN.	

### Figure 44. Tork Coefficients

# LOOK-UP CARD FOR TORSION ANALYSIS

$$\left[ C_{m_{c/4}} / \left( C_{\eta_b} \right)_{\delta_F} \right] = f (C_F/C, \delta_F)$$

## SINGLE SLOTTED FLAP - BLC OFF

$\delta_F$	$C_F/C = .15$	$C_F/C = .20$	$C_F/C = .25$	
10	-.443	-.406	-.368	} ATTACHED
20	-.432	-.398	-.364	
30	-.419	-.387	-.354	
40	-.403	-.372	-.340	
50	-.384	-.352	-.318	} TRANSITION
60	-.353	-.318	-.286	
65	-.339	-.305	-.273	
70	-.328	-.293	-.259	} SEPARATED
80	-.305	-.266	-.230	
90	-.280	-.237	-.199	

## PLAIN FLAP - BLC OFF

$\delta_F$	$C_F/C = .15$	$C_F/C = .20$	$C_F/C = .25$
10	-.419	-.393	-.368
20	-.419	-.392	-.369
30	-.407	-.384	-.361
40	-.390	-.367	-.344
50	-.367	-.343	-.320
60	-.340	-.316	-.292

**SUCTION FLAP - BLC ON - ATTACHED**

$\delta_F$	$C_F/C = .15$	$C_F/C = .20$	$C_F/C = .25$
15	-.415	-.390	-.364
30	-.402	-.375	-.349
45	-.380	-.349	-.325
60	-.349	-.315	-.288
75	-.312	-.275	-.248
90	-.272	-.234	-.204

**BLOWN FLAP - BLC ON - ATTACHED**

$\delta_F$	$C_F/C = .15$	$C_F/C = .20$	$C_F/C = .25$
30	-.426	-.388	-.352
45	-.404	-.367	-.332
60	-.375	-.340	-.305
75	-.344	-.308	-.274
90	-.310	-.274	-.240

## OPERATING PROCEDURES

I Titles	BLC Airfoil Lift Data	(1148)
----------	-----------------------	--------

## Finite Step Method for Calculation of Span Loading (1048)

<u>II Originator</u>	J. Burich	Programmer	T. Paulson
	R. Gusky		R. Dickie

III Set-up      Have program tape already mounted (rewound) on drive 1.  
During execution, tapes 4 through 7 will also be expected.  
Place data deck into card reader. (First card must be "\*1148"  
or "\*1048".)

Ready card reader.  
Hit "Clear" key.  
Hit "Load Tape" key.  
Card reader will require an end-of-file.  
While output is being printed, only tape 6 is needed.  
Normal completion of the program is indicated by a program-stop  
after printing a console-scoop.

IV Hardware IBM 704 (32K, floating-trap)  
on-line card reader  
on-line printer  
on-line card punch  
tape drives 1, 4, 5, 6 and 7.

V Time Estimate = 4 minutes per case.  
(-1, if there is a "LIFT ONLY" control card)  
(-1, if there is a "NO TORQUE" control card)  
(x 2, if there is a "CALALPHA" control card)

VI Wrap up Return program tape to file.  
Telephone user, announcing completion of task.

APPENDIX III - SYSTEM OF EQUATIONS FOR THE SOLUTION  
OF TWO-DIMENSIONAL MIXING FLOW OF CONCENTRIC  
STREAMS OF FLUIDS

In general, prediction of fluid/dynamics behavior is one of considerable complexity in all but the simplest cases. In a jet pump system, there exists the problem of mixing of concentric streams. Many approximations have been made on similar systems, but all are limited in range and application owing to complexity. Before an attempt can be made to optimize a jet pump for BLC application, a sound theoretical approach is necessary. The following is a possible approach which could satisfy the theoretical requirements.

The symbols used in this appendix are shown separately herein, for the convenience of the reader. Their choice has been made to agree with the conventions of Cartesian and cylindrical coordinate systems in order to preserve the generality of the concept.

$x, y, z$  - Cartesian coordinates

$r, \theta, z$  - Cylindrical coordinates

$\bar{R}, \bar{\theta}, \bar{Z}$  - Body forces in cylindrical coordinates

$u, v, w$  - Velocities in  $x, y$ , and  $z$  directions

$V_r, V_\theta, V_z$  - Velocities in  $r, \theta$ , and  $z$  directions ;

$t$  - Time

$\rho$  - Density (mass)

$\mu$  - Viscosity (dynamic)

$$\frac{D}{Dt} = \frac{\partial}{\partial t} + V_r \frac{\partial}{\partial r} + \frac{V_\theta}{r} \frac{\partial}{\partial \theta} + V_z \frac{\partial}{\partial z}$$



$$\text{DIV. } \mathbf{V} = -\frac{1}{r} \frac{\partial(r V_r)}{\partial r} + \frac{1}{r} \frac{\partial V_\theta}{\partial \theta} + \frac{\partial V_z}{\partial z}$$

If a section of the jet pump is considered as one of a closed surface drawn at some arbitrary point and if the fluid is assumed to be in continuous motion, then the mass within the section at any time interval must equal the excess of mass that flows in over the mass that flows out, or in equation form:

$$\frac{\partial \rho}{\partial t} + \frac{\partial(\rho u)}{\partial x} + \frac{\partial(\rho v)}{\partial y} + \frac{\partial(\rho w)}{\partial z} = 0 \quad (1)$$

In cylindrical coordinates, the equation can be expressed as

$$\frac{\partial \rho}{\partial t} + \frac{1}{r} \frac{\partial(\rho V_r r)}{\partial r} + \frac{1}{r} \frac{\partial(\rho V_\theta)}{\partial \theta} + \frac{\partial(\rho V_z)}{\partial z} = 0 \quad (2)$$

When the second law of motion, which states that the sum of the forces acting on an enclosed fluid mass is equal to the time rate of change of the linear momentum, is considered, a set of equations can be generated. They can be expressed mathematically in cylindrical coordinates by three equalities, which are as follows:

$$\begin{aligned} \frac{DV_r}{Dt} = & R + \frac{V_\theta^2}{r} - \frac{1}{\rho} \frac{\partial \rho}{\partial r} + \frac{1}{\rho} \frac{\partial}{\partial r} \left[ \mu \left( \frac{2 \partial V_r}{\partial r} - \frac{2}{3} \text{DIV. } \mathbf{V} \right) \right] \\ & + \frac{1}{\rho r} \frac{\partial}{\partial \theta} \left[ \mu \left( \frac{1}{r} \frac{\partial V_r}{\partial \theta} + \frac{\partial V_\theta}{\partial r} - \frac{V_\theta}{r} \right) \right] + \frac{1}{\rho} \frac{\partial}{\partial z} \left[ \mu \left( \frac{\partial V_r}{\partial z} + \frac{\partial V_z}{\partial r} \right) \right] \\ & + \frac{2\mu}{\rho r} \left( \frac{\partial V_r}{\partial r} - \frac{1}{r} \frac{\partial V_\theta}{\partial \theta} - \frac{V_r}{r} \right) \end{aligned} \quad (3)$$

$$\begin{aligned}
\frac{D V_{\theta}}{Dt} = & \bar{\theta} - \frac{V_r V_{\theta}}{\rho} - \frac{1}{r\rho} \frac{\partial P}{\partial \theta} + \frac{1}{r\rho} \frac{\partial}{\partial \theta} \left[ \mu \left( \frac{2}{r} \frac{\partial V_{\theta}}{\partial \theta} - \frac{2}{3} \text{DIV. } V \right) \right] \\
& + \frac{1}{\rho} \frac{\partial}{\partial z} \left[ \mu \left( \frac{1}{r} \frac{\partial V_z}{\partial \theta} + \frac{\partial V_{\theta}}{\partial z} \right) \right] + \frac{\partial}{\partial r} \left[ \mu \left( \frac{1}{r} \frac{\partial V_r}{\partial \theta} + \frac{\partial V_{\theta}}{\partial r} - \frac{V_{\theta}}{r} \right) \right] \\
& + \frac{2\mu}{\rho r} \left[ \frac{1}{r} \frac{\partial V_r}{\partial \theta} + \frac{\partial V_{\theta}}{\partial r} - \frac{V_{\theta}}{r} \right] \quad (4)
\end{aligned}$$

$$\begin{aligned}
\frac{D V_z}{Dt} = & \bar{z} - \frac{1}{\rho} \frac{\partial \rho}{\partial z} + \frac{1}{\rho} \frac{\partial}{\partial z} \left[ \mu \left( 2 \frac{\partial V_z}{\partial z} - \frac{2}{3} \text{DIV. } V \right) \right] \\
& + \frac{1}{\rho r} \frac{\partial}{\partial r} \left[ \mu r \left( \frac{\partial V_r}{\partial z} + \frac{\partial V_z}{\partial r} \right) \right] + \frac{1}{\rho r} \frac{\partial}{\partial \theta} \left[ \mu \left( \frac{1}{r} \frac{\partial V_z}{\partial \theta} + \frac{\partial V_{\theta}}{\partial z} \right) \right] \quad (5)
\end{aligned}$$

If the assumptions are made that the flow is axially symmetrical, that the temperature and density are constant, that viscosity is negligible, and that the body forces are zero, then the above five equations can be reduced to the following three:

$$\frac{\partial V_r}{\partial r} + \frac{V_r}{r} + \frac{\partial V_z}{\partial z} = 0 \quad (6)$$

$$\frac{\partial V_r}{\partial t} + V_r \frac{\partial V_r}{\partial r} + V_z \frac{\partial V_r}{\partial z} = -\frac{1}{\rho} \frac{\partial \rho}{\partial r} \quad (7)$$

$$\frac{\partial V_z}{\partial t} + V_r \frac{\partial V_z}{\partial r} + V_z \frac{\partial V_z}{\partial z} = -\frac{1}{\rho} \frac{\partial \rho}{\partial z} \quad (8)$$

Solution of these three equations is possible with  $V_r$ ,  $V_z$ , and  $P$  as the unknowns and with  $r$  and  $z$  as the independent variables.

An exact analytical solution to these equations is questionable, but they do lend themselves to a numerical-type solution. Once the equations are set up on a computer and solutions are obtained, a number of pump sizes and variations could be run with a considerable saving in time and effort over experimental development of similar cases. There are also the advantages that equations can be used to predict the effect of different flow parameters on the overall pumping characteristics and that they can be modified to show more complex flows.

## APPENDIX IV - SMOKE TUNNEL TESTS

### SMOKE TUNNEL

The flow characteristics about six airfoil sections, representative of the BLC-adapted Caribou wing and tail sections, were investigated in the Ryan smoke tunnel with tests conducted during November and December 1963. The purpose of the tests was to evaluate the effectiveness of varying amounts of suction and blowing for increasing lift and controllability of the Caribou.

#### Description of the Test Items

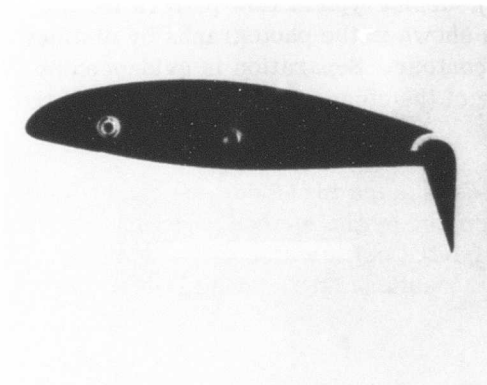
All of the six airfoils tested were scaled-down sections representative of either the Caribou wing or the horizontal tail. Each of the test items was 1.9 inches wide (span), so as to fit snugly between the walls of the smoke tunnels. The individual sections tested were:

1. Inboard suction flap airfoil;  $t/c = .17$ ;  $c_F/c = .255$ ;  $s/c = .02$
2. Outboard suction flap airfoil;  $t/c = .15$ ;  $c_F/c = .225$ ;  $s/c = .02$
3. Blowing flap airfoil;  $t/c = .17$ ;  $c_F/c = .1885$ ;  $s/c = .0175$ ; drooped leading edge
4. Blowing aileron airfoil;  $t/c = .15$ ;  $c_F/c = .195$ ;  $s/c = .015$
5. Blowing elevator airfoil;  $t/c = .125$ ;  $c_F/c = .40$ ;  $s/c = .0026$
6. Suction elevator airfoil;  $t/c = .125$ ;  $c_F/c = .40$ ;  $s/c = .0051$

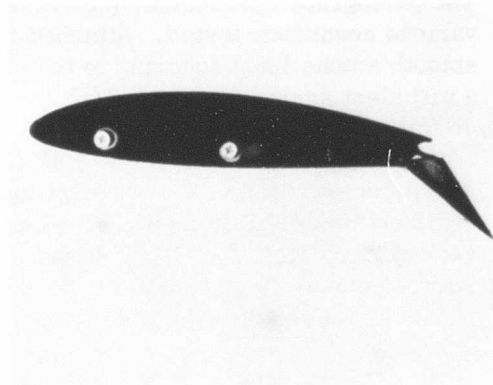
Figure 45 shows the models tested.

#### DATA ACQUISITION

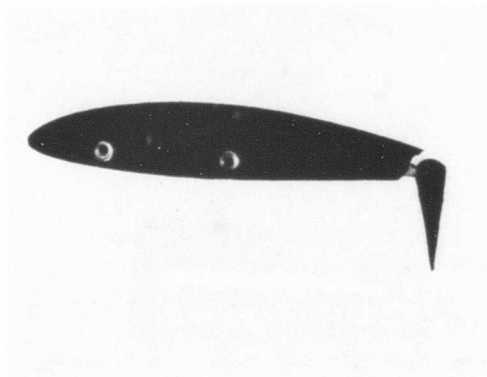
Two forms of data were obtained: (1) visual evidence of flow attachment and separation and (2) lift estimates, obtained through measurement of flow lines displacement.



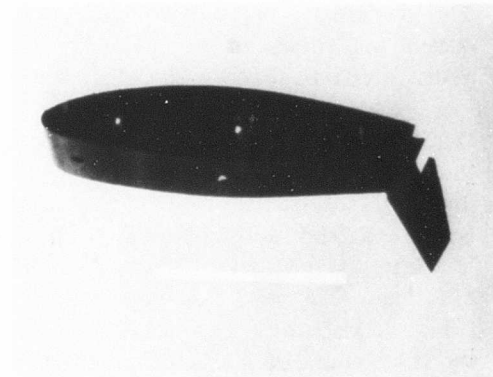
SK-171-0008 Blowing Airfoil Flap



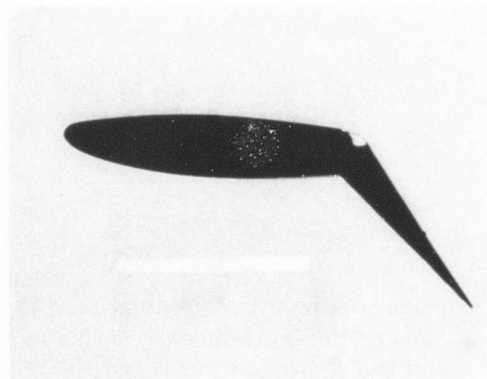
SK-171-0008 Suction Airfoil Flap



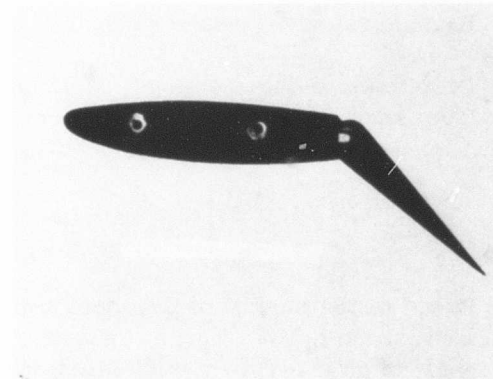
SK-171-0009 Blowing Aileron Airfoil



SK-171-0009 Suction Flap Airfoil



SK-171-00010 Blowing Elevator Airfoil



SK-171-0010 Suction Elevator Airfoil

Figure 45. Model Airfoils Tested

The photographs presented, (see Figure 59), depict typical flow pattern for the various conditions tested. Attached flow is shown in the photographs by distinct smooth smoke lines adhering to the airfoil contour. Separation is evidenced by a turbulent smoke pattern and/or departure of the adjacent smoke lines from the airfoil contour.

A brief description of the corresponding tests is given in the corresponding List of Illustrations. Lift coefficients were estimated by the method given in "A Theoretical Investigation on the Determination of Lift Coefficients in Two Dimensional Smoke Tunnels", Princeton University, Aeronautical Engineering Dept., Report No. 289, which gives the following formula:

$$C_{l\Gamma} = A (1 + \Delta) \tan \theta$$

The streamline angular displacement,  $\theta$ , was measured with the aid of a transparent protractor at a point 1/2 chord length forward of the airfoil leading edge, and it was measured with reference to the direction of flow in the tunnel.

Qualitative data can be readily obtained when the above method is used. Such is the case of lift induced by angle of attack and reasonably so for the case of lift due to flap deflection. However, when angle of attack and flap deflection are combined, the method becomes so reliant upon theory as to negate its value for obtaining quantitative lift data. The use of boundary layer control and/or the existence of partial flow separation further complicates the analysis. An additional shortcoming of smoke tunnel tests is the low Reynolds number at which the tests must be operated. At the higher Reynolds number, boundary layer does not build up as rapidly as at very low Reynolds number, and so either BLC requirements for a particular lift increment are lessened or greater lift may be achieved for a particular BLC setting. In any event, the effect of the low Reynolds number requires conservatism in the use of test results.

Despite these shortcomings, much useful information can be and was obtained from smoke tunnel testing. Because of the difficulty in accurately determining  $\Delta$  for each individual test point, lift is represented in the analysis by the term

$$\left[ C_{l\Gamma} / (1 + \Delta) \right] .$$

Based on the method of the above reference, a value for the term A was chosen to correspond to lift acting at the quarter chord, so that for incremental lift due to angle of attack,  $\Delta$  is negligible. However,  $\Delta$  is of the order of 0.4 for incremental lift due to flap deflection and BLC, provided the increase lift due to flap

deflection does not introduce leading edge stall characteristics. The presence of leading edge stall will increase the value of  $\Delta$ .

#### DATA ANALYSIS

Lift data are presented in the figures in the form of plots depicting

$$\left[ C_{l_T} / (1 + \Delta) \right]$$

versus angle of attack. These data illustrate qualitatively how BLC increases the lift capability and control effectiveness of the airplane. Some quantitative evaluation of the data could be achieved by a point-by-point evaluation of  $\Delta$ . However, there is little to warrant an extensive study of this nature.

The data presented herein are qualitative in nature. The test results selected for presentation are from those test conditions that will give the greater representation of the effects of boundary layer control applied to the airfoil configurations tested.

#### FIFTEEN-PERCENT-THICK SUCTION FLAP AIRFOIL

For the takeoff design condition,  $\delta F \approx 50^\circ, 60^\circ$ , almost fully attached flow is evidenced at  $C_{QS} = 0.04$  (lowest  $C_Q$  tested), whereas with flaps deflected  $80^\circ$  and  $90^\circ$ , appreciable flow attachment was not incurred except at  $C_Q > 0.04$ . However, at  $C_Q = .11$  (second point tested), fully attached flow was evidenced. The photograph indicates that the combination of large suction ( $C_Q = .265$ ) and very low tunnel velocity (10 fps) produced reversed flow over the flap and recurrence of separation. When lift is increased by flow attachment over the flap, the incremental lift due to angle of attack deteriorates, indicating a leading edge stall condition. However, as  $C_{QS}$  is increased beyond the requirement for flow attachment over the flap, the lift increment due to angle of attack is partially recovered, indicating that the added suction induces reattachment of the leading edge bubble.

#### SEVENTEEN-PERCENT-THICK SUCTION FLAP AIRFOIL

The above discussion is applicable to the 17-percent-thick section with the exception that with flaps deflected  $80^\circ$  or  $90^\circ$ , higher  $C_{QS}$  was required to induce flow attachment than was the case for the 15-percent-thick section.

#### SEVENTEEN-PERCENT-THICK BLOWING FLAP AIRFOIL

The lift increment due to blowing shows a radically different pattern than does lift increment due to suction. Instead of the sharp rise to the point of flow attachment and subsequent flattening out of the curve, the lift due to blowing increment for  $\delta_F = 50^\circ$  increases continuously with increased  $C_{QS}$  throughout the range tested and the lift term  $\Delta [C_{LT} / (1 + \Delta)]$  attained a maximum value four times that achieved with suction. This, however, may reflect a difference in the term  $\Delta$  and warrants further study before conclusions may be drawn.

The lift of the  $50^\circ$  deflected flap rose immediately upon the introduction of  $C_{QB}$ , whereas the lift of the  $60^\circ$  deflected flap did not rise significantly until  $C_{QB}$  was equal to .03; this lift then increased more rapidly than that of the  $50^\circ$  deflected flap. The delay in the lift rise was probably due to flow separation at  $60^\circ$  flap deflection. Since the blowing flap is a single slotted flap, it could probably maintain attached flow without BLC until nearly  $50^\circ$  flap deflection. As shown in the curves, BLC had a much less favorable effect on the flaps at very high deflection angle.

The maximum lift increment due to angle of attack on the blowing flap decreases with increasing  $C_{QB}$ . This most likely is the result of increased circulation of the jet flap which increases the leading edge negative pressure peak so that the critical pressure for flow separation occurs at a lower angle of attack.

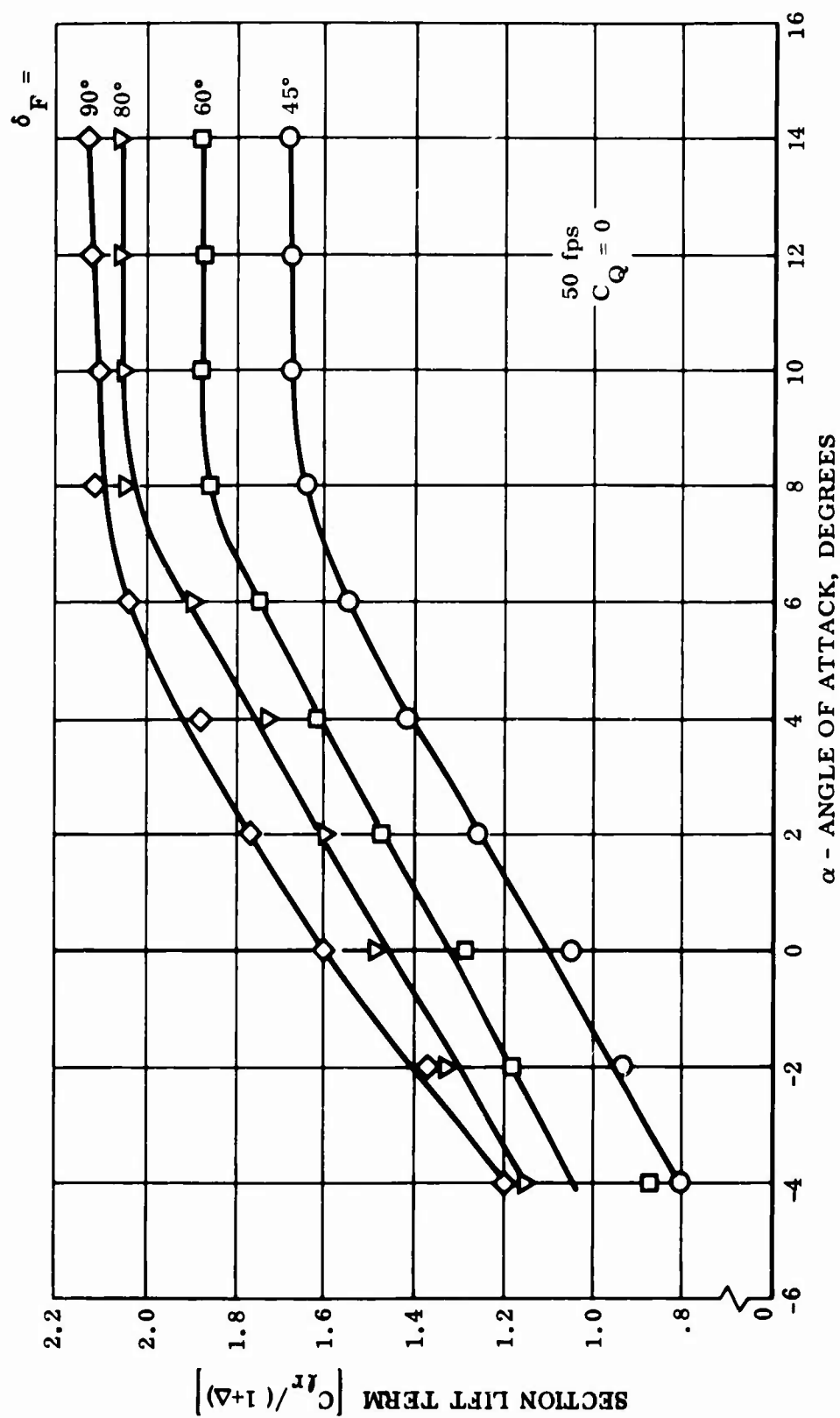


Figure 46. Fifteen-Percent-Thick Suction Flap Airfoil - Smoke Tunnel Test Runs 3, 6, 9, and 12



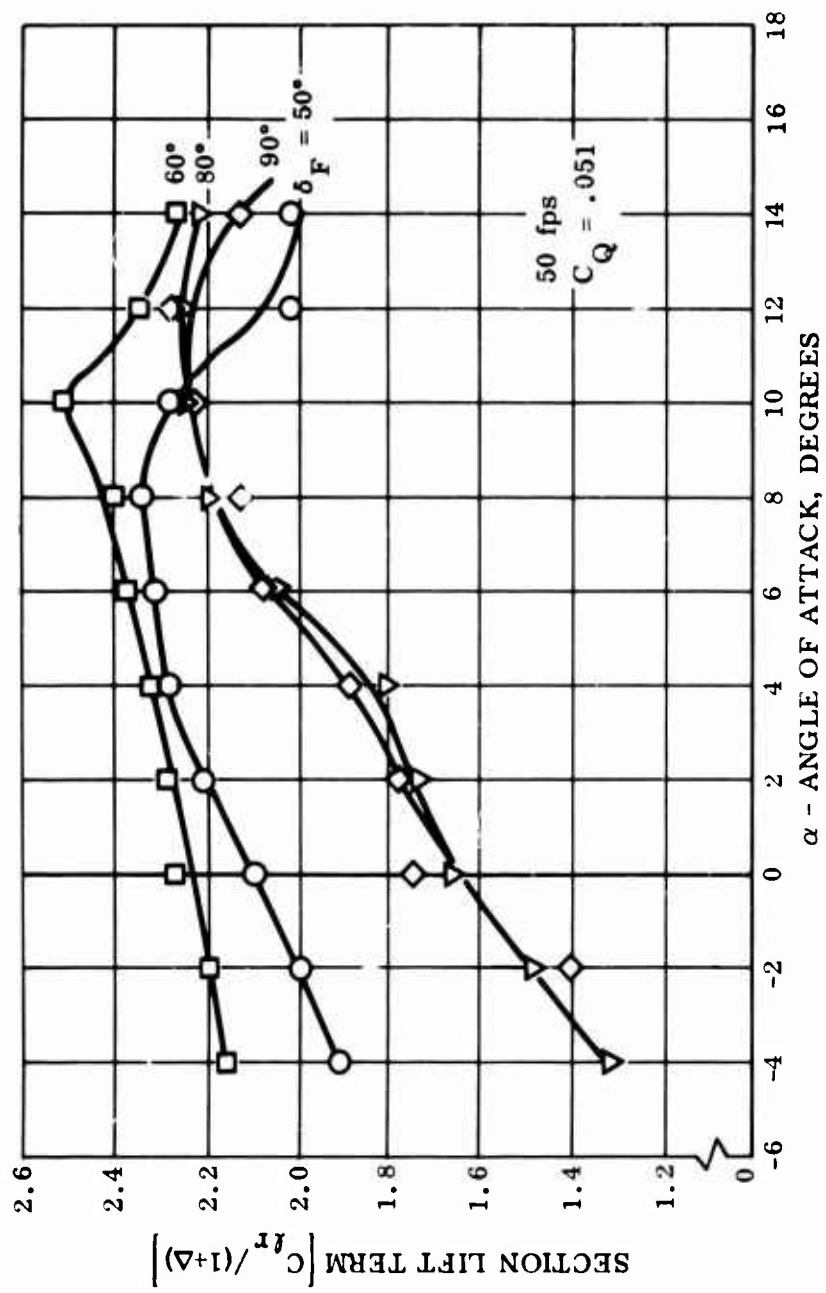


Figure 47. Fifteen-Percent-Thick Suction Flap Airfoil - Smoke Tunnel Test Runs 15, 18, 21, and 24

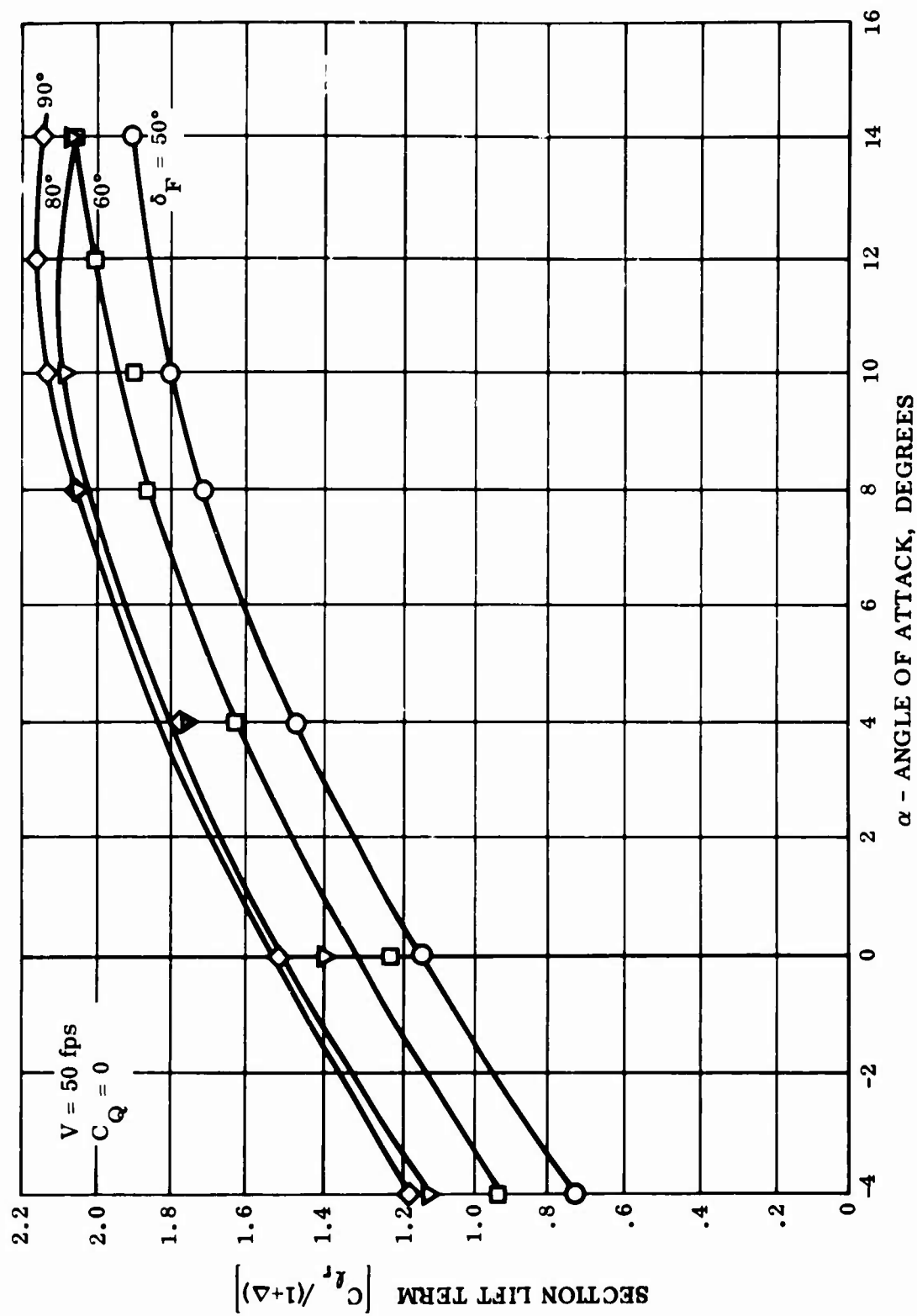


Figure 48. Seventeen-Percent-Thick Suction Flap Airfoil - Smoke Tunnel Test Runs 27, 30, 33, and 36

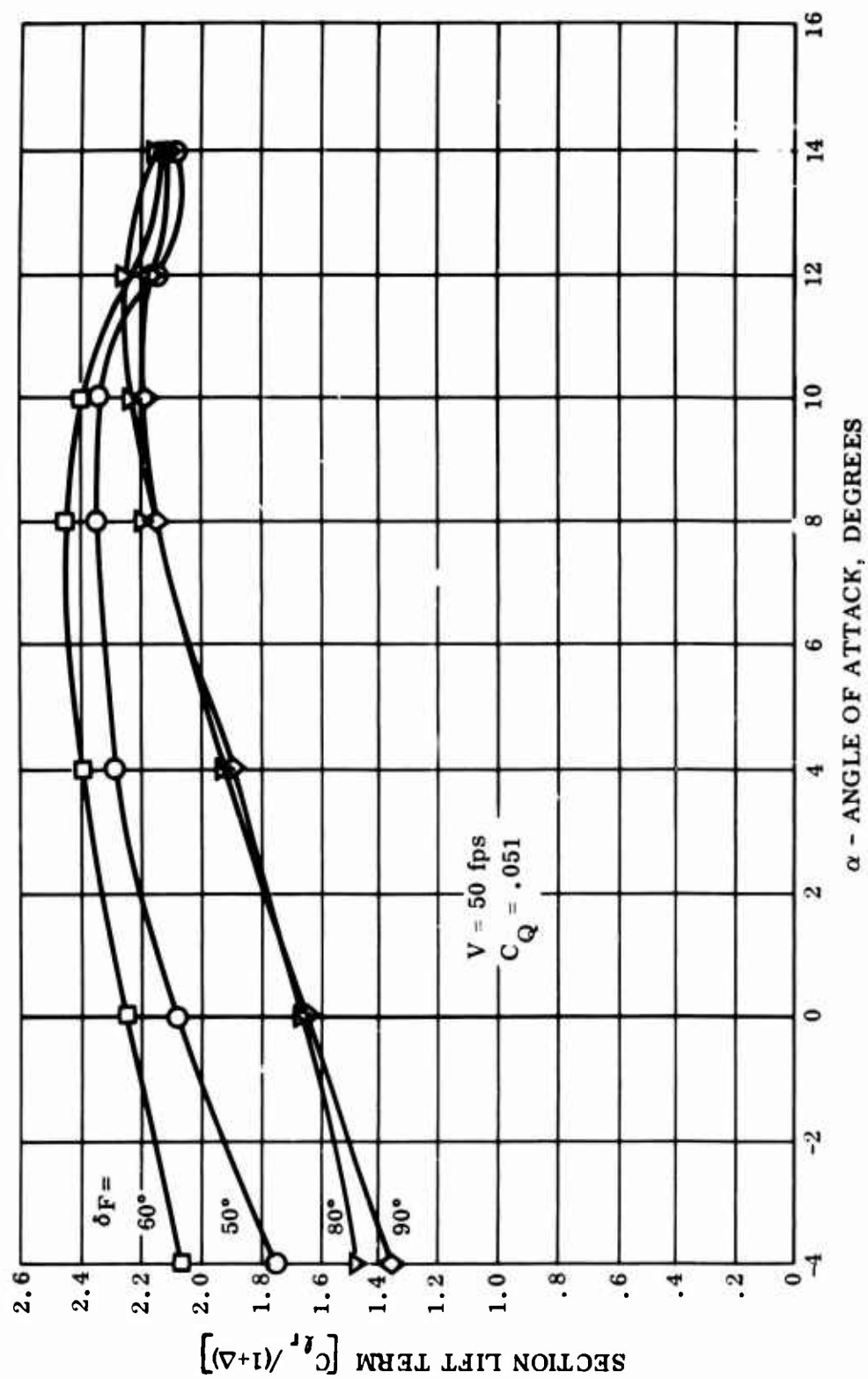


Figure 49. Seventeen-Percent-Thick Suction Flap Airfoil - Smoke Tunnel Test Runs 39, 42, and 48

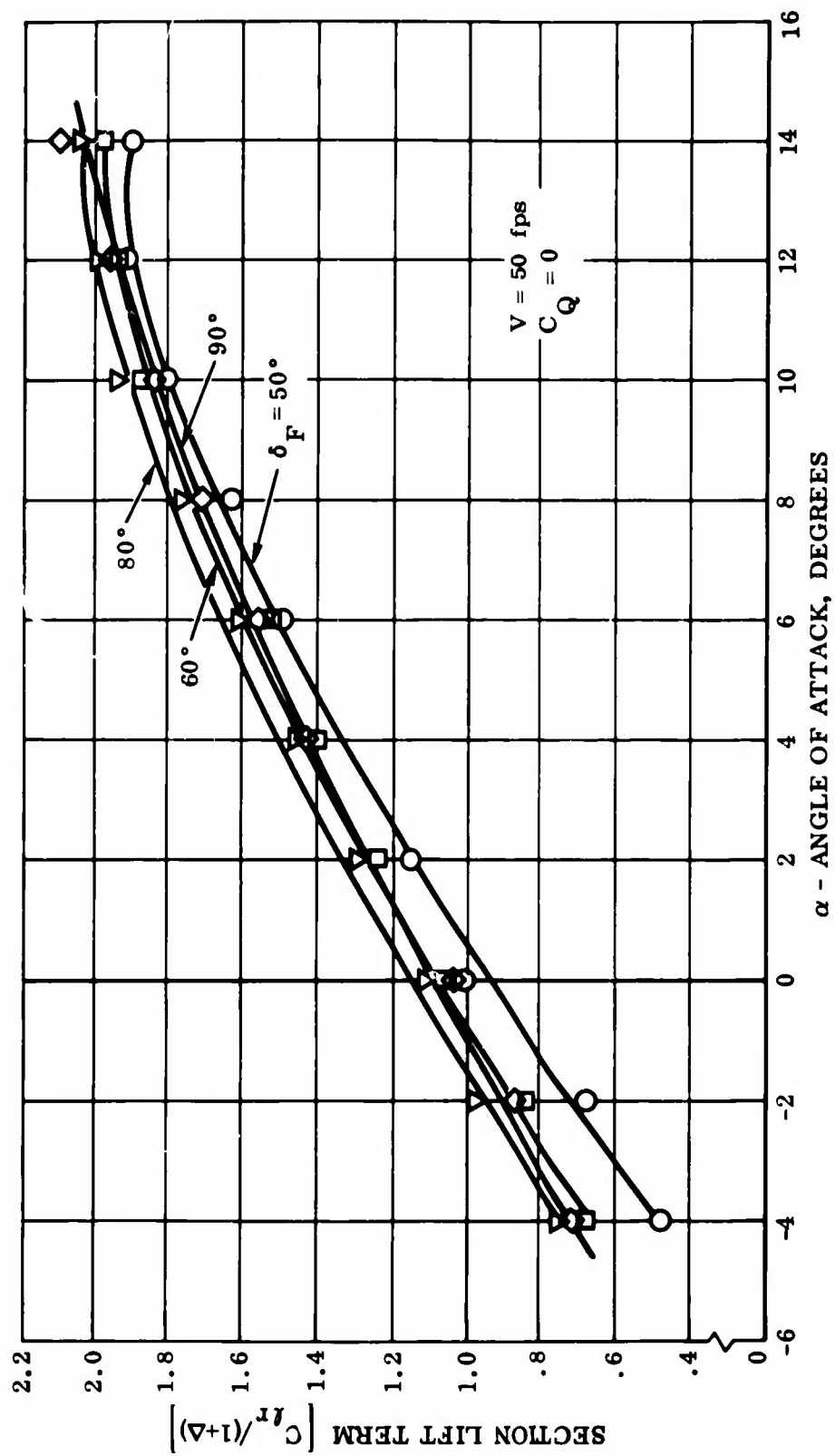


Figure 50. Blowing Flap Airfoil - Smoke Tunnel Test Runs 59, 62, 65, and 68

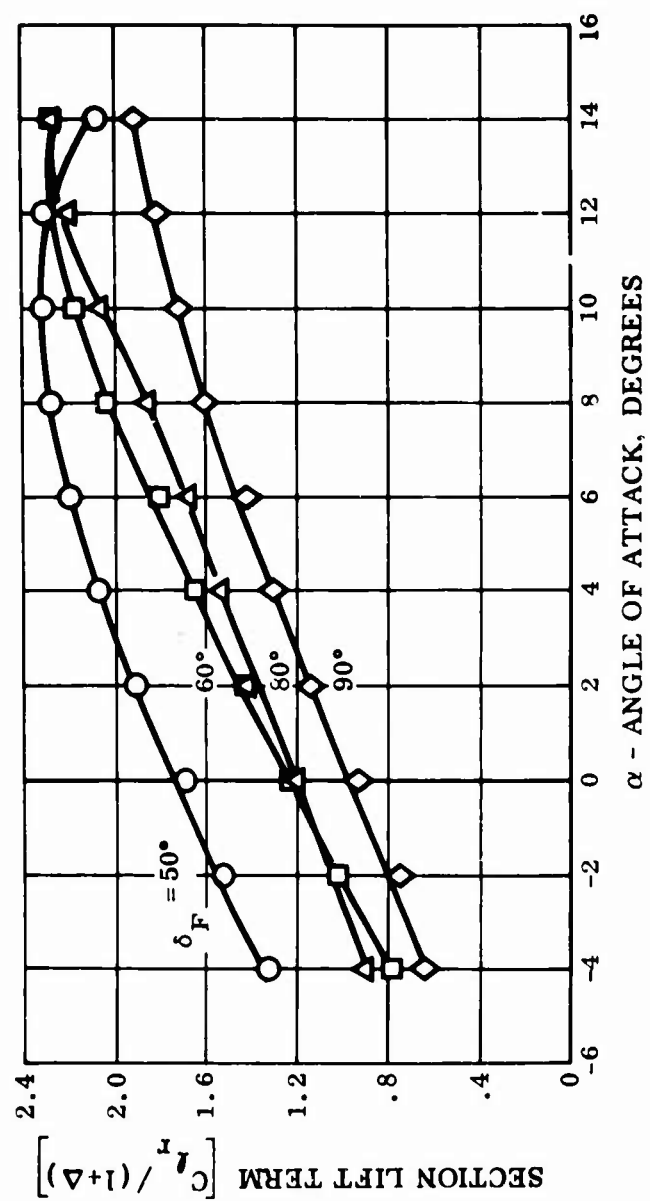


Figure 51. Blowing Flap Airfoil - Smoke Tunnel Test Runs 71, 74, 77, and 80

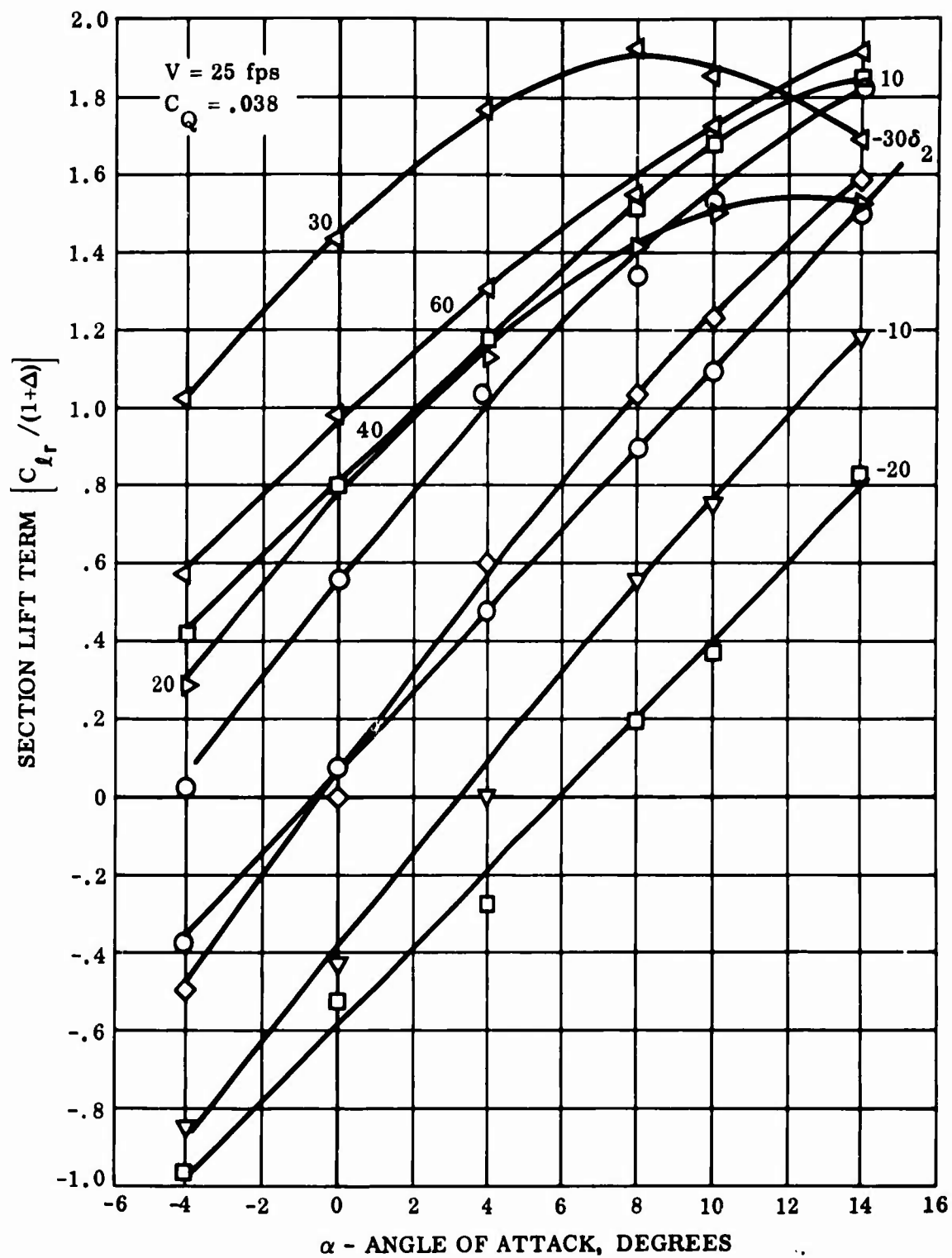


Figure 52. Blowing Aileron - Smoke Tunnel Test Runs 90 Through 98

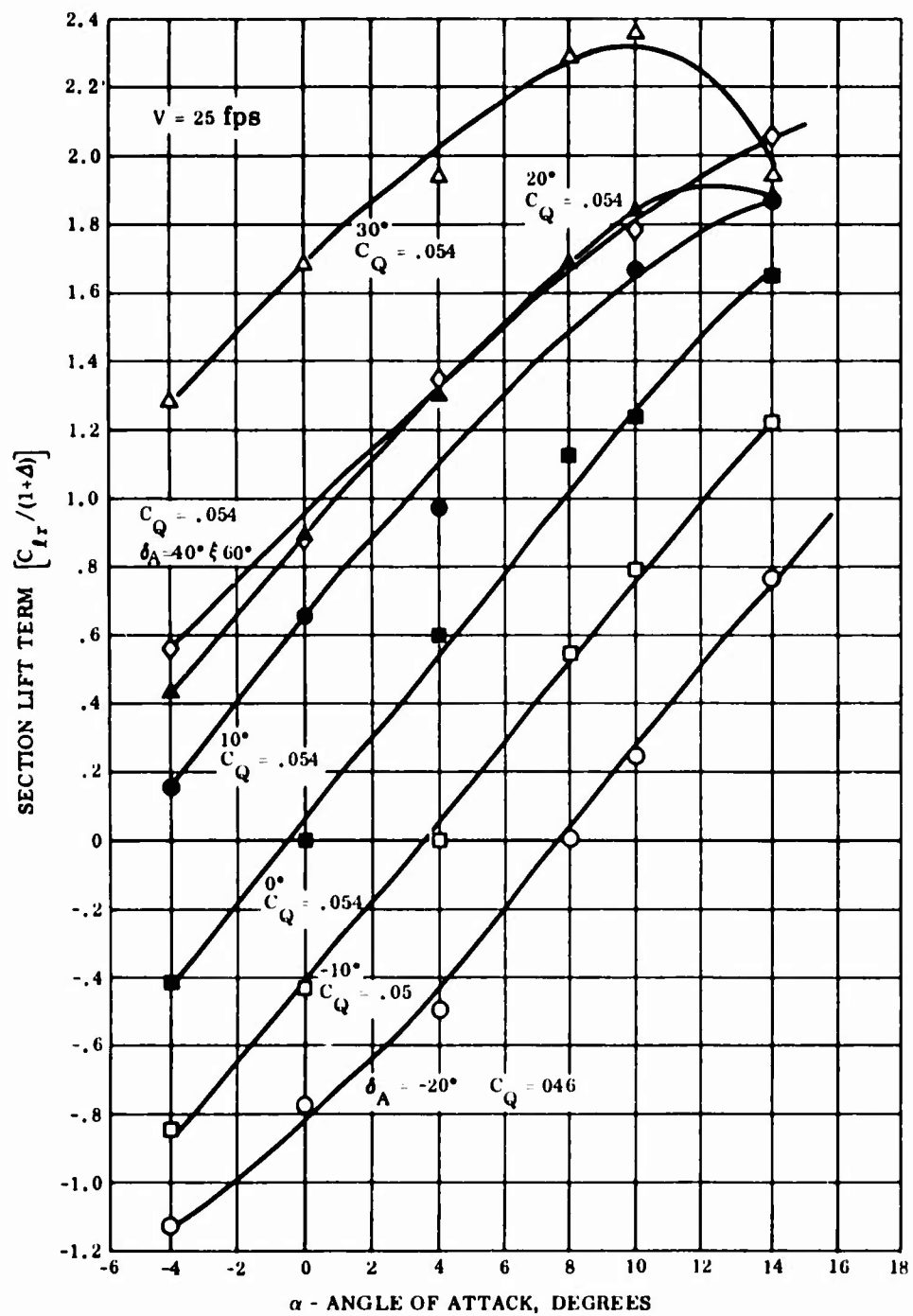


Figure 53. Blowing Aileron - Smoke Tunnel Test Runs 99 Through 106

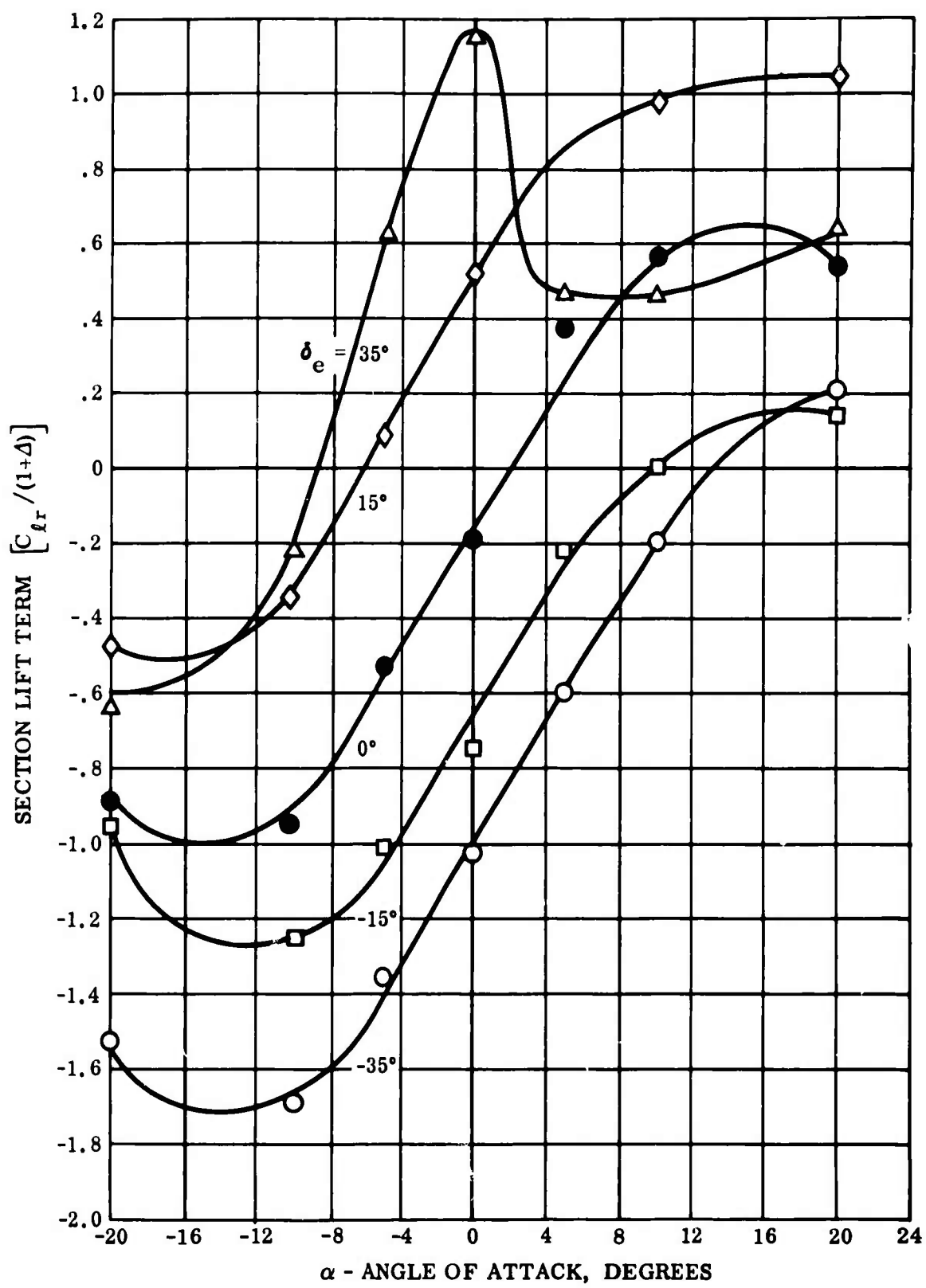


Figure 54. Suction Elevator Airfoil - Smoke Tunnel Test Runs 49 Through 53



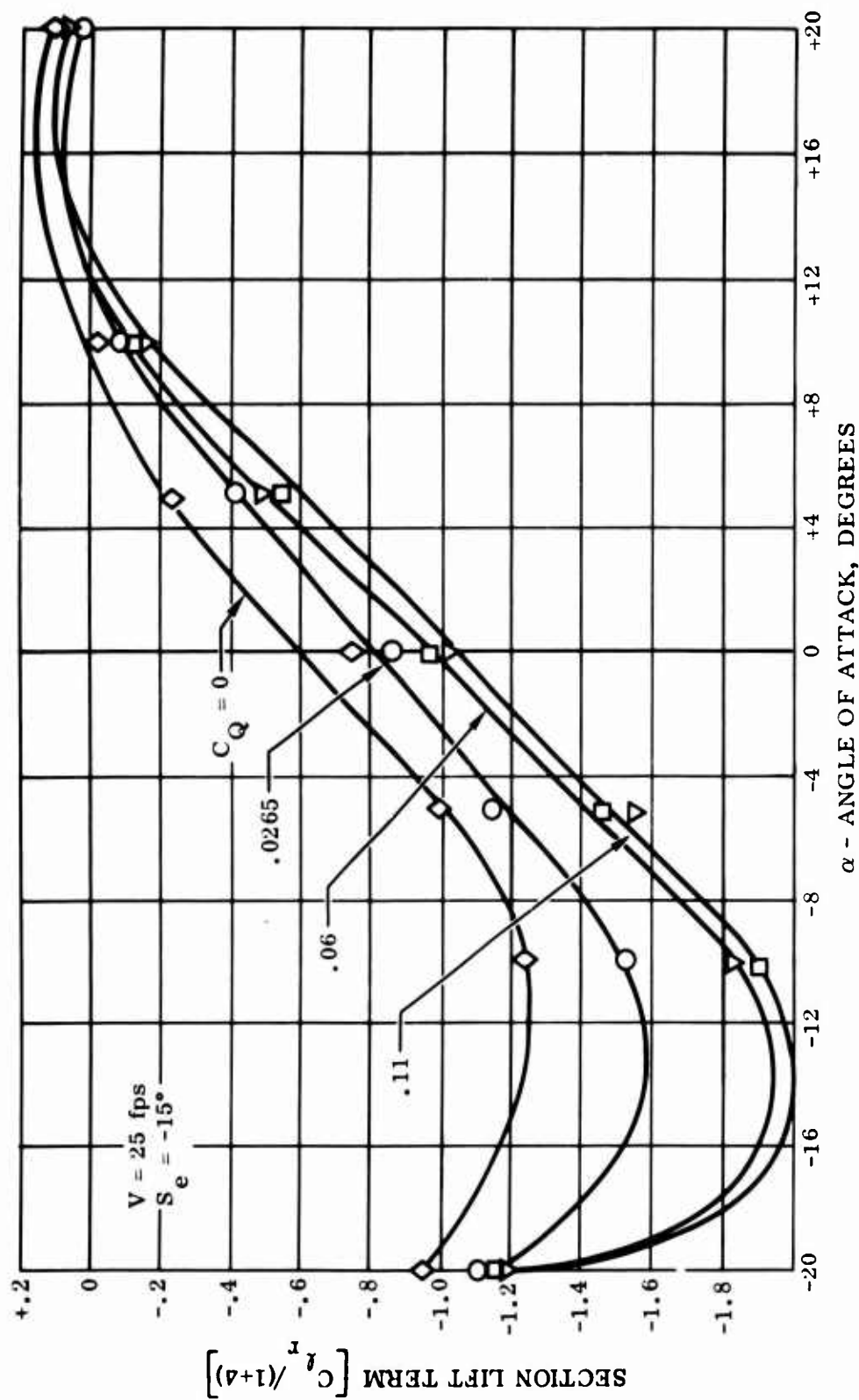


Figure 55. Suction Elevator Airfoil - Smoke Tunnel Test Runs 50 Through 56

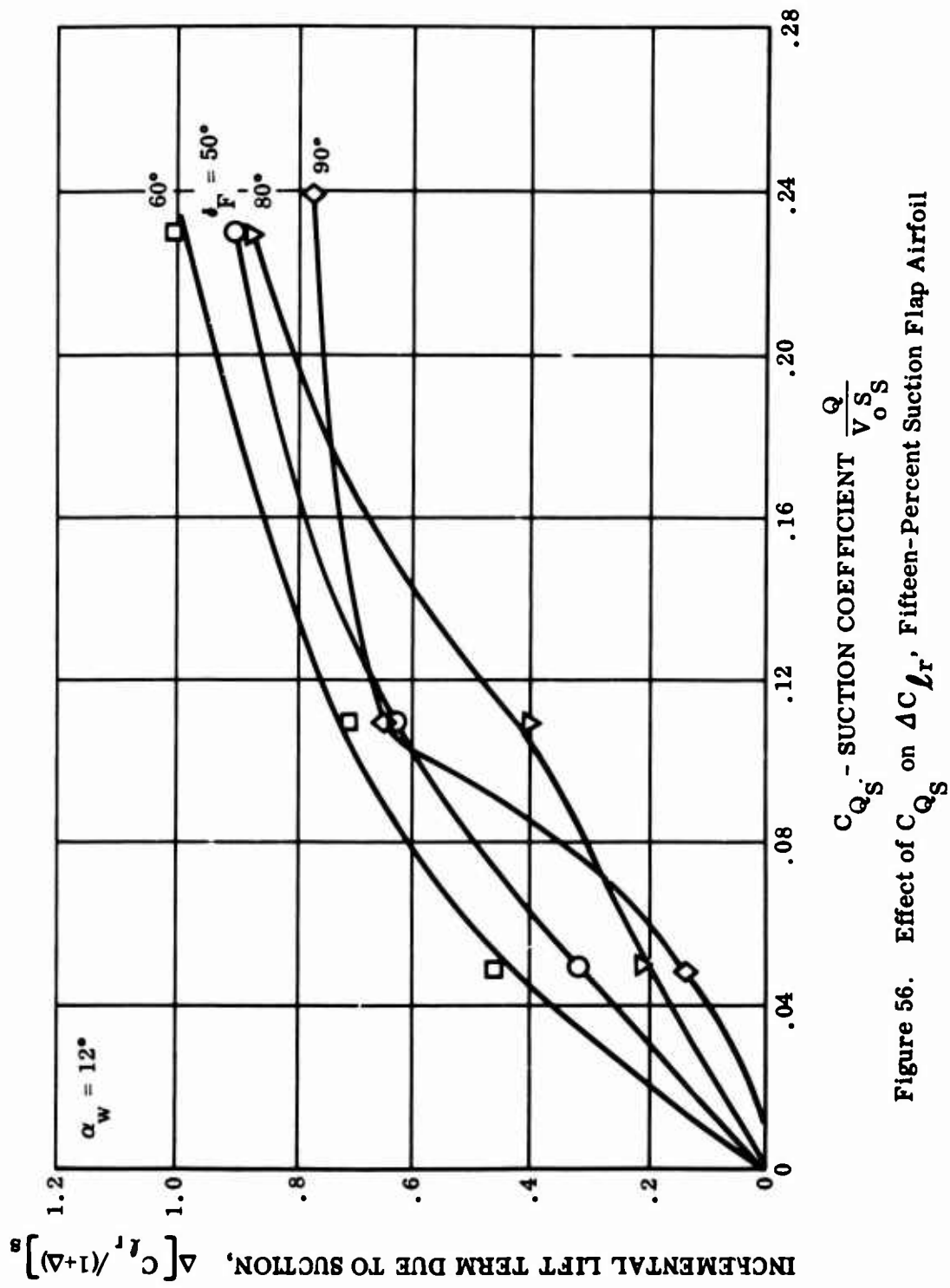


Figure 56. Effect of  $C_{Q_s}$  on  $\Delta C_{l_r}$ , Fifteen-Percent Suction Flap Airfoil

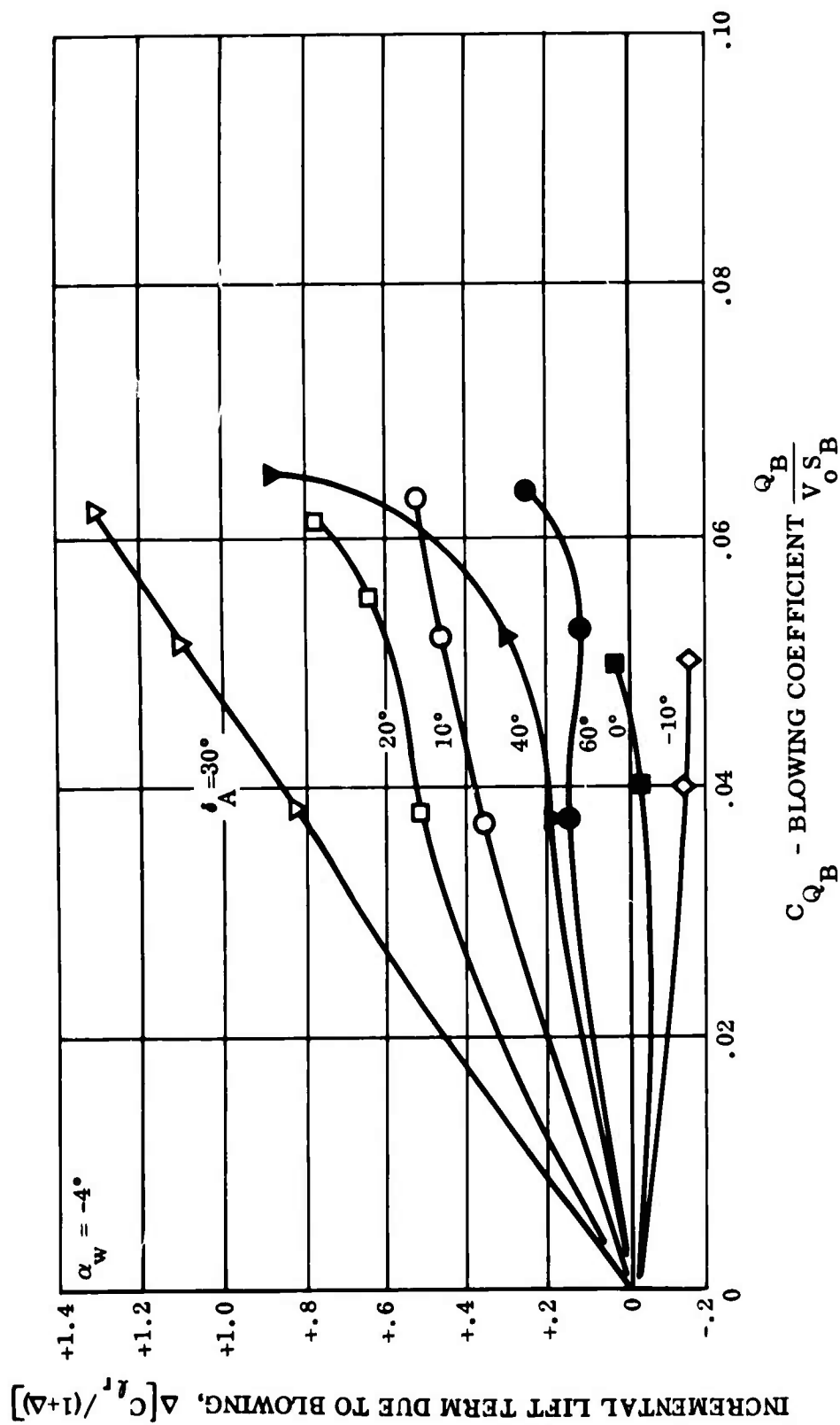


Figure 57. Effect of  $C_{Q_B}$  on  $\Delta C_{l_r}$ , Blowing Aileron

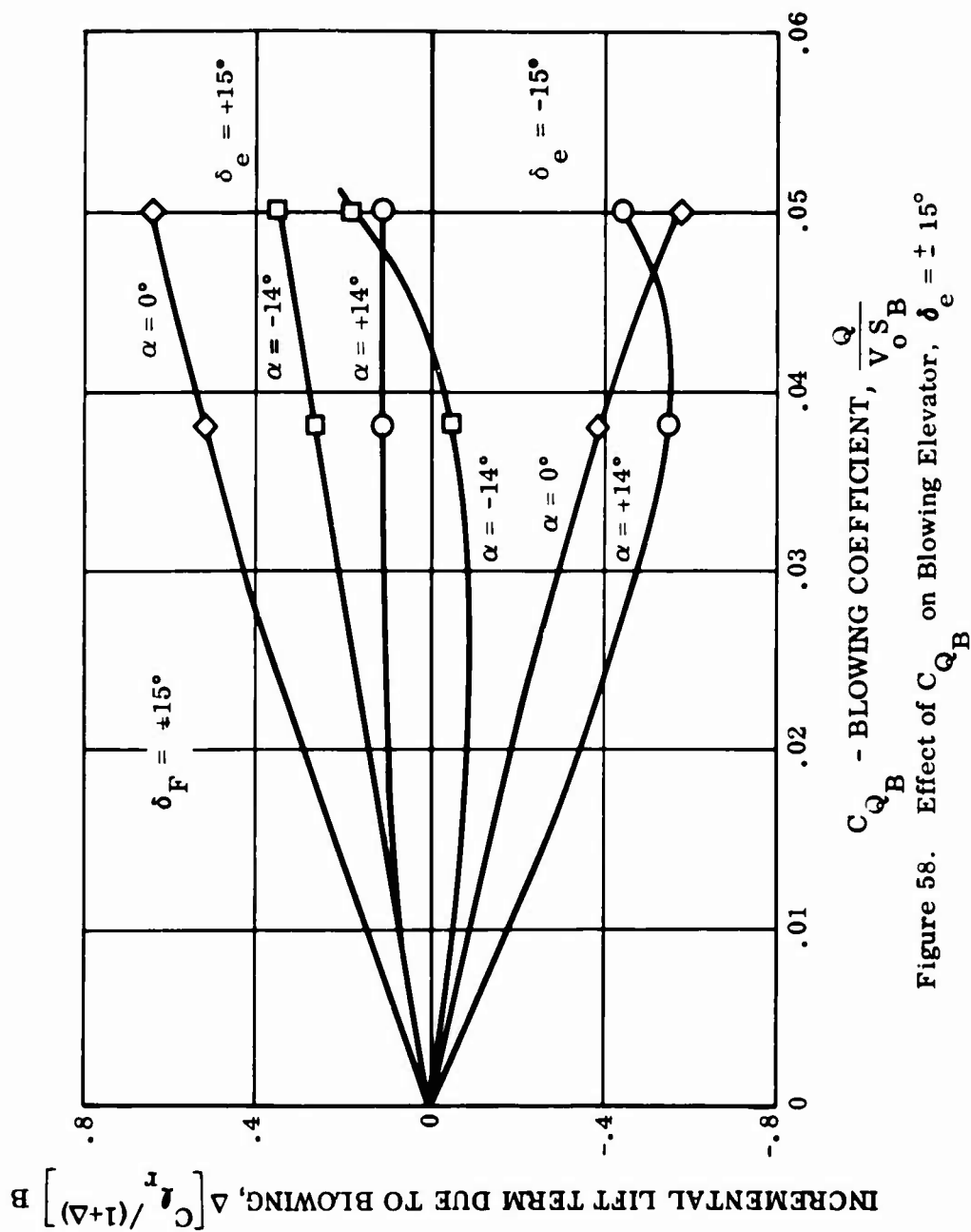
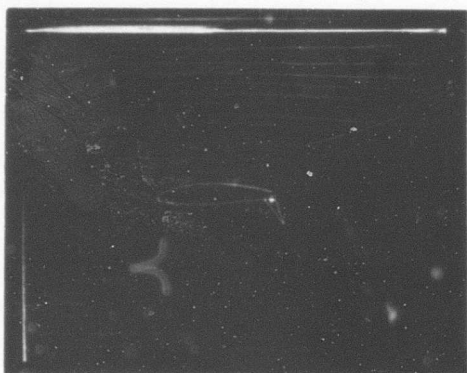
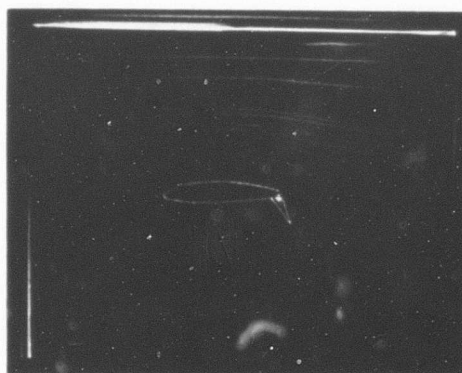


Figure 58. Effect of  $C_{Q_B}$  on Blowing Elevator,  $\delta_e = \pm 15^\circ$



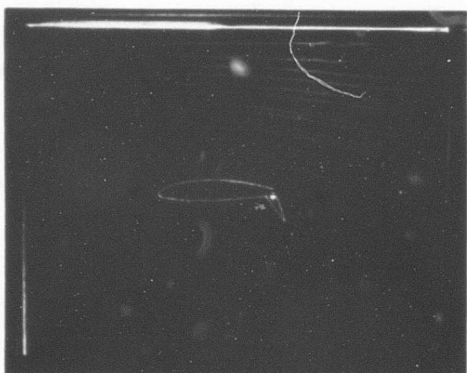
$C_Q = 0, V = 25 \text{ fps}$

(A)



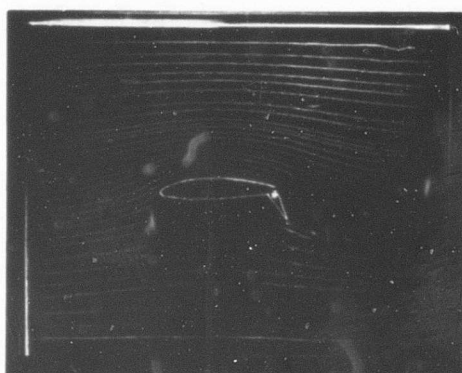
$C_Q = .051, V = 50 \text{ fps}$

(B)



$C_Q = .110, V = 25 \text{ fps}$

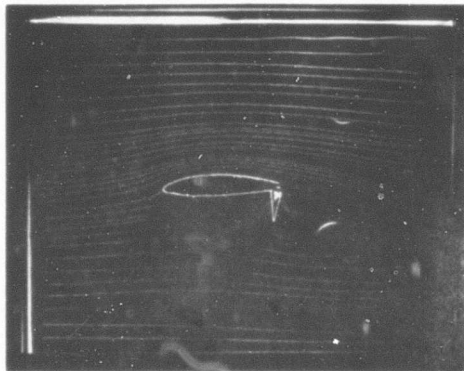
(C)



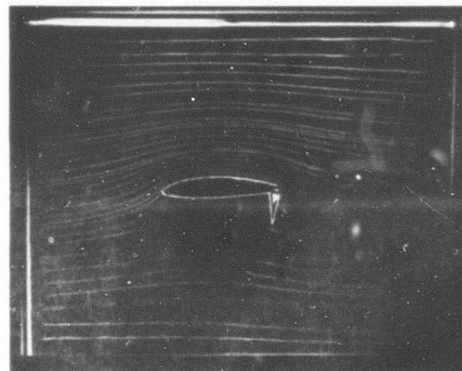
$C_Q = .265, V = 10 \text{ fps}$

(D)

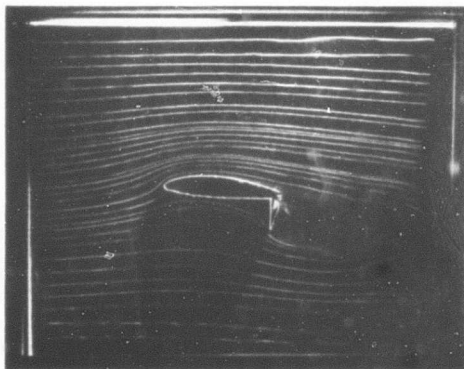
Figure 59. Fifteen-Percent-Thick Airfoil With Suction Flat Deflected  $60^\circ$  at Zero Angle of Attack



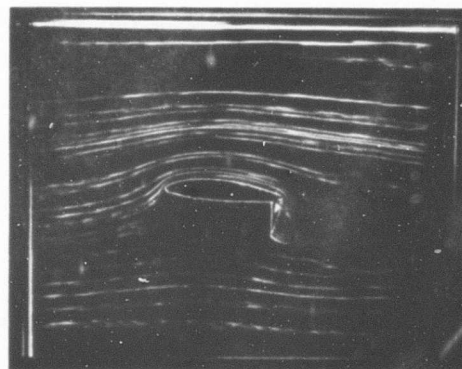
$C_Q = 0, \alpha = 0^\circ$   
(A)



$C_Q = .110, \alpha = 0^\circ$   
(B)

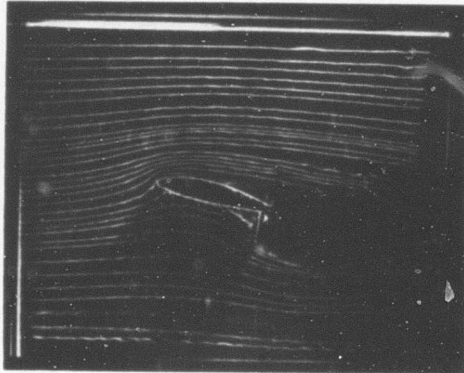


$C_Q = 0, \alpha = 6^\circ$   
(C)



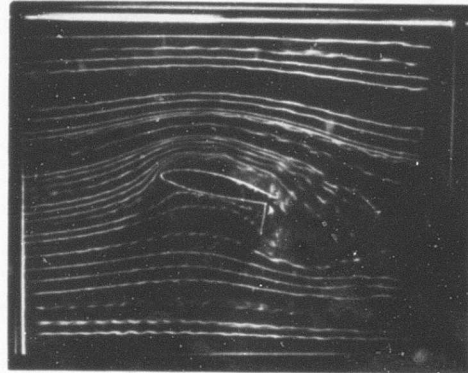
$C_Q = .110, \alpha = 6^\circ$   
(D)

Figure 60. Fifteen-Percent-Thick Airfoil With Suction Flap Deflected  $90^\circ$  at 25 fps Tunnel Velocity



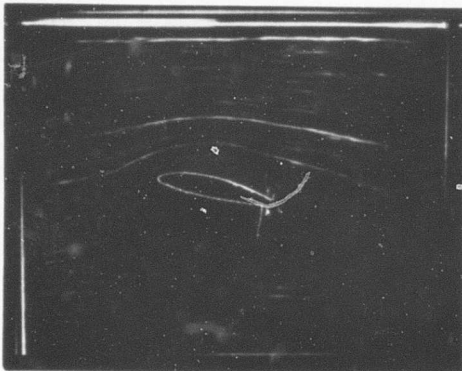
$C_Q = 0, V = 10 \text{ fps}$

(A)



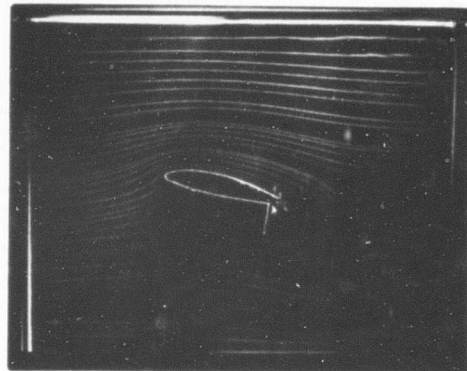
$C_Q = .265, V = 10 \text{ fps}$

(B)



$C_Q = .110, V = 25 \text{ fps}$

(C)

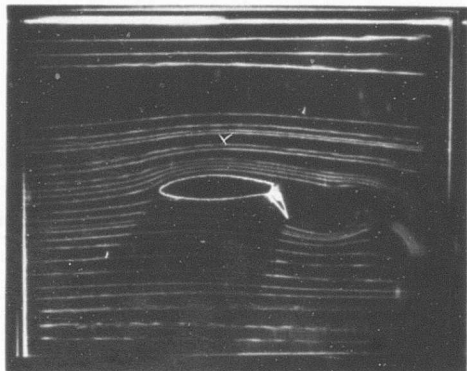


$C_Q = .110, V = 25 \text{ fps}$

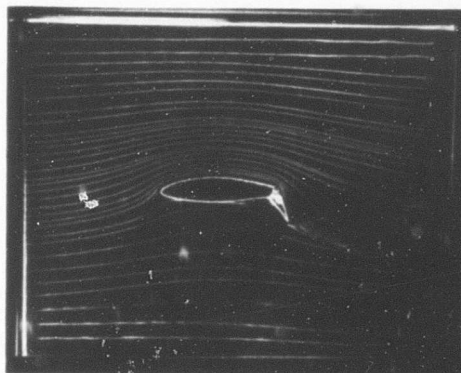
(D)

Photographs (C) and (D) illustrate oscillatory flow separation and reattachment that occurred at  $C_Q = .110, V = 25 \text{ fps}$ .

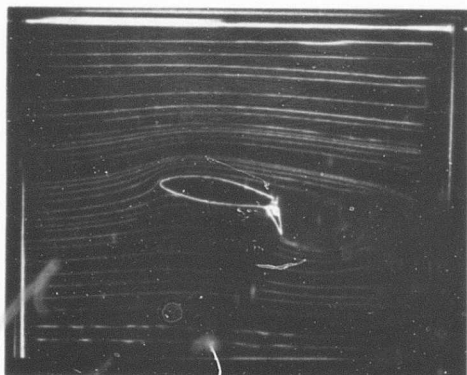
Figure 61. Fifteen-Percent-Thick Airfoil With Suction Flap Deflected  $90^\circ$  at  $14^\circ$  Angle of Attack.



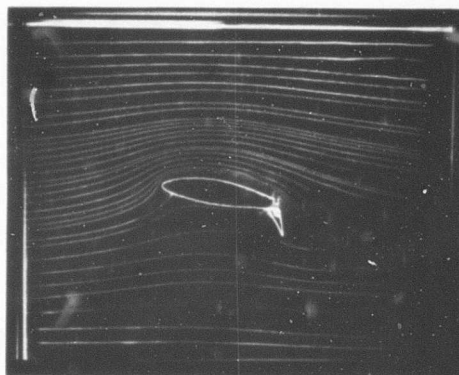
$C_Q = 0, \alpha = 0^\circ$   
(A)



$C_Q = .110, \alpha = 0^\circ$   
(B)



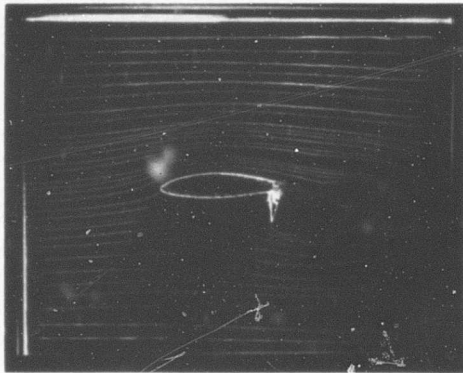
$C_Q = 0, \alpha = 10^\circ$   
(C)



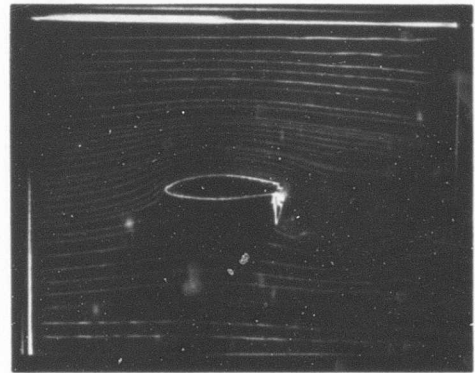
$C_Q = .110, \alpha = 10^\circ$   
(D)

Figure 62. Seventeen-Percent-Thick Airfoil With Suction Flap Deflected  $60^\circ$  at 25 fps Tunnel Velocity

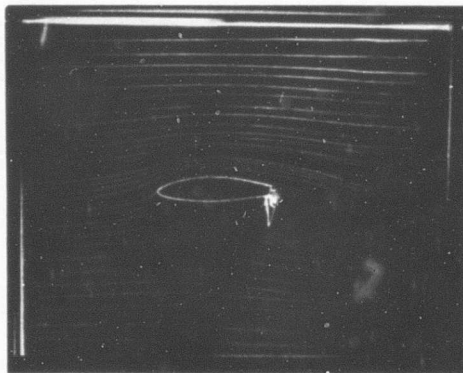




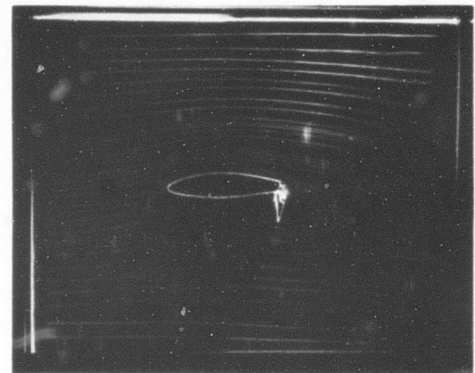
$C_Q = 0, V = 25 \text{ fps}$   
(A)



$C_Q = .110, V = 25 \text{ fps}$   
(B)

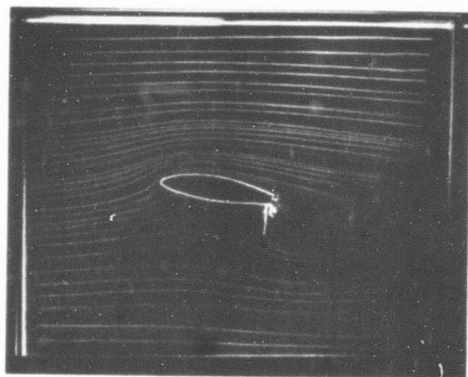


$C_Q = 0, V = 50 \text{ fps}$   
(C)

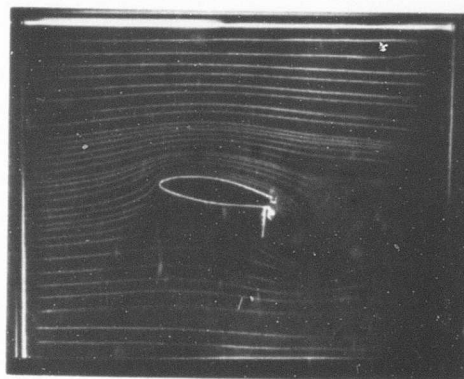


$C_Q = .051, V = 50 \text{ fps}$   
(D)

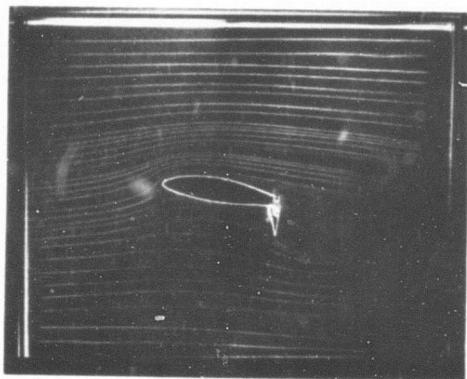
Figure 63. Seventeen-Percent-Thick Airfoil With Suction Flap Deflected  $90^\circ$  at Zero Angle of Attack



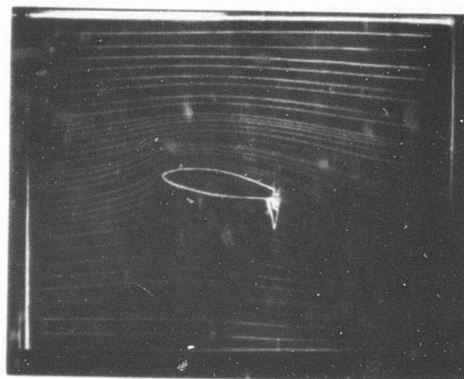
$C_Q = 0, \delta_F = 90^\circ$   
(A)



$C_Q = .110, \delta_F = 90^\circ$   
(B)

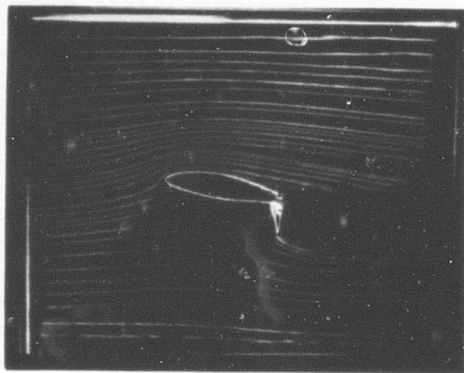


$C_Q = 0, \delta_F = 80^\circ$   
(C)

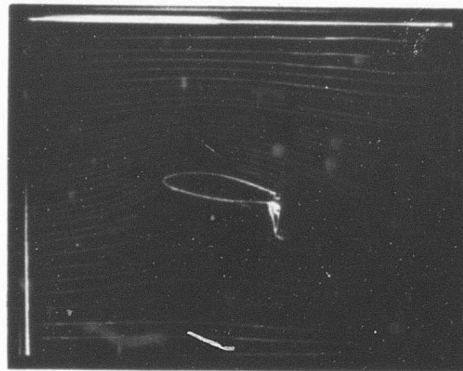


$C_Q = 0, \delta_F = 80^\circ$   
(D)

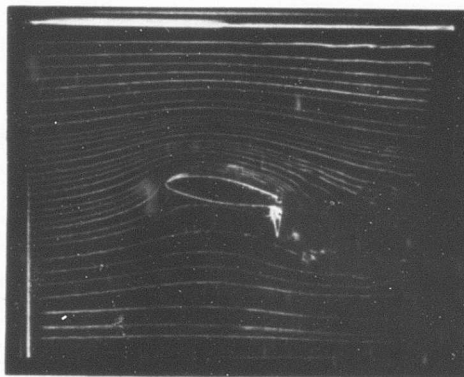
Figure 64. Seventeen-Percent-Thick Airfoil With Suction Flap Deflected  $90^\circ$  and  $80^\circ$  at  $10^\circ$  Angle of Attack and 50 fps Tunnel Velocity



$C_Q = 0$ ,  $V = 25$  fps  
(A)

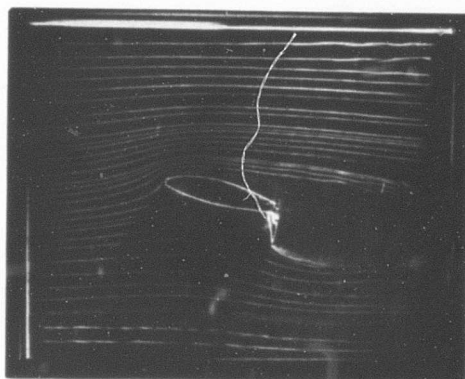


$C_Q = .110$ ,  $V = 25$  fps  
(B)



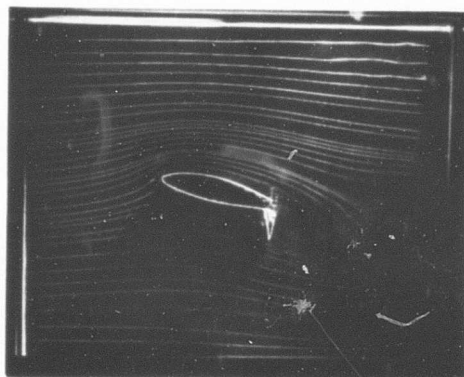
$C_Q = .265$ ,  $V = 10$  fps  
(C)

Figure 65. Seventeen-Percent-Thick Airfoil With Suction Flap Deflected  $80^\circ$  at  $10^\circ$  Angle of Attack



$$C_Q = 0$$

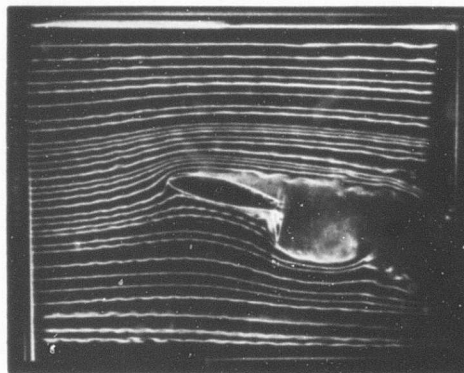
(A)



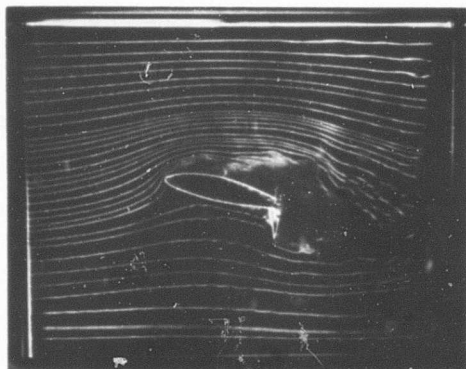
$$C_Q = .110$$

(B)

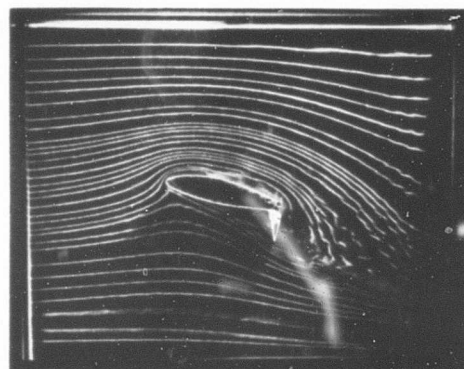
Figure 33. Seventeen-Percent-Thick Airfoil With Suction Flap Deflected  $80^\circ$  at 25 fps Tunnel Velocity



$C_Q = 0$   
(A)



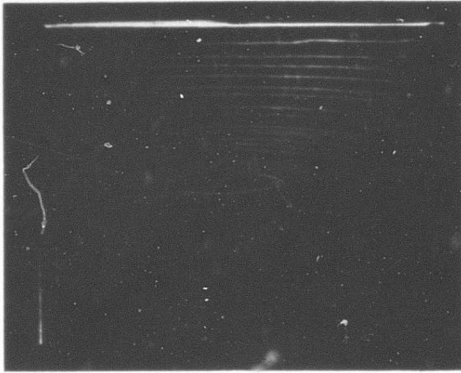
$C_Q = .265$   
(B)



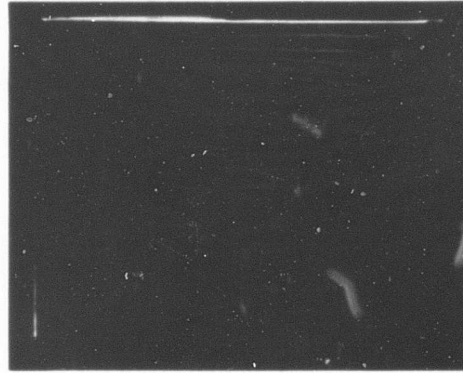
$C_Q = .265$   
(C)

Photographs (B) and (C) illustrate oscillatory flow separation and reattachment at  $C_Q = .265$ ,  $V = 10$  fps.

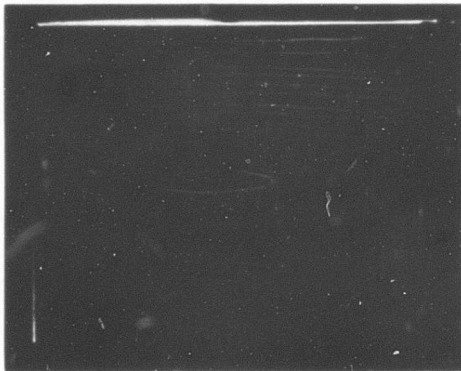
Figure 67. Seventeen-Percent-Thick Airfoil With Suction Flap Deflected  $80^\circ$  at 10 fps Tunnel Velocity and  $14^\circ$  Angle of Attack



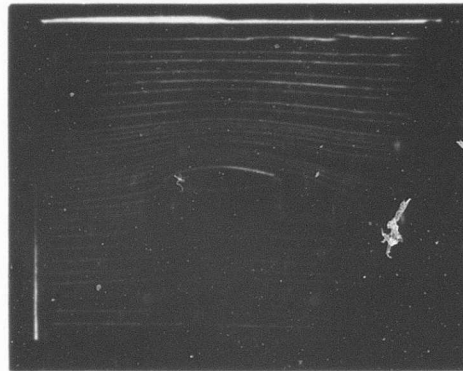
$C_Q = 0, \delta_F = 60^\circ$   
(A)



$C_Q = .070, \delta_F = 60^\circ$   
(B)

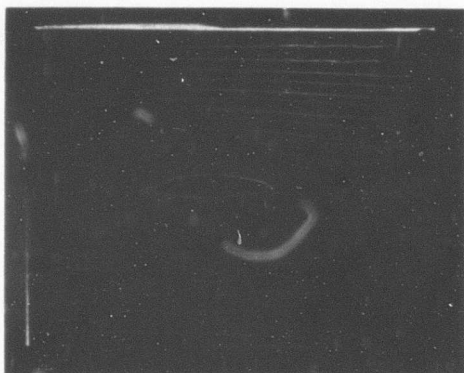


$C_Q = 0, \delta_F = 80^\circ$   
(C)



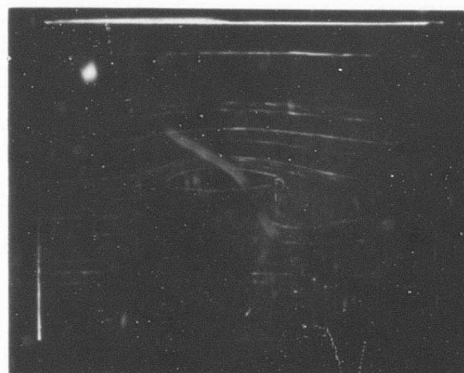
$C_Q = .070, \delta_F = 80^\circ$   
(D)

Figure 68. Seventeen-Percent-Thick Airfoil With Blowing Flap Deflected  $60^\circ$  and  $80^\circ$  at Zero Angle of Attack and 25 fps Tunnel Velocity



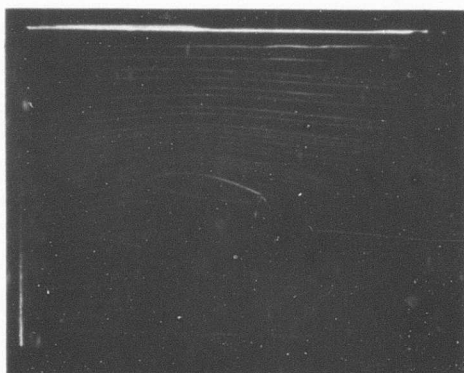
$$C_Q = 0, \alpha = 0^\circ$$

(A)



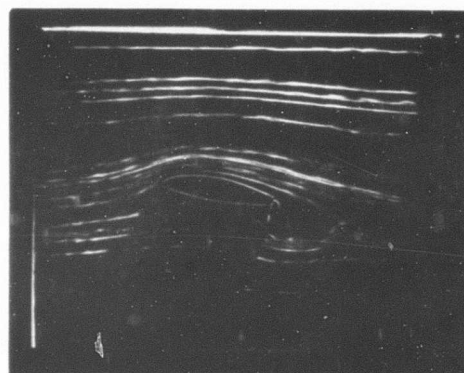
$$C_Q = .070, \alpha = 0^\circ$$

(B)



$$C_Q = 0, \alpha = 10^\circ$$

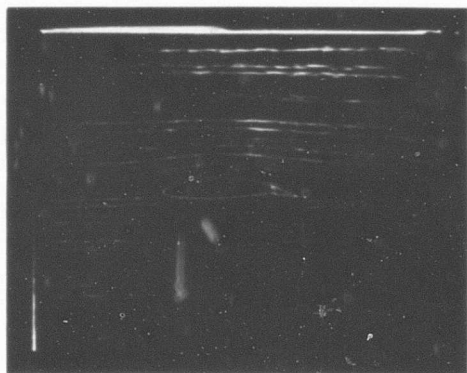
(C)



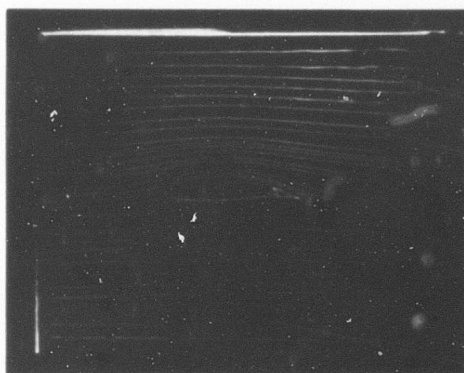
$$C_Q = .070, \alpha = 10^\circ$$

(D)

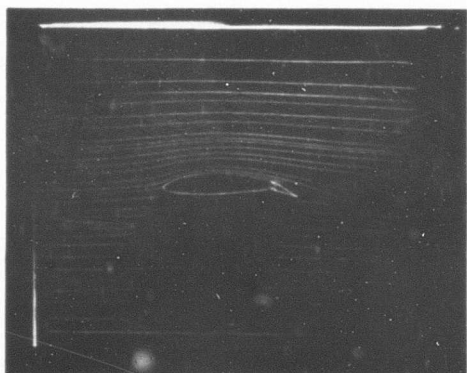
Figure 69. Seventeen-Percent-Thick Airfoil With Blowing Flap Deflected  $90^\circ$  at 25 fps Tunnel Velocity



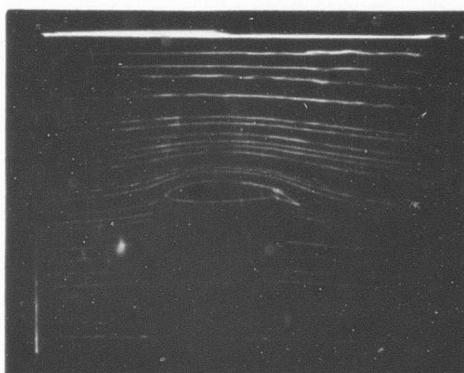
$C_Q = 0, \delta_a = +10^\circ$   
(A)



$C_Q = .062, \delta_a = +10^\circ$   
(B)



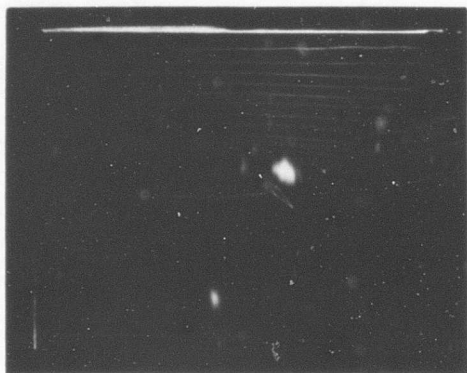
$C_Q = 0, \delta_a = +20^\circ$   
(C)



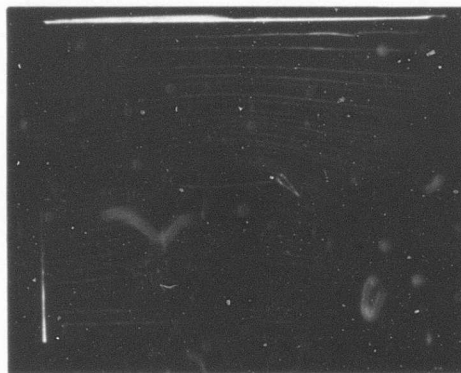
$C_Q = .062, \delta_a = +20^\circ$   
(D)

Figure 70. Airfoil With Blowing Aileron Deflected  $10^\circ$  and  $20^\circ$  at Zero Angle of Attack and 25 fps Tunnel Velocity

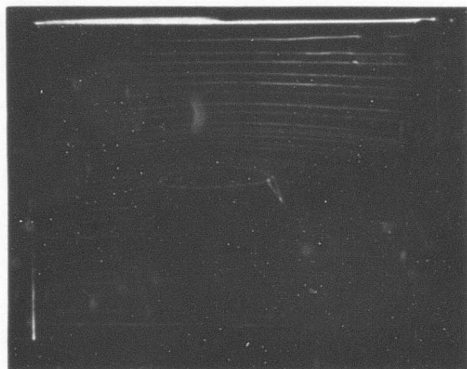




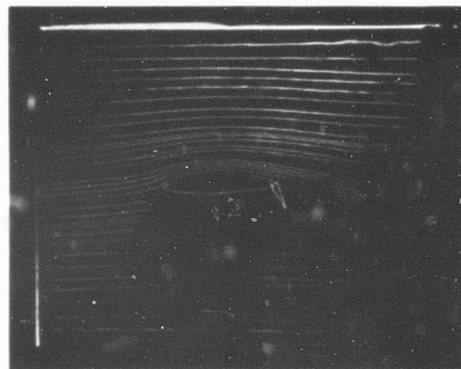
$C_Q = 0, \delta_a = +40^\circ$   
(A)



$C_Q = .062, \delta_a = +40^\circ$   
(B)

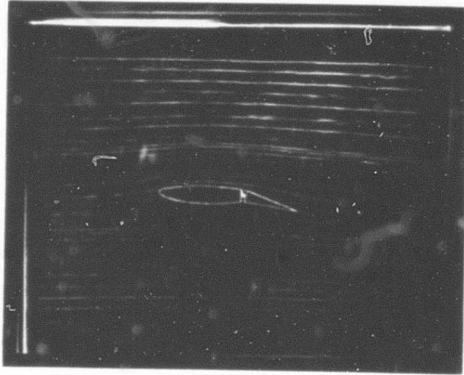


$C_Q = 0, \delta_a = +60^\circ$   
(C)



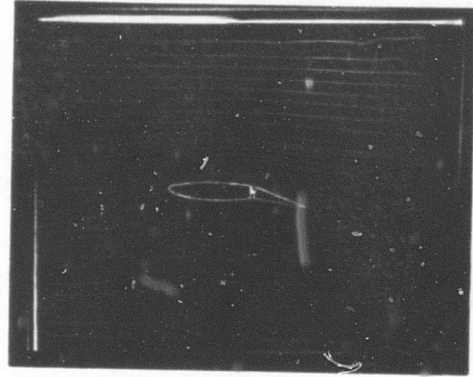
$C_Q = .062, \delta_a = +60^\circ$   
(D)

Figure 71. Airfoil With Blowing Aileron Deflected  $40^\circ$  and  $60^\circ$  at Zero Angle of Attack and 25 fps Tunnel Velocity



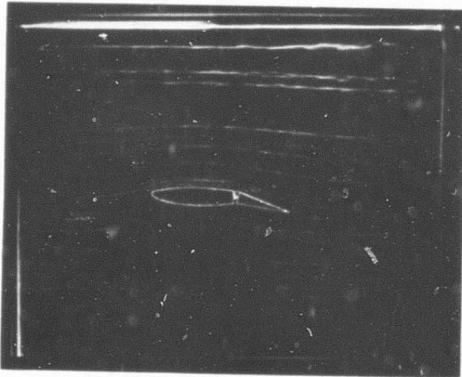
$$C_Q = 0$$

(A)



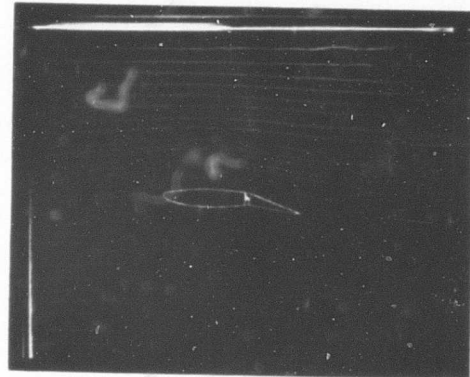
$$C_Q = .028$$

(B)



$$C_Q = .060$$

(C)



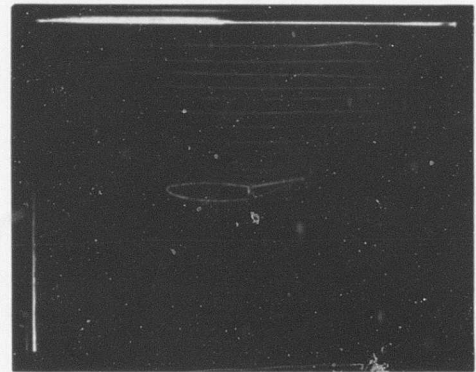
$$C_Q = .110$$

(D)

Figure 72. Airfoil With Suction Elevator Deflected +15° at Zero Angle of Attack and 25 fps Tunnel Velocity



$C_Q = 0$   
(A)



$C_Q = .027$   
(B)



$C_Q = .060$   
(C)

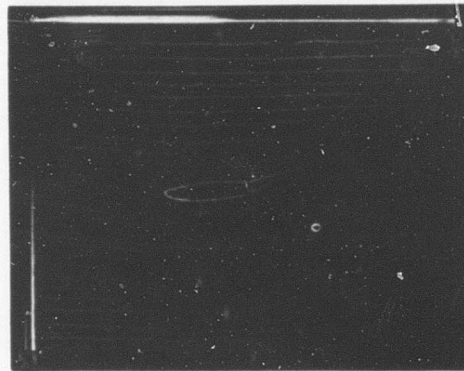


$C_Q = .110$   
(D)

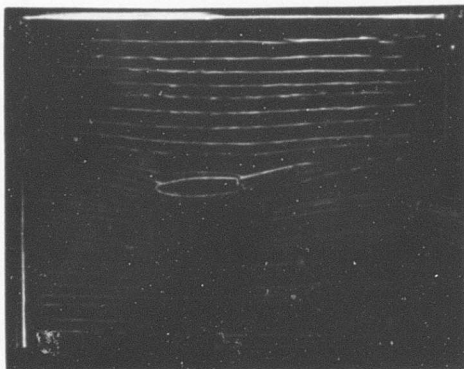
Figure 73. Airfoil With Suction Elevator Deflected -  $15^\circ$  at Zero Angle of Attack and 25 fps Tunnel Velocity



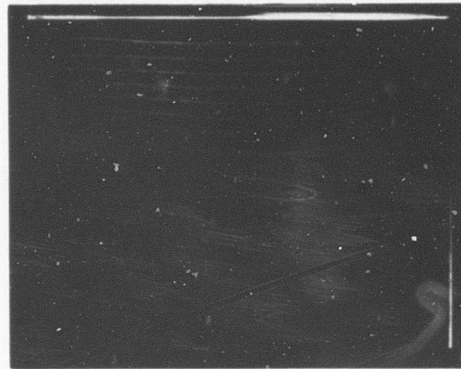
$C_Q = 0, \alpha = -4^\circ$   
(A)



$C_Q = 0, \alpha = 16^\circ$   
(B)

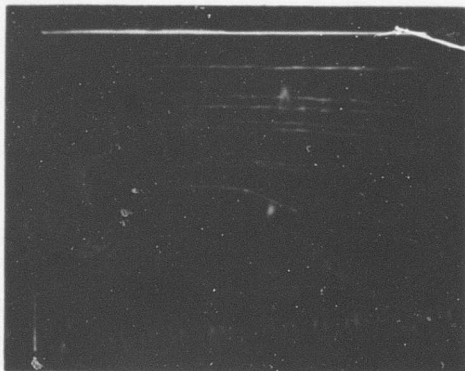


$C_Q = .110, \alpha = -4^\circ$   
(C)



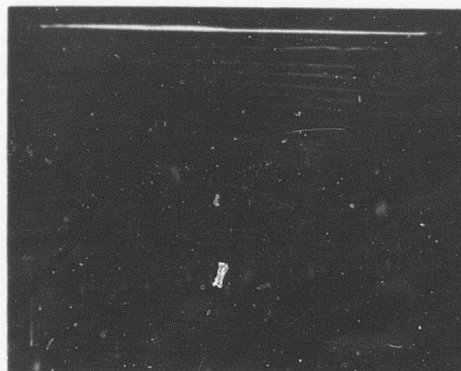
$C_Q = .110, \alpha = -6^\circ$   
(D)

Figure 74. Airfoil With Suction Elevator Deflected  $-15^\circ$  at 25 fps Tunnel Velocity



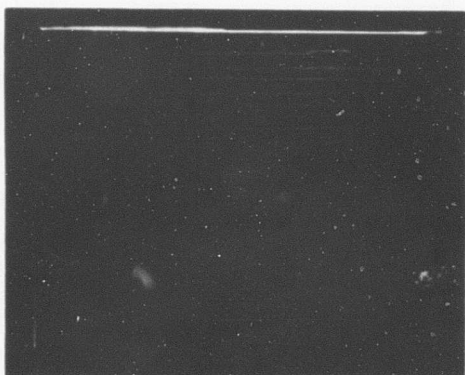
$$C_Q = 0, \delta_e = +15^\circ, \alpha = 0^\circ$$

(A)



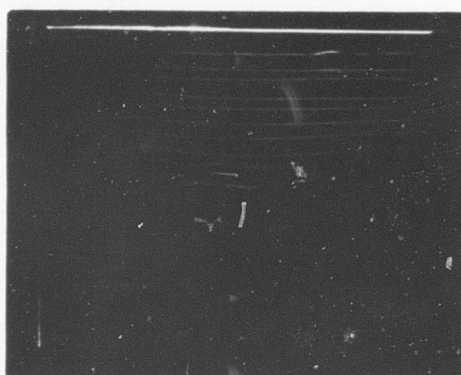
$$C_Q = .05, \delta_e = +15^\circ, \alpha = 0^\circ$$

(B)



$$C_Q = 0, \delta_e = -15^\circ, \alpha = -4^\circ$$

(C)



$$C_Q = .05, \delta_e = -15^\circ, \alpha = -4^\circ$$

(D)

Figure 75. Airfoil With Blowing Elevator Deflected  $\pm 15^\circ$  at 25 fps Tunnel Velocity

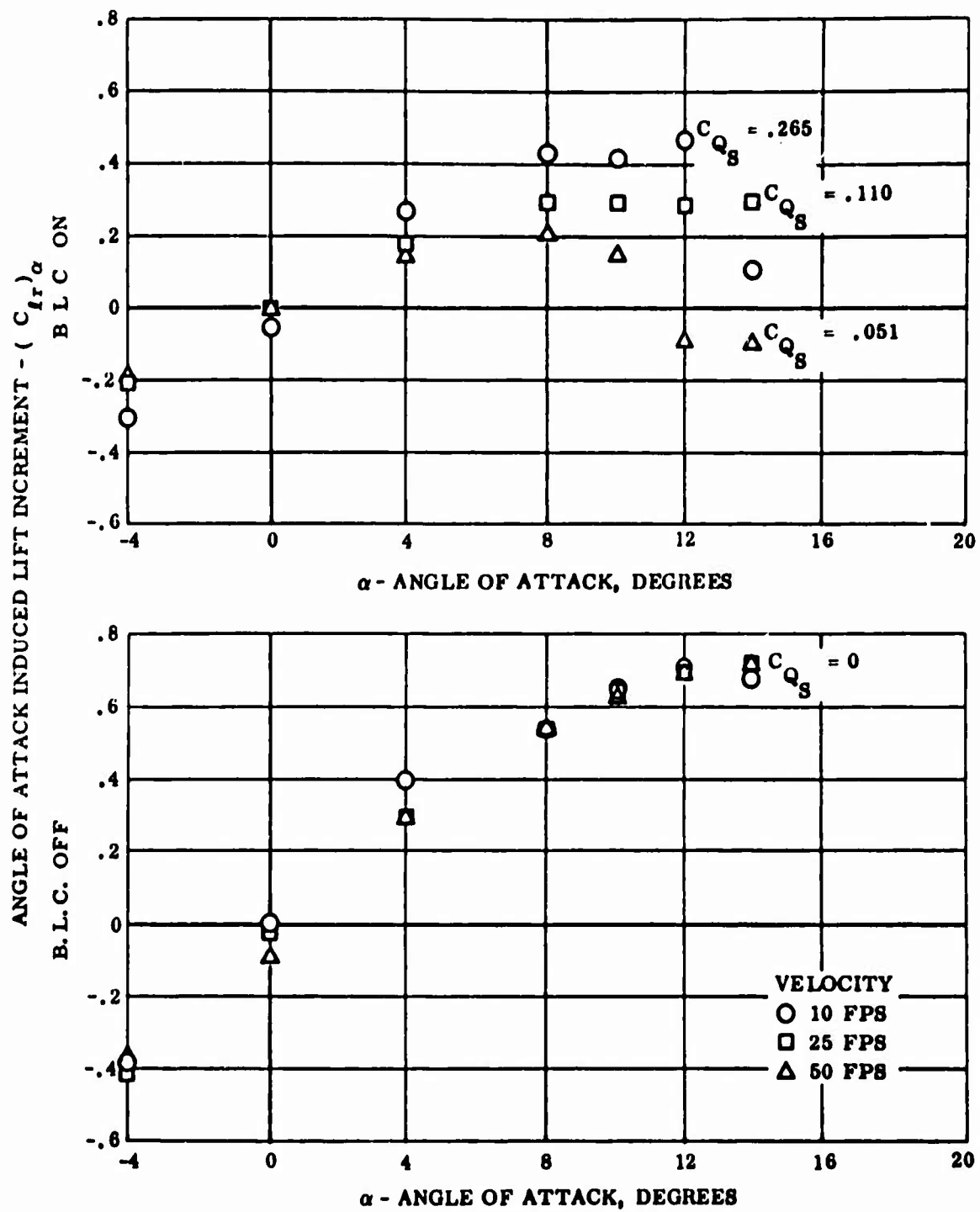


Figure 76. Seventeen-Percent-Thick Suction Flap Airfoil,  $\delta_F = 60^\circ$

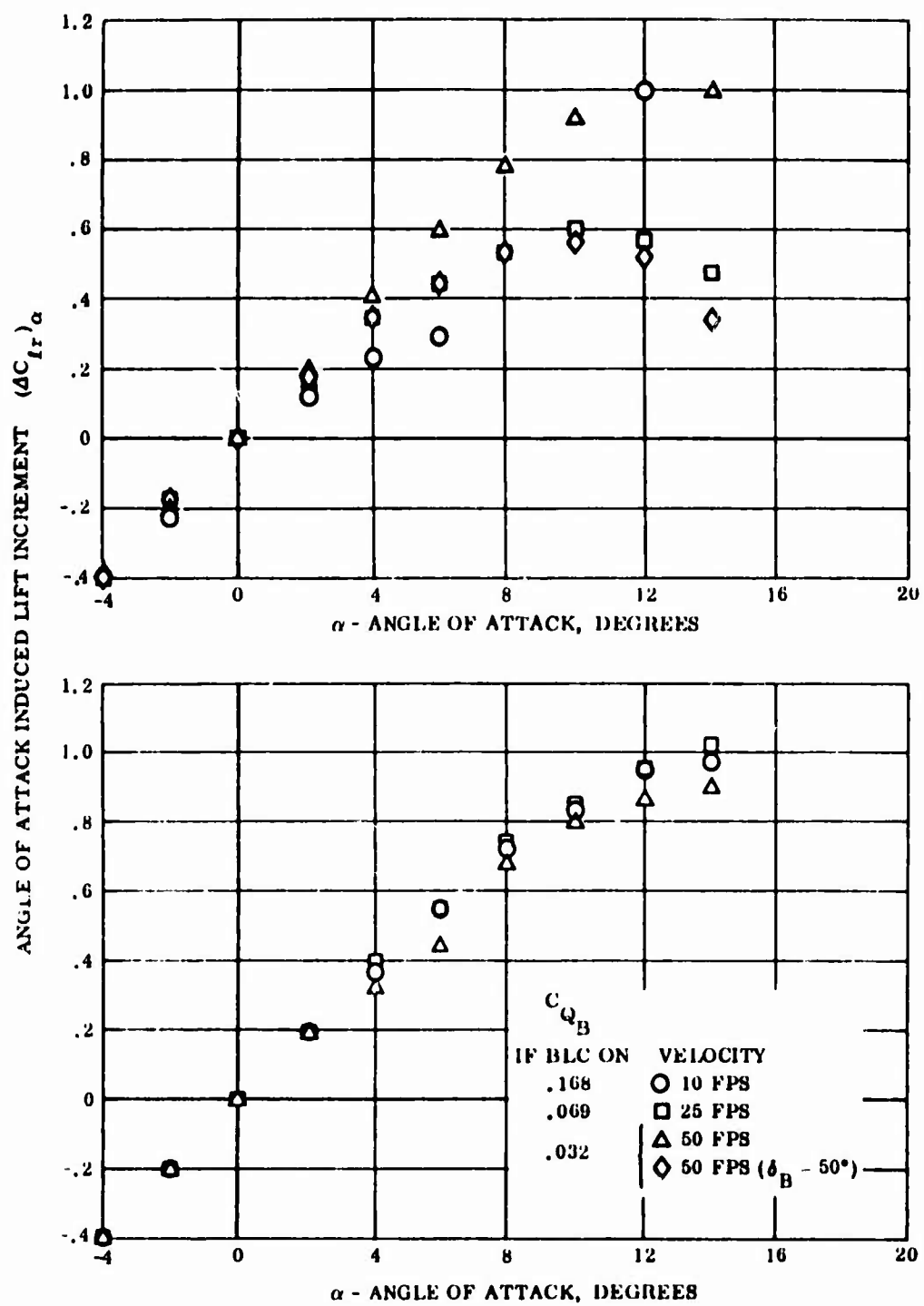


Figure 77. Blowing Flap Airfoil,  $\delta_F = 60^\circ$



Unclassified

Security Classification

DOCUMENT CONTROL DATA - R&D		
<small>(Security classification of title, body of abstract and indexing annotation must be entered when the overall report is classified)</small>		
1. ORIGINATING ACTIVITY (Corporate author) Ryan Aeronautical Company San Diego, California		2a. REPORT SECURITY CLASSIFICATION Unclassified
		2b. GROUP
3. REPORT TITLE Boundary Layer Control System Installation for the YCV-2B Airplane		
4. DESCRIPTIVE NOTES (Type of report and inclusive dates) Final Report		
5. AUTHOR(S) (Last name, first name, initial) Cordner, C. A.		
6. REPORT DATE May 1967	7a. TOTAL NO. OF PAGES 201	7b. NO. OF REFS 11
8a. CONTRACT OR GRANT NO. DA 44-177-AMC-35(T) b. PROJECT NO. Task 1P121401A14178 c. d.	9a. ORIGINATOR'S REPORT NUMBER(S) USAAVLABS Technical Report 66-33 9b. OTHER REPORT NO(S) (Any other numbers that may be assigned this report) Ryan Report No. 65B017A	
10. AVAILABILITY/LIMITATION NOTICES Distribution of this document is unlimited.		
11. SUPPLEMENTARY NOTES	12. SPONSORING MILITARY ACTIVITY US Army Aviation Materiel Laboratories Fort Eustis, Virginia	
13. ABSTRACT The report presents the findings of a research and development contract for the investigation of the feasibility of installing a high lift boundary layer control (BLC) system in a YCV-2B airplane. Work was to be conducted in the areas of preliminary design, technical analysis, and development testing to the extent necessary to determine the feasibility and practicability of improvement of takeoff and landing performance of YCV-2B aircraft.  Primary effort was directed to the development of a compressed air/gasoline fuel primary motor for driving the jet pump system. Secondary effort was directed to the design and evaluation of the system and to the performance characteristics. Also, smoke tunnel tests were conducted to determine qualitatively the effects of BLC on lift characteristics of the YCV-2B airfoils. Difficulty was experienced in the development of the primary motor owing to its inability to contain high temperatures. However, the experimental prototype model was satisfactory for obtaining limited jet pump data. The performance of the jet pump was not able to improve takeoff and landing characteristics of the aircraft. Design and technical analysis studies showed that the BLC system could not be installed and operated in the YCV-2B airplane with any reasonable expectancy of success.  Included as a part of this report are equations, computer programs and methods for predicting design parameters, and performance characteristics of jet pumps and boundary layer controls systems.		

DD FORM 1473  
1 JAN 64

Unclassified

Security Classification



Unclassified  
Security Classification

14. KEY WORDS	LINK A		LINK B		LINK C	
	ROLE	WT	ROLE	WT	ROLE	WT

**INSTRUCTIONS**

**1. ORIGINATING ACTIVITY:** Enter the name and address of the contractor, subcontractor, grantee, Department of Defense activity or other organization (*corporate author*) issuing the report.

**2a. REPORT SECURITY CLASSIFICATION:** Enter the overall security classification of the report. Indicate whether "Restricted Data" is included. Marking is to be in accordance with appropriate security regulations.

**2b. GROUP:** Automatic downgrading is specified in DoD Directive 5200.10 and Armed Forces Industrial Manual. Enter the group number. Also, when applicable, show that optional markings have been used for Group 3 and Group 4 as authorized.

**3. REPORT TITLE:** Enter the complete report title in all capital letters. Titles in all cases should be unclassified. If a meaningful title cannot be selected without classification, show title classification in all capitals in parenthesis immediately following the title.

**4. DESCRIPTIVE NOTES:** If appropriate, enter the type of report, e.g., interim, progress, summary, annual, or final. Give the inclusive dates when a specific reporting period is covered.

**5. AUTHOR(S):** Enter the name(s) of author(s) as shown on or in the report. Enter last name, first name, middle initial. If military, show rank and branch of service. The name of the principal author is an absolute minimum requirement.

**6. REPORT DATE:** Enter the date of the report as day, month, year, or month, year. If more than one date appears on the report, use date of publication.

**7a. TOTAL NUMBER OF PAGES:** The total page count should follow normal pagination procedures, i.e., enter the number of pages containing information.

**7b. NUMBER OF REFERENCES:** Enter the total number of references cited in the report.

**8a. CONTRACT OR GRANT NUMBER:** If appropriate, enter the applicable number of the contract or grant under which the report was written.

**8b, 8c, & 8d. PROJECT NUMBER:** Enter the appropriate military department identification, such as project number, subproject number, system numbers, task number, etc.

**9a. ORIGINATOR'S REPORT NUMBER(S):** Enter the official report number by which the document will be identified and controlled by the originating activity. This number must be unique to this report.

**9b. OTHER REPORT NUMBER(S):** If the report has been assigned any other report numbers (*either by the originator or by the sponsor*), also enter this number(s).

**10. AVAILABILITY/LIMITATION NOTICES:** Enter any limitations on further dissemination of the report, other than those imposed by security classification, using standard statements such as:

- (1) "Qualified requesters may obtain copies of this report from DDC."
- (2) "Foreign announcement and dissemination of this report by DDC is not authorized."
- (3) "U. S. Government agencies may obtain copies of this report directly from DDC. Other qualified DDC users shall request through \_\_\_\_\_."
- (4) "U. S. military agencies may obtain copies of this report directly from DDC. Other qualified users shall request through \_\_\_\_\_."
- (5) "All distribution of this report is controlled. Qualified DDC users shall request through \_\_\_\_\_."

If the report has been furnished to the Office of Technical Services, Department of Commerce, for sale to the public, indicate this fact and enter the price, if known.

**11. SUPPLEMENTARY NOTES:** Use for additional explanatory notes.

**12. SPONSORING MILITARY ACTIVITY:** Enter the name of the departmental project office or laboratory sponsoring (*paying for*) the research and development. Include address.

**13. ABSTRACT:** Enter an abstract giving a brief and factual summary of the document indicative of the report, even though it may also appear elsewhere in the body of the technical report. If additional space is required, a continuation sheet shall be attached.

It is highly desirable that the abstract of classified reports be unclassified. Each paragraph of the abstract shall end with an indication of the military security classification of the information in the paragraph, represented as (TS), (S), (C), or (U).

There is no limitation on the length of the abstract. However, the suggested length is from 150 to 225 words.

**14. KEY WORDS:** Key words are technically meaningful terms or short phrases that characterize a report and may be used as index entries for cataloging the report. Key words must be selected so that no security classification is required. Identifiers, such as equipment model designation, trade name, military project code name, geographic location, may be used as key words but will be followed by an indication of technical context. The assignment of links, rules, and weights is optional.

Unclassified

Security Classification

4099-67